Utah State University

DigitalCommons@USU

All Graduate Theses and Dissertations   Graduate Studies

8-2021

An Analysis of Electromagnetic Flowmeters: A Numerical Study

Kade J. Beck
Utah State University

Follow this and additional works at: https://digitalcommons.usu.edu/etd

Part of the Civil and Environmental Engineering Commons

UtahState University
MERRILL-CAZIER LIBRARY

AN ANALYSIS OF ELECTROMAGNETIC FLOWMETERS: A NUMERICAL STUDY

by

Kade J. Beck

A dissertation submitted in partial fulfillment
of the requirements for the degree

of

DOCTOR OF PHILOSOPHY

in

Civil and Environmental Engineering

Approved:

_____
Michael C. Johnson, Ph.D., P.E.
Major Professor

_____
Steven L. Barfuss, M.S., P.E.
Committee Member

_____
Todd K. Moon, Ph.D.
Committee Member

_____
Zachary B. Sharp, Ph.D., P.E.
Committee Member

_____
Som Dutta, Ph.D.
Committee Member

_____
D. Richard Cutler, Ph.D.
Interim Vice Provost of Graduate Studies

UTAH STATE UNIVERSITY
Logan, Utah

2021

ABSTRACT

An Analysis of Electromagnetic Flowmeters: A Numerical Study

by

Kade J. Beck, Doctor of Philosophy

Utah State University, 2021

Major Professor: Michael C. Johnson, Ph.D., P.E.
Department: Civil and Environmental Engineering

Water meters are critical to the conservation of water by enabling improved water management. Electromagnetic (magnetic) flowmeters are often used in both the drinking water distribution and wastewater collection industries. The focus of this research was threefold. The first objective was to optimize the arc electrode flowmeter and multipoint electrode flowmeter, thereby warranting better meters may exist than in operation today. The second objective was to validate an alternative method to analyze magnetic flowmeter performance for a group of researchers who have historically been unable to do so. The third objective was to explore and evaluate the sensitivity of magnetic flowmeter output signal to higher fidelity flow field models. To that end, this dissertation reviews the required physics for analysis, justifies the present work by providing context of what has previously been accomplished in the literature and identifies three remaining knowledge gaps, presents three studies to demonstrate how the objectives were accomplished, and concludes with the contribution of the present research and its limitations.

(123 pages)

PUBLIC ABSTRACT

An Analysis of Electromagnetic Flowmeters: A Numerical Study

Kade J. Beck

As water scarcity increases, improved water management through better water measurement is of critical global significance. Today, the most common way to measure water in drinking water and wastewater systems is to use an electromagnetic (magnetic) flowmeter. A magnetic flowmeter has many components, and their accuracy can be compromised if not installed or calibrated correctly. The purpose of the present study was threefold. Each of the three components has been named to help the reader understand the context of the study without getting lost in the details.

The Idealist. Using mathematical programs, the spacing of two types of magnetic flowmeter sensors was optimized and the performance of these sensors was numerically compared to the standard sensors in use today.

The Egalitarian. Not all researchers who are interested in magnetic flowmeter analysis are trained to understand how they work. Thus, some researchers are limited in their abilities to identify improvements to water measurement practices. Consequently, an alternative magnetic flowmeter analysis method was compared to the traditional magnetic flowmeter analysis method and found good agreement, thereby enabling a new group of researchers to analyze magnetic flowmeters.

The Capitalist. Computer models can be used to predict the flow of water through pipes. Some models match laboratory observations better than others but are more expensive to use. This segment of research explored how sensitive magnetic flowmeters are to less expensive and more expensive models and found that they appear to exhibit some sensitivity to the choice of model.

ACKNOWLEDGMENTS

CONTENTS

LIST OF TABLES

LIST OF FIGURES

CHAPTER 1

INTRODUCTION

According to Renzetti and Dupont (2016), if water consumption habits don't change, "Water demand will exceed supply by about 55% by the year 2050." The American Water Works Association (AWWA) has stated, "No tool available to water [managers] has played a greater role in the conservation of water than the water meter"(AWWA 2002). Thus, the ability to measure water accurately and thereby wisely manage water resources continues to have critical global significance.

1.1 Background

Electromagnetic (magnetic) flowmeters are a type of volumetric flowmeter that can be very accurate when installed and calibrated correctly (Beck et al. 2019). A recent study found that the drinking water and wastewater markets are responsible for more sales of magnetic flowmeters than any other industry (FlowResearch 2017). This same study also found that magnetic flowmeters generate more revenue than any other type of flowmeter worldwide (\$ 1.4B/year).

Magnetic flowmeters employ Faraday's law of induction to measure a volumetric flowrate. A typical magnetic flowmeter has electrodes located at the springline of the pipe as shown in Figure 1.1. Faraday's law of induction states that as a conductor of width D, with a velocity $\mathbf{v}$, moves normal to a magnetic field of strength $\mathbf{B}$, an electric potential $\tilde{U}$, is created as shown in Equation 1.1.

$$\tilde{U} = \mathbf{v}\mathbf{B}D \tag{1.1}$$

Although magnetic flowmeters do not generally cause system energy losses like other differential pressure meters or Coriolis meters, they are sensitive to the velocity profile at the cross section of measurement. This dissertation uses computational fluid dynamics (CFD)
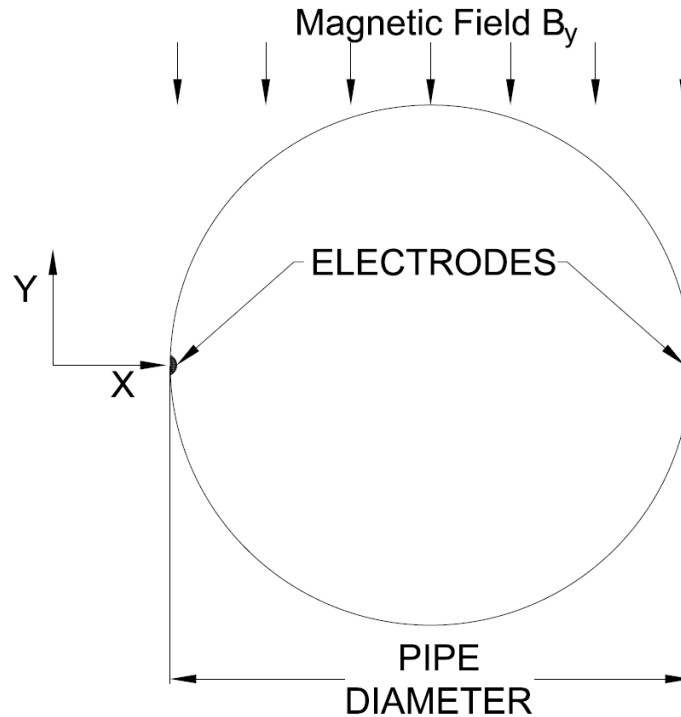
Figure 1.1: Typical Single Point Magnetic Flowmeter

to analyze ways to improve their performance and evaluate the effect of distorted flow profiles on magnetic flowmeters.

1.2   Overview

This section provides an overview of the remaining structure of the dissertation. Chapter 2 presents a review of the existing relevant literature to provide context and establish the basis for the three research objectives. Chapter 3 introduces the fundamental physics required to analyze magnetic flowmeters and explains the modeling process employed for the study to ensure repeatable and reproducible results. Chapter 4 optimizes two different types of magnetic flowmeter electrodes and evaluates their performance in distorted flows. Chapter 5 compares the traditional method of magnetic flowmeter analysis with a numerical solution available in most commercial CFD packages and concludes that there is good agreement between the two methods. Chapter 6 evaluates the effect of higher fidelity flow field models on the output signal of a magnetic flowmeter and asserts there is a difference

between the various flow field models available for magnetic flowmeter analysis in distorted flows. The concluding chapter of the dissertation summarizes the contribution of the research to the field and presents a few of the author's opinions about possible future research topics.

Due to the multipaper format of this dissertation, Chapters 4, 5, and 6 were written as original research papers and submitted to journals for publication. Thus, they can be read and understood independent of the rest of the dissertation. However, the remainder of the dissertation is written in a way to provide additional context and perspective between the three original research papers as a whole that would be difficult to capture without reading the entire dissertation. Furthermore, the reader is reminded that the results of this dissertation are limited to the specific geometries explored, ranges of flows modeled, and the numerical uncertainties reported due to discretization of the mesh.

CHAPTER 2

LITERATURE REVIEW

This chapter reviews the history and development of magnetic flowmeters to provide context for the work conducted as part of this dissertation. The breadth of magnetic flowmeter research is briefly introduced and acknowledged by citing samples of existing research. However, only the most relevant research is reviewed in depth to provide greater context and substantiate the need for the work conducted herein. The section concludes by defining the scope of work and the objectives of the research.

2.1 History and Development

The earliest known attempt to measure flowrate using electromagnetic induction was carried out by Faraday (Shercliff 1962) when he tried to use the earth's magnetic field and large electrodes to measure the flow in the River Thames. Although this attempt was unsuccessful, later researchers like Fabre developed a magnetic flowmeter which was used successfully to measure instantaneously the flow of blood in arteries (Shercliff 1962). After being introduced as flow measurement devices in the medical industry, magnetic flowmeters were also employed to measure the flow of liquid metals in nuclear reactors (Shercliff 1962). The use of magnetic flowmeters as flow measurement devices continues to increase.

2.2 Research Breadth

To help the reader understand the breadth of the research landscape of magnetic flowmeters, a distinction is made between the various components of the flowmeter. The primary elements are those parts which are in direct contact with the fluid being measured such as the magnetic field, meter lining, and the electrodes. The secondary elements of the meter include the components of the meter that are not in direct contact with the fluid which include the signal amplifier and post processing algorithm of the signal. In addi-

tion to active research continuing on the secondary and primary elements of the flowmeter, researchers have explored new methods of analysis and substantiated previous analysis methods with analytical proofs. More recently, researchers have applied magnetic flowmeters to multi-phase flows both as the primary flow measurement device and as a means to reconstruct the velocity profile of the multi-phase flow. Research has been conducted to modify magnetic flowmeter designs and evaluate their performance in annular flows. Experimentalists have explored the effect of various piping configurations on magnetic flowmeter performance. The following sections cite several examples of the work mentioned above to furnish the reader with a panoramic view before narrowing the focus to the research most directly related to the work of this dissertation.

2.3 Sensitivity to Velocity Profile

Shercliff (1954) was the first to note magnetic flowmeters' sensitivity to the velocity profile of the fluid at the cross section of measurement (i.e., the velocity profile at the electrode plane). Shercliff (1962) proposed using a weighted calculation of the velocity profile to account for the effect that distorted velocity profiles have on flowmeter accuracy. He termed this weighted calculation a weight function which is dependent on the electrode geometry and meter shape. Building upon the work of Shercliff, Bevir (1969) proposed using what he called a "weight vector" which included the magnetic field and a "virtual current." Bevir described the virtual current as "the potential due to unit flux flowing from one electrode to the other under identical electrical conditions to those in the flowmeter in normal operation, and may be obtained as the ∇G (apart from a scaling factor), by imposing a fixed voltage between the electrodes and measuring the size and direction of the resulting current field" (Bevir 1969). Although Bevir included the magnetic field as part of the weight vector, many researchers simply refer to the virtual current as the weight function and do not include the magnetic field when referring to the weight function. This dissertation adopts that approach by referring to the virtual current as the weight function. As explained by Bevir above, the virtual current is a theoretical means of determining the distribution of the weight function for a given magnetic flowmeter shape and electrode

configuration. Although Smyth (1971) proposed a similar method around the same time, Bevir's virtual current theory is typically the standard method employed to analyze the performance of magnetic flowmeters and is adopted in this study.

If the velocity profile of the fluid is axisymmetric, the magnetic flowmeter will not be negatively affected. However, two problems exist. First, most practical installation conditions for magnetic flowmeters do not allow for long lengths of straight pipe upstream of the meter due to facility footprint constraints. Thus, many meters are often installed downstream of elbows, valves, tees, etc. The second problem is that the exact shape of the distorted velocity profile caused by the upstream piping is not known beforehand. Thus, a magnetic flowmeter user can be under the erroneous assumption that the magnetic flowmeter will be reading the flow accurately, when that may not be the case. Thus, the majority of the research after Shercliff's identification of this deficiency is focused on improving the accuracy of the magnetic flowmeter. The majority of magnetic flowmeter research appears to be aimed at minimizing the effects of distorted velocity profiles to improve magnetic flowmeter accuracy. These efforts can be broadly grouped into one of three categories (Horner and Mesch 1995). First, researchers have tried to identify ways to rectify the velocity profile in the pipe by increasing the distance between the magnetic flow meter and any upstream disturbances (e.g., valves, tees, elbows, etc.), or by installing flow conditioners (Luntta and Halttunen 1989). Flow conditioners are devices like multi-hole orifice plates whose purpose is to redistribute the flow, thereby reducing the distance for the flow profile to return to straight pipe conditions. In contrast to the first approach, where the attempt is to directly influence the velocity profile, the second and third approaches indirectly attempt to minimize the effect of the velocity profile. The second approach includes altering the flowmeter's magnetic field to reduce the effect of the distorted velocity profile (Cao et al. 2014). The third approach is to improve the weight function of the meter by changing the flowmeter's electrode geometry (Al-Khazraji 1979; Horner and Mesch 1995).

2.4   Electrode Configurations

This section reviews the research employing the third method of improving the weight function by altering the configuration and size of the electrodes.

2.4.1   Arc/Large Electrodes

Significant results have been achieved by efforts to improve the weight function. Bevir (1969) appears to be the first researcher to evaluate the possible performance gains from electrodes of various sizes and shapes. An arc electrode flowmeter has electrodes that extend in an arc shape along the interior wall of the meter. As shown in Figure 4.2, the arc electrodes are represented by the thick black lines. Bevir noted that a meter with arc electrodes with an angle of 133 degrees would have a very uniform weight function. However, it appears that he did not explicitly state 133 degrees would be the optimum angle of the arc electrode meter (Bevir 1969). Later, Al-Khazraji (1979) conducted research on what he termed large electrode flowmeters. Much of this research was focused on determining the loss of accuracy that would accompany fouling of the electrodes from material build up on the electrode surface while the flowmeter is in operation. Shi et al. (2015) proposed that the optimum angle for an arc electrode flowmeter is 100 degrees. Although the authors were able to replicate the weight functions produced by Bevir (1969) and Shercliff (1962), they were unable to replicate the results of Shi et al. (2015). Consequently, the literature is inconclusive regarding the optimum angle for an arc electrode flowmeter.

2.4.2   Multipoint Electrodes

Horner et al. (1996) proposed using a flowmeter with more than a one-point electrode pair to measure the flowrate. They evaluated various combinations of multiple electrodes and concluded that the addition of electrodes produces a significant improvement in flowmeter accuracy. Later, Horner (1998) proposed two additional electrode pairs at 45-degree angles from the standard diametrically opposed pair. The results showed much less sensitivity to the distorted profiles created by various orifice plates upstream of the meter without excessive electrode pairs. Other researchers (Xu et al. 2005; Wang et al. 2007; Lucas and

Leeungculsatien 2010) have extensively explored additional electrodes as a means of reconstructing the velocity profile using a method proposed by Engl (1970). As far as can be surmised without a formal and complete translation, Kong et al. (2015) numerically analyzed the weight function distribution of various configurations of the 6-electrode flowmeter and concluded the 6-electrode flowmeter is better than the single-point flowmeter due to a more uniform weight function. However, it is unclear what the optimum spacing would be for the 6-electrode flowmeter. Furthermore, there does not appear to be research conducted that compares the results of optimized arc and multipoint (6-total electrodes) flowmeters against single-point electrode flowmeters downstream of practical and common installation conditions in the water industry, which is the basis for the first research objective.

2.5   The Evolution of Analysis Methods

This section describes the evolution of magnetic flowmeter analysis methods. The specific articles highlighted in this section do not represent a comprehensive list of all the researchers who have contributed to the field over the years. Rather, the articles mentioned below are intended to describe a change in focus to a more complete analysis of magnetic flowmeters which is possible largely because of increased computing power.

As the following paragraphs illustrate, researchers were often limited by the available tools and had to make assumptions about the velocity profile, magnetic field, or both when analyzing magnetic flowmeter performance. Furthermore, it is apparent from the literature that other researchers who are very interested in the sensitivity and accuracy of magnetic flowmeters in varied hydraulic conditions do not appear to be aware of or capable of analyzing magnetic flowmeters performance numerically and thus rely on other correlative methods like those described by Martim et al. (2019) and Beck et al. (2019) as a substitute. In some cases, researchers appear to be as comfortable with the fluid mechanics involved in solving the flow field as they are in understanding the computations required to produce a voltage output for the magnetic flowmeter being modeled. However, this appears to be the exception rather than the norm. Thus, the interest in enabling the many researchers interested in the measurement errors that are produced from common magnetic flowmeter

installation conditions.

Even research conducted by some magnetic flowmeter manufacturers like SeaMetrics (Peery 2006) appears to indicate a gap between the way manufacturers develop and test magnetic flowmeters and the present capabilities of software when used correctly to model magnetic flowmeter performance. Thus, from both a design and operational perspective, the advancement of holistic flowmeter analysis methods is of significant interest.

Around the same time Bevir (1969) introduced his weight vector and virtual current theory, Smyth (1971) derived weight functions using a similar approach and produced a similar weight function to Shercliff (1962). Using the weight function method (WFM), Bevir et al. (1981) presented a method for which the performance of a magnetic flowmeter could be predicted based upon constraints on the velocity profile being "rectilinear and axisymmetric" (i.e., no distortion in the flow). Later, O'Sullivan and Wyatt (1983) presented a method employing the weight function that removed the axisymmetric but not the rectilinear flow restriction.

Luntta and Halttunen (1989) used the computer program PHEONICS to model the flow profile for a distorted flow and, using the weight function, computed the expected error for a magnetic flowmeter. Lim and Chung (1998) modeled the flow field and compared the results of the WFM with a solution to the flowmeter equation using the finite volume method (they do not state whether they wrote the code or used a commercial package). They noted that the results of each method were sensitive to the direction and combination of various grid refinements. Wang et al. (2006) created a 3D model for a magnetic flowmeter and employed a numerical weight function based on the work of Shercliff (1962) including a numerical solution of the flow field. Fu et al. (2010) proposed a method for calibrating magnetic flowmeters by coupling the weight function, magnetic field, and velocity profile data using a finite element solver in MatLab.

It appears that Lu et al. (2013) was the first to use commercially available software that employed both the magnetohydrodynamic (MHD) equations and the Navier-Stokes equations to analyze magnetic flowmeters. They concluded that the MHD coupled solver

method agreed well with the WFM for a laminar and turbulent flow in straight pipe conditions without modeling the actual electrodes and the associated solid-fluid interaction. They also evaluated the effect of the Lorentz force on the magnetic flowmeter output for both a laminar and turbulent flow. They concluded that the effect of the Lorentz force was "negligible" for the fluid modeled which had a low electric conductivity. However, Lu et al. (2013) only compared the WFM and MHD for straight pipe conditions and did not evaluate the capability of the MHD method to model alternative electrode configurations (e.g., multipoint electrodes). There does not appear to be any literature that compares the WFM with the MHD method for flows downstream of distortions or with alternative electrode configurations (e.g., multipoint electrodes), which is the basis for the second objective.

2.6   Flow Field Studies

A limited number of studies have incorporated an evaluation of the flow field to varying degrees of complexity. At the most basic level, some researchers like Al-Khazraji (1979) and Bevir (1969) employed velocity log laws for straight pipe turbulent flow in their analyses. Luntta and Halttunen (1989) employed the numerical code PHOENICS to analyze a magnetic flowmeter in a distorted flow condition. Later, Lim and Chung (1999) evaluated the flowmeter signal with laminar flow because "the numerical solution of [turbulent flows] depends strongly on the model adopted, [and] it is almost impossible to distinguish the true installation effects from erroneous results due to the inadequate turbulence model." In a study conducted by Fu et al. (2010), the velocity profile was modeled in an attempt to validate an approach to dry calibrating magnetic flowmeters. However, the authors do not state how they solved the flow field other than stating they solved the Navier-Stokes equations, and they acknowledge that the uncertainty of the flow field is a significant factor in fluid mechanics and higher fidelity models. Furthermore, all of the testing was conducted using a reference flowmeter. Reference flowmeters can introduce additional errors if not calibrated properly and thus leave some questions as to the absolute errors associated with Fu et al.'s work. Later, Cao et al. (2014) optimized the magnetic field to reduce the effect of a distorted velocity profile on the flowmeter output using the commercial CFD solver

FLUENT. Cao et al. (2014) did not state which turbulence model was employed for the numerical modeling as it appears the focus was on the relative difference of between the unoptimized and optimized magnetic fields. In another magnetic flowmeter analysis study Lu et al. (2013) used the κ-ϵ turbulence model in COMSOL to model the flow field in straight pipe conditions. Simão et al. (2018) used the κ-ϵ turbulence model and COMSOL as well and acknowledged the tradeoff between higher fidelity models and the associated computation cost increases accompanying those models. Other researchers have long explored the deficiencies of Reynolds-averaged Navier-Stokes (RANS) models compared to higher fidelity models in distorted flow conditions like those downstream of an elbow. In a review of turbulent flow in curved pipes, Vester et al. (2016) noted that RANS models struggle to predict the flow accurately due to "the anisotropic nature of turbulence [and] the secondary motion imposed by the curvature." However, it is unclear how much this apparent limitation of RANS models influences the flowmeter output, which is the basis for the third objective.

2.7   Magnetic Flowmeter Analysis Theory

Some researchers have found alternative ways to arrive at the same result of the weight function using various theoretical derivations. For example, around the time of Bevir (1969), Smyth (1971) solved for the weight function differently by using Green's Theorem and conformal mapping. Davidović et al. (1991) attempted to "provide a more intuitive insight into flowmeter operation to electrical engineers" by providing a "physically transparent and mathematically rigorous" derivation of the voltage output of a magnetic flowmeter using electrostatics. Yin and Li (2013) presented a new approach to solving weight functions using resistive network modeling with an assertion that the approach is simpler and more intuitive.

2.8   Secondary Elements

Due to the low magnitude of a typical magnetic flowmeter voltage output (on the order of microvolts) signal amplification and noise cancellation methods have also been improved.

Ge et al. (2020) presented a new method based on a differential correlation technique to reduce the noise and interference of the flowmeter signal for low flow limits.

2.9   Multiphase Flow

Magnetic flowmeters have been employed as a means to measure multiphase flows (Cha et al. 2002; Li et al. 2019). They have also combined with other measurement technologies to reconstruct the velocity profile (Wang et al. 2006, 2007; Lucas and Leeungculsatien 2010) based on the work of Engl (1970).

2.10   Open Channel

Magnetic flowmeters have even been employed as flow measurement devices for open channel flows (Michalski et al. 2001; Watral et al. 2015) in addition to understanding their performance in partially full pipes (Ismael et al. 2017).

2.11   Magnetic Field Optimization

Bevir (1969) evaluated the conditions that would be necessary to create an ideal flowmeter. He noted that due to the practical limitations of constructing the magnetic field the meter couldn't be made ideal. However, other researchers have explored other ways to optimize the magnetic field using Helmholtz coils (Lucas and Leeungculsatien 2010). In addition to exploring battery powered magnetic flowmeters (Katutis and Virbalis 2007), others, like Lim (2008) explored energy consumption reduction and claimed a reduction of 54.7% less power consumption over the conventional magnetic flowmeter. Magnetic fields have also been optimized for reduced port flowmeters (Liu and Zhang 2014). A global flowmeter manufacturer, ABB, has written that a magnetic field that is the inverse of the weight function "can only be approached in practical designs" (Frenzel et al. 2011) This statement appears to suggest that magnetic flowmeter manufacturers intentionally design the magnetic field to complement the meter's weight function, thereby reducing the sensitivity of the meter to flow profile distortions.

2.12 Physical Laboratory Testing

A more pragmatic approach, which is also the most accurate to ensuring flowmeter performance is that of physical laboratory testing. This is done by installing the flowmeter and testing the flowmeter in the exact same piping configuration that it will be operated in and experimentally determining the performance as done by Beck et al. (2018). This approach ensures that the meter being tested is subjected to a simulated velocity profile passing through the meter that replicates what will be seen in the field when the meter is permanently installed.

2.13 Objectives

This section outlines the three primary objectives for this study.

1) Determine the optimum angle of arc electrodes and the optimum spacing for the multipoint electrode meter with 6 electrodes in order to demonstrate the superior performance of the arc electrode flowmeter.

2) Determine the validity of direct MHD/CFD solutions to flowmeter analysis in distorted flows by comparing with the traditional WFM and explore the capability of using MHD/CFD to evaluate alternative magnetic flowmeter electrode configurations besides the standard single-point electrode flowmeter.

3) Evaluate whether or the not numerical accuracy of a magnetic flowmeter is affected by the fidelity of the flow field model.

CHAPTER 3

METHODOLOGY

This chapter presents the fundamental principles of electromagnetics and fluid mechanics required to understand magnetic flowmeters and the subsequent analysis methods. The first section is devoted to reviewing electromagnetics and MHD. It concludes by reviewing how the software packages used for the research program (MatLab and STAR CCM+) employed the mathematics for the electromagnetic and MHD research components. The second section briefly describes Simcenter STAR CCM+, which was the CFD package employed for the study.

3.1 Electromagnetics and Magnetohyrodynamics

This section reviews the fundamental equations of MHD which govern the analysis of magnetic flowmeters. The solution to the governing flowmeter equation by means of the WFM and the MHD coupled solver method, respectively, is addressed. The Reynolds Magnetic Number (Re_{mag}) is introduced in the concluding portion of the section.

The MHD equations describe the interaction between magnetic fields and electrically conducting fluids. Ohm's law for the case when a conducting fluid passes through a magnetic field is given by

$$\mathbf{J} = \sigma(\mathbf{E} + \mathbf{v} \times \mathbf{B}), \tag{3.1}$$

where $\mathbf{J}$ is the current density vector, σ the fluid conductivity, $\mathbf{E}$ is the electric field, $\mathbf{v}$ is the fluid velocity vector, and $\mathbf{B}$ is the magnetic field (Hughes and Young 1966). $\mathbf{E}$ can be substituted with $-\nabla U$, where U is the electric potential and because of conservation of charge the induced electric current within the meter satisfies Equation 3.2

$$\nabla \cdot \mathbf{J} = 0. \tag{3.2}$$

Using the identity that $\nabla \cdot (\nabla U) = \nabla^2 U$ and assuming isotropic conductivity Equation 3.1 can be rearranged as,

$$\nabla^2 U = \nabla \cdot (\mathbf{v} \times \mathbf{B}) \tag{3.3}$$

which is commonly called the flowmeter equation (Shercliff 1962).

At the time of Shercliff, it appears that numerical computational methods were not robust enough to solve the flowmeter equation directly. Consequently, Shercliff proposed the weight function as an alternative method of solution to the flowmeter equation. The process for deriving the weight function as presented by Bevir (1969) is summarized in what follows. Let G be a potential function that satisfies Laplace's equation (Equation 3.4) and has boundary conditions of a positive and negative unit voltage on opposing electrodes as shown in Equation 3.5 (Bevir 1969).

$$\nabla^2 G = 0. \tag{3.4}$$

$$\left. \frac{\partial G}{\partial r} \right|_{r=R} = \begin{cases} \text{right electrode} = 1 \\ \\ \text{left electrode} = -1 \\ \\ \text{otherwise} = 0 \end{cases} \tag{3.5}$$

The author's analytical derivation of the weight function boundary conditions using the method of separation of variables is included in Appendix B. The weight function is obtained by taking the gradient of G perpendicular to the flow direction (z) and the magnetic field (negative y)

$$\nabla G = j_x, \tag{3.6}$$

where j_x represents the values of the weight function at each point in the flowmeter. Using the weight function method, the flowmeter signal is found by solving Equation 3.7

$$\Delta U = \int_\Omega v_z j_x B_y d\Omega, \tag{3.7}$$

where ΔU is the voltage difference between the electrodes, v_z is the velocity profile in the pipe, j_x is the weight function, B_y is the y-component of the magnetic field in the meter, and Ω is the measuring volume or plane for a 3D or 2D analysis, respectively (Bevir 1969).

The solution to Equation 3.7 requires the derivation of the weight function of the flowmeter and a knowledge of the magnetic field and velocity data at each grid of the domain. Thus, it often requires writing one's own post-processing code to solve Equation 3.7, which can be extensive effort beyond that of solving the flow field of interest. Hence, it is desirable to eliminate any unnecessary steps in the process without compromising the fidelity of the magnetic flowmeter analysis. Appendix A includes the author's MatLab code for extracting the weight function values corresponding to the flow field geometry as well as the MatLab code written by the author for deriving the single-point, multipoint, and arc electrode flowmeters.

In contrast to the WFM, many commercial multiphysics solvers have the capability to solve the flowmeter equation directly without the need for the weight function. For example, the commercial software Simcenter STAR CCM+, which is used in this study, solves for the voltage by discretizing an integral form of Equation 3.3 over the entire domain using the finite volume method (SIEMENS 2021). The ability to solve Equation 3.7 directly is a significant advantage when considering the time savings and flexibility of a comprehensive solver.

Another important concept to introduce is the Reynolds Magnetic Number (Re_{mag}) which is a dimensionless number that relates the ratio of the induced and prescribed magnetic flux densities and is defined as,

$$Re_{mag} = \mu_0 \sigma U L \tag{3.8}$$

where μ_0 is the permeability constant, σ is the electric conductivity of the fluid, U is the characteristic flow velocity in the pipe, and L is the diameter of the pipe (SIEMENS 2021). For low Re_{mag} values, the induced magnetic flux densities are negligible. Due to the low electrical conductivity of water, the present study falls in the low Re_{mag} regime.

3.2   Computational Fluid Dynamics

CFD employs numerical methods to solve the Navier-Stokes equations which describe the flow of fluid. For laminar flows, analytical solutions exist. However, for turbulent flows, analytical treatment becomes impossible. Modeling flow fields has a tradeoff between the cost to run the model and the associated accuracy of the model. The flow field was solved using Simcenter STAR CCM+, which is a commercially available CFD package. Simcenter STAR CCM+ is a multiphysics solver with many capabilities of modeling flow fields and other physical and chemical processes. The specific methods used for each study are described in chapter corresponding to that study. For each study conducted, the uncertainty of the numerical model due to the discretization was determined using the process described by Celik et al. (2008).

CHAPTER 4

THE SUPERIOR ACCURACY OF THE ARC ELECTRODE FLOWMETER: A

NUMERICAL STUDY

4.1 Abstract

The superior accuracy of the arc electrode magnetic flowmeter is demonstrated by optimizing its weight function and comparing its performance downstream of a 90-degree elbow and gate valve (50% open) with that of an optimized multipoint (six-electrode) and single-point electrode flowmeter. Research literature is inconclusive on the necessary angle of arc electrode magnetic flowmeters, as well as the required spacing for multipoint flowmeters to optimize meter accuracy. This article determines the optimum configurations for both arc and multipoint flowmeters using the coefficient of variation of the weight function as the basis for optimization. This study illustrates that the accuracy of multipoint electrode flowmeters exhibits the same oscillatory behavior of single-point flowmeters, but the magnitude of the deviation is greatly reduced. The numerical study also provides supporting evidence that the optimized arc electrode flowmeter is superior to the optimized multipoint and single-point electrode flowmeters.

4.2 Introduction

This article identifies a gap in current research regarding electromagnetic (magnetic) flowmeter accuracy compared with previous results and presents a numerical study conducted to illustrate the superiority of the arc electrode magnetic flowmeter.

Since the first magnetic flowmeter was proposed by Fabre in 1932 (Shercliff 1962), their use has continued to expand from the medical industry into many other industries (e.g., drinking water distribution and wastewater collection). Magnetic flowmeters employ Faraday's law of induction to measure a volumetric flowrate. A schematic of a typical single-

point electrode flowmeter is shown below in Figure 4.1. The electrodes are diametrically opposed and located at the springline of the pipe. The magnetic field B_y is in the $-y$ direction and flow is in the positive z direction (i.e., out of the page). Due to their non-intrusive nature, they do not cause any system pressure loss, and they can be very accurate when installed properly (Beck et al. 2018).
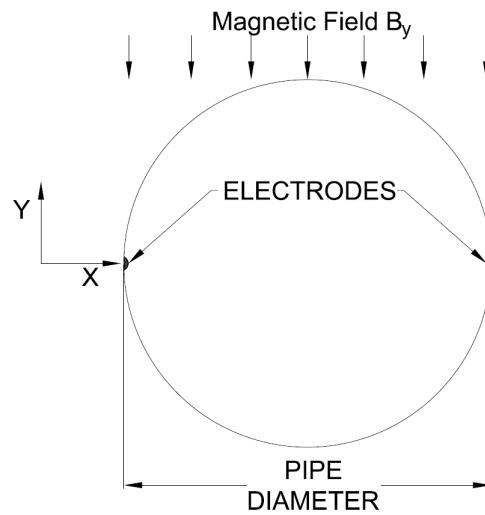
Figure 4.1: Magnetic Flowmeter Schematic

Shercliff (1954) was the first to note magnetic flowmeters' sensitivity to the velocity profile at the cross section of measurement (i.e., the velocity profile at the electrode plane). Shercliff (1962) proposed using a weighted calculation of the velocity profile to account for the effect that distorted velocity profiles have on flowmeter accuracy. He termed this weighted calculation a weight function which is dependent on the electrode geometry and meter shape.

Since then, significant research has been conducted to minimize the effects that distorted velocity profiles have on magnetic flowmeter accuracy. These efforts can be broadly grouped into one of three categories (Horner and Mesch 1995). First, researchers have tried to identify ways to rectify the velocity profile in the pipe by increasing the distance between the magnetic flow meter and any upstream disturbances (e.g., valves, tees, elbows, etc.), or

by installing flow conditioners (Luntta and Halttunen 1989). Flow conditioners are devices like multi-hole orifice plates whose purpose is to redistribute the flow, thereby reducing the distance for the flow profile to return to straight pipe conditions. In contrast to the first approach, where the attempt is to directly influence the velocity profile, the second and third approaches indirectly attempt to minimize the effect of the velocity profile. The second approach includes altering the flowmeter's magnetic field to reduce the effect of the distorted velocity profile (Cao et al. 2014). The third approach is to improve the weight function of the meter by changing the flowmeter's electrode geometry (Al-Khazraji 1979; Horner and Mesch 1995). This study falls under the third approach by optimizing the electrode geometry for arc and multipoint flowmeters.

4.2.1 Virtual Current Theory

One of the greatest contributions to magnetic flowmeter analysis was given by Bevir (1969) who expanded the work of Shercliff (1962). He proposed using what he called a "weight vector" which included the magnetic field and a "virtual current." Bevir described the virtual current as "the potential due to unit flux flowing from one electrode to the other under identical electrical conditions to those in the flowmeter in normal operation, and may be obtained as the ∇G (apart from a scaling factor,) by imposing a fixed voltage between the electrodes and measuring the size and direction of the resulting current field" (Bevir 1969). Although Bevir included the magnetic field as part of the weight vector, many researchers simply refer to the virtual current as the weight function and do not include the magnetic field when referring to the weight function. This paper adopts that approach by referring to the virtual current as the weight function. As explained by Bevir above, the virtual current is a theoretical means of determining the distribution of the weight function for a given electromagnetic flowmeter shape and electrode configuration. Although Smyth (1971) proposed a similar method around the same time, Bevir's virtual current theory is typically the standard method employed to analyze the performance of magnetic flowmeters and is adopted in this study.

4.2.2   Arc/Large Electrodes

Significant results have been achieved by efforts to improve the weight function. Bevir (1969) appears to be the first researcher to evaluate the possible performance gains from electrodes of various sizes and shapes. An arc electrode flowmeter has electrodes that extend in an arc shape along the interior wall of the meter. As shown in Figure 4.2, the arc electrodes are represented by the thick black lines. Bevir noted that a meter with arc electrodes with an angle of 133 degrees would have a very uniform weight function. However, it appears that he did not explicitly state 133 degrees would be the optimum angle of the arc electrode meter (Bevir 1969). Later, Al-Khazraji (1979) conducted research on what he termed large electrode flowmeters. Much of this research was focused on determining the loss of accuracy that would accompany fouling of the electrodes from material build up on the electrode surface while the flowmeter is in operation. Shi et al. (2015) proposed that the optimum angle for an arc electrode flowmeter is 100 degrees. Although the authors were able to replicate the weight functions produced by Bevir (1969) and Shercliff (1962), they were unable to replicate the results of Shi et al. (2015). Consequently, the literature is inconclusive regarding the optimum angle for an arc electrode flowmeter.

4.2.3   Multipoint Electrodes

Horner et al. (1996) proposed using a flowmeter with more than a one-point electrode pair to measure the flowrate. He evaluated various combinations of multiple electrodes and concluded that the addition of electrodes produces a significant improvement in flowmeter accuracy. Later, Horner (1998) proposed two additional electrode pairs at 45-degree angles from the standard diametrically opposed pair. The results showed much less sensitivity to the distorted profiles created by various orifice plates upstream of the meter without excessive electrode pairs. Other researchers (Xu et al. 2005; Wang et al. 2007; Lucas and Leeungculsatien 2010) have extensively explored additional electrodes as a means of reconstructing the velocity profile using a method proposed by Engl (1970). As far as can be surmised without a formal and complete translation, Kong et al. (2015) numerically analyzed the weight function distribution of various configurations of the 6-electrode flowmeter

and concluded the 6-electrode flowmeter is better than the single-point flowmeter due to a more uniform weight function. However, it is unclear what the optimum spacing would be for the 6-electrode flowmeter. Furthermore, there does not appear to be research conducted that compares the results of optimized arc and multipoint (6-total electrodes) flowmeters against single-point electrode flowmeters downstream of practical and common installation conditions in the water industry.

4.2.4   Objective

This study was undertaken to optimize the multipoint electrode magnetic flowmeter spacing and clarify the optimum angle of the arc electrode magnetic flowmeter. The purpose of this paper is to demonstrate the significance of the numerical accuracy increases of arc and multipoint electrode magnetic flowmeters as compared to single-point electrode magnetic flowmeters downstream of a 90-degree elbow and a gate valve which is 50% open.

4.3   Governing Equations

Based on Bevir's virtual current theory, the voltage of a magnetic flowmeter is described by

$$\Delta U = \int_\Omega v_z j_x B_y d\Omega, \tag{4.1}$$

where ΔU is the voltage difference between the electrodes, v_z is the velocity profile in the pipe, j_x is the weight function of the meter obtained by calculating the virtual current with the appropriate boundary conditions for the meter, B_y is the y-component of the magnetic field in the meter, and Ω is the measuring volume or plane for a 3D or 2D analysis, respectively (Bevir 1969). All analyses conducted herein were 2D. The process for calculating the weight function was also described by Bevir (1969). Let G be a potential function that satisfies Laplace's equation, with the boundary conditions of a positive unit voltage on one electrode and a negative unit voltage on the other that is a solution to the Laplacian as shown in Equation 4.2.

$$\nabla^2 G = 0 \tag{4.2}$$

By taking the gradient of this function G in the same direction as the electrodes, the weight function is obtained

$$\nabla G = j_x. \tag{4.3}$$

4.4 Electrode Optimization

The arc and multipoint electrode configurations were optimized by determining the weight function's coefficient of variation for a range of angles. Using the Partial Differential Equation (PDE) Toolbox in MatLab, a potential function G was found using the boundary conditions described in Equation 4.4.

$$\left.\frac{\partial G}{\partial r}\right|_{r=R} = \begin{cases} \text{right hand side electrode} =1 \\ \text{left hand side electrode} = -1 \\ \text{otherwise} = 0 \end{cases} \tag{4.4}$$

Once this potential function G was found, the weight function was obtained by employing Equation 4.3. The standard deviation (S_d) and mean (M) of the weight function (j_x) were used to calculate the coefficient of variation as shown in Equation 4.5.

$$C_v = \frac{S_d}{M} \tag{4.5}$$

The coefficient of variation is a way to measure the uniformity or dispersion of a dataset. Thus, a smaller value of the coefficient of variation for the weight function is an indication of reduced sensitivity of the flowmeter to the velocity profile throughout the cross-section of measurement. For this reason, the coefficient of variation was plotted at varying ranges of angles for the arc and multipoint electrode configurations to determine the optimal configuration.

4.4.1 Arc Electrode

The optimum angle of the arc electrode was determined by calculating the weight function of the meter and then determining the coefficient of variation. When the coefficient of variation was at a minimum, the arc electrode meter was considered optimized. Interestingly, the minimum coefficient of variation occurred at an angle of 130 degrees. This confirms Bevir's results that the optimum angle for the arc electrode flow meter is at or near 133 degrees. Figure 4.2 depicts the arc electrode flowmeter. Figure 4.3 presents a plot of the electrode angle in degrees vs the coefficient of variation for the arc electrode meter. An angle of 130 degrees was used throughout this study for simplicity.
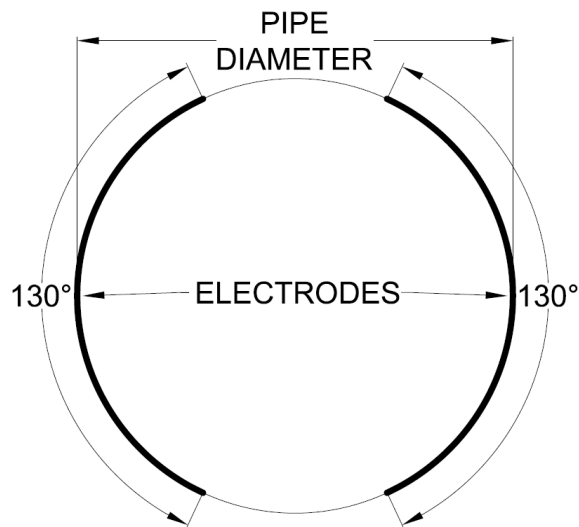
Figure 4.2: Optimized Arc Electrode Flowmeter
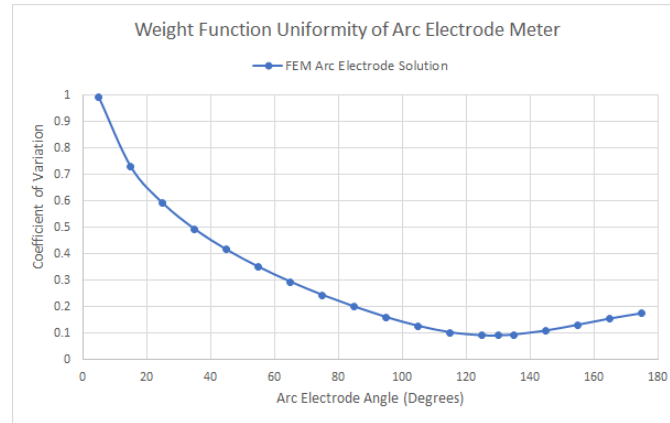
Figure 4.3: Coefficient of Variation for Arc Electrode Flowmeter

Figure 4.4 shows the results of the numerical simulation of the weight function corresponding to an arc electrode flowmeter 130-degrees. Several contour lines are shown in black with white labels indicating the value of the weight function.
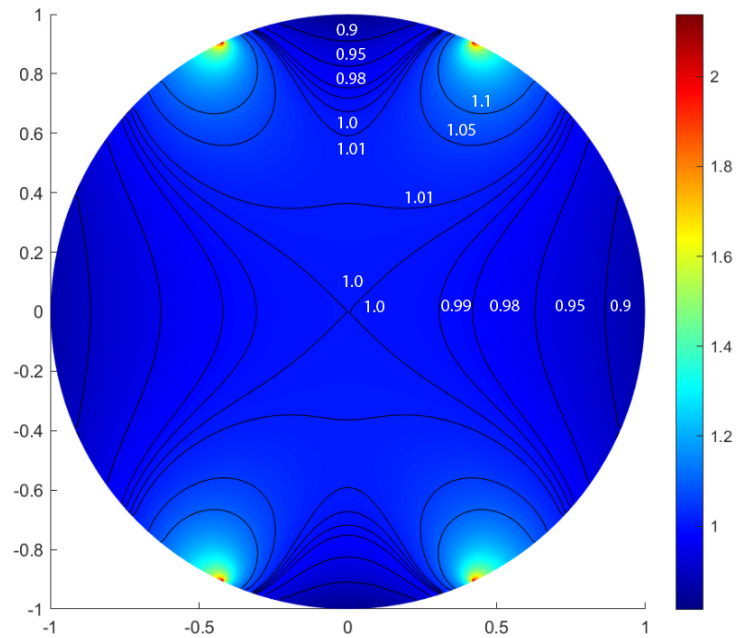
Figure 4.4: Weight Function of Optimized Arc Electrode Flowmeter

4.4.2   Multipoint Electrode

The optimum spacing between the electrodes for the multipoint meter was also determined by calculating the coefficient of variation of the weight function for different angles between the electrodes. Only the top and bottom pairs of electrodes were moved incrementally farther away from the diametrically opposed pair in stages of 5 and eventually 2.5 degrees when determining the optimum angle. The minimum coefficient of variation occurred when the spacing between the electrodes was 25 degrees as shown in Figures 4.5 and 4.6.
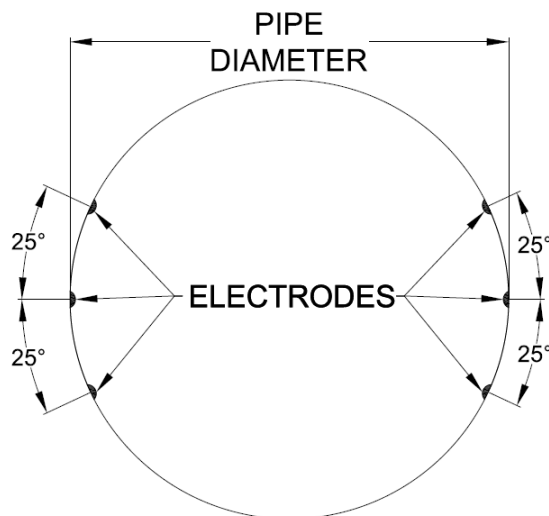
Figure 4.5: Optimized Multipoint Electrode Flowmeter
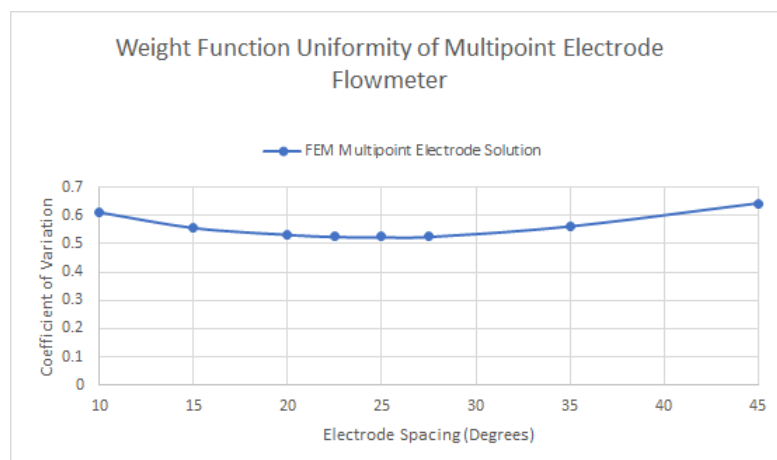
Figure 4.6: Coefficient of Variation for Multipoint Electrode Flowmeter

The weight function corresponding to the optimized multipoint flowmeter is shown in Figure 4.7. Several contour lines are shown in black with white labels indicating the value of the weight function.
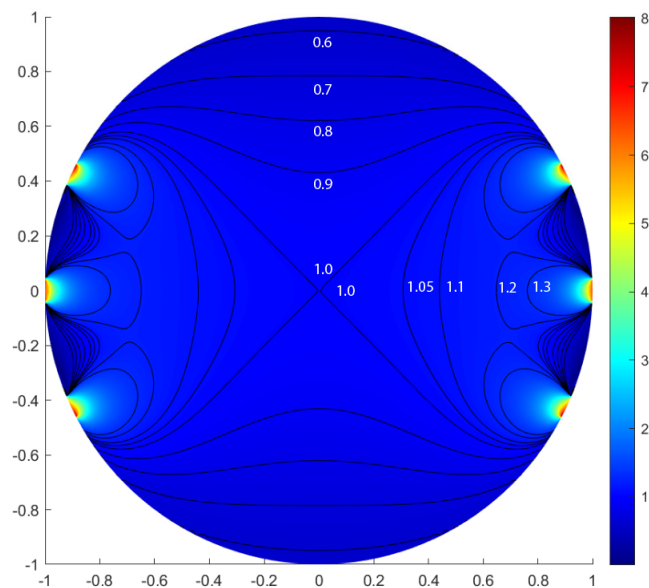
Figure 4.7: Weight Function of Optimized Multipoint Electrode Flowmeter

For reference and comparison, the weight function of the single-point electrode flowmeter is also shown in Figure 4.8.
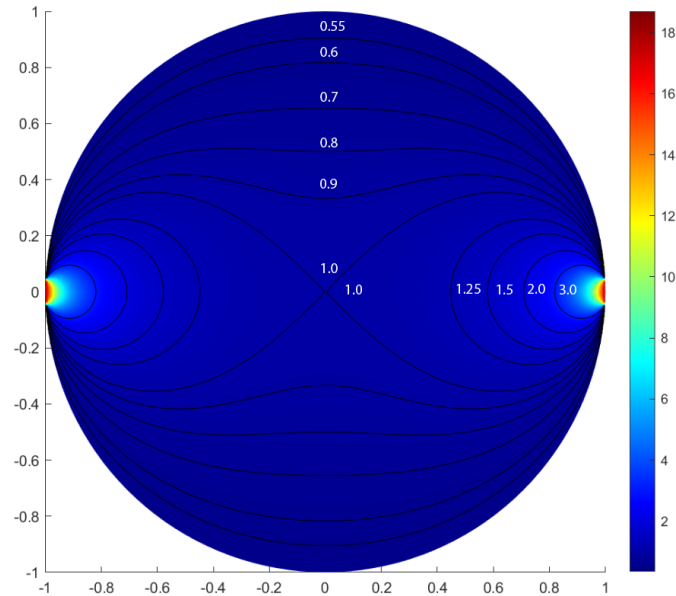
Figure 4.8: Weight Function of single-point electrode flowmeter

4.5   Results and Practical Applications

A 6-inch 90-degree long radius (1.5D) elbow (a) and a gate valve (50% open) as shown in Figure 4.9 (a) and (b), respectively, were selected as the flow disturbances to provide two distinct, yet typical, installation conditions. The flow was modeled as a constant density fluid using Star CCM+, which employed the Reynolds-Averaged Navier-Stokes (RANS) equations. The simulations used the $\kappa - \epsilon$ turbulence model along with the two layer all y+ wall treatment and the segregated flow solver. Two flow rates corresponding to mean pipeline velocities of 2 feet-per-second (fps) and 10-fps were simulated. Fully developed velocity profiles were created by using a periodic boundary condition on a pipe segment and letting the simulation run until the velocity magnitude was unchanging with increasing iterations. This fully developed velocity profile was used as the input for three simulations. The first simulation represents an ideal straight pipe condition with no distorted profile.
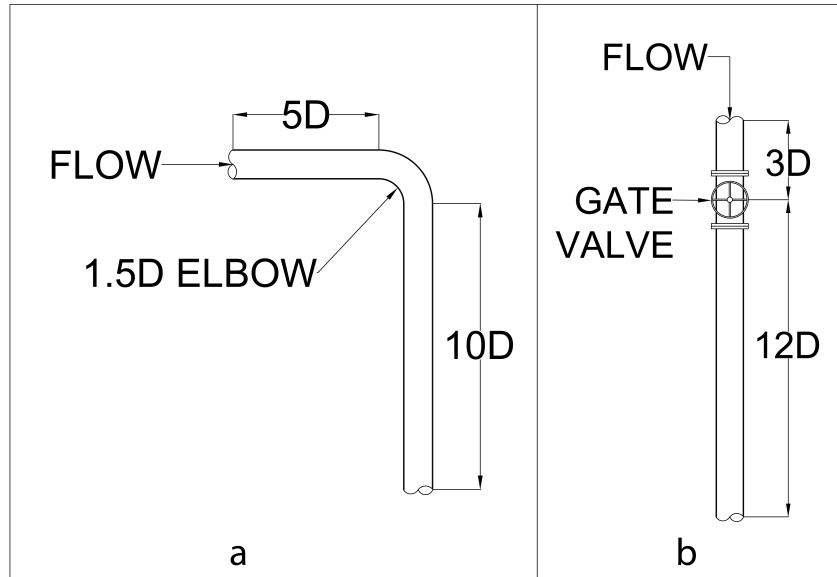
Figure 4.9: Numerical Model Geometry

The second and third simulations were segments of pipe as shown in Figure 4.9 (a) and (b), respectively. The third simulation only included the mean pipeline velocity of 10 fps because there did not appear to be a significant difference between the 2 fps and 10 fps 90-degree elbow simulation. The uncertainty due to the discretized mesh was calculated for each of the simulations following the procedure outlined by Celik et al. (2008). The discretization uncertainty for the 2 fps and 10 fps 90-degree elbow simulations was 0.02% and 0.12%, respectively, while the uncertainty for the 10 fps gate valve 50% open simulation was 0.85%.

The voltage calculations assumed a uniform magnetic field which is often not possible to achieve exactly in practice (The numerical analysis conducted herein indicates that more accurate electrode configurations exist than are currently being manufactured. However, numerical analyses do not replace physical laboratory calibrations and are used here as a means to assert that the optimized meters modeled are worth manufacturer's considerations. Furthermore, as noted by Al-Khazraji (1979), the authors acknowledge electrode fouling

needs to be considered but is beyond the scope of this paper.). The flowmeter voltage was calculated in straight pipe conditions and was used as the reference voltage. The voltage was also calculated for the second and third simulations at different diameters downstream of the installation conditions shown in Figure 4.9. The deviation was determined by subtracting the straight pipe voltage value from the voltage at the ith diameter downstream and dividing by the straight pipe voltage value as shown in Equation 4.6.

$$\%Deviation = \frac{(V_{iD} - V_{straight})}{V_{straight}} \times 100\% \qquad (4.6)$$

This comparison is the numerical equivalent of a flowmeter that received a physical straight pipe laboratory calibration as opposed to an off the shelf meter that has not received a physical straight pipe laboratory calibration. The 0-diameter (0D) location corresponds to the case where the upstream flange of the flowmeter is bolted directly to the downstream flange of the elbow or gate valve. The flowmeter used in this model was 12-inches long, with the electrode plane in the center of the meter. The results for the 90-elbow simulation are shown below in Figures 4.10 and 4.11.
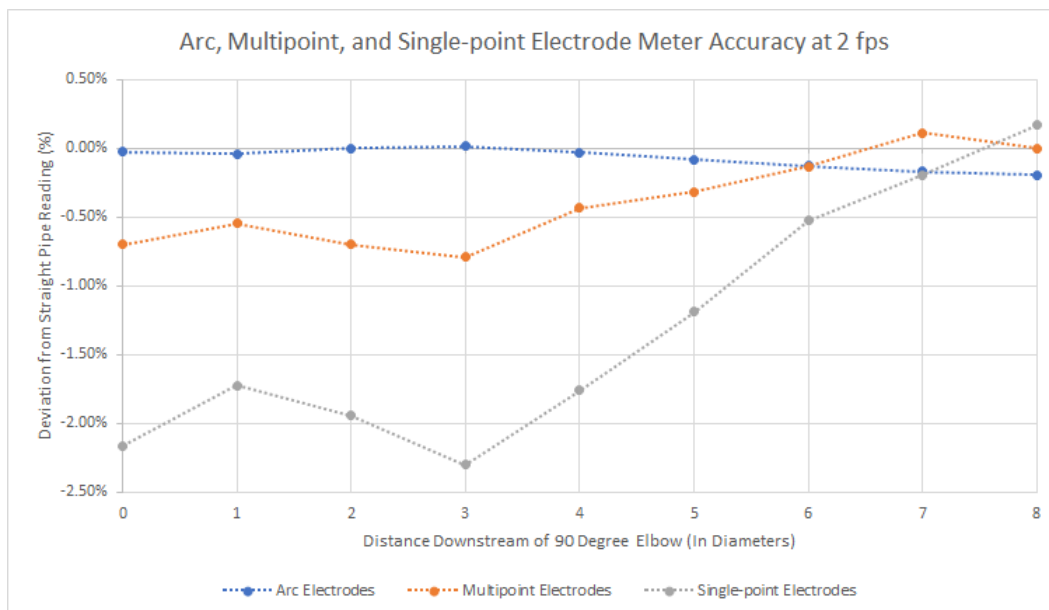
Figure 4.10: Accuracy comparison for arc, multipoint, and single-point electrode configurations downstream of 90-degree elbow at a mean pipe velocity of 2 ft/s
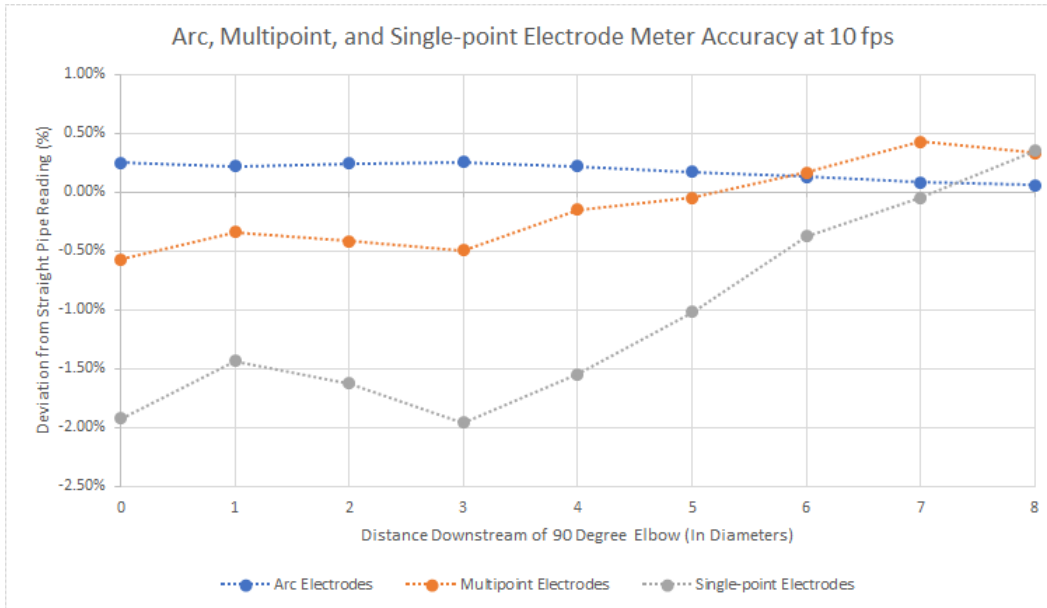
Figure 4.11: Accuracy comparison for arc, multipoint, and single-point electrode configurations downstream of 90-degree elbow at a mean pipe velocity of 10 ft/s

The velocity profile contours at each of the diameters shown on the plot from the 90-degree elbow simulation corresponding to a mean pipeline velocity of 10 fps is shown in Figure 4.12 along with the straight pipe contour, labeled SP, representing the fully developed flow profile.
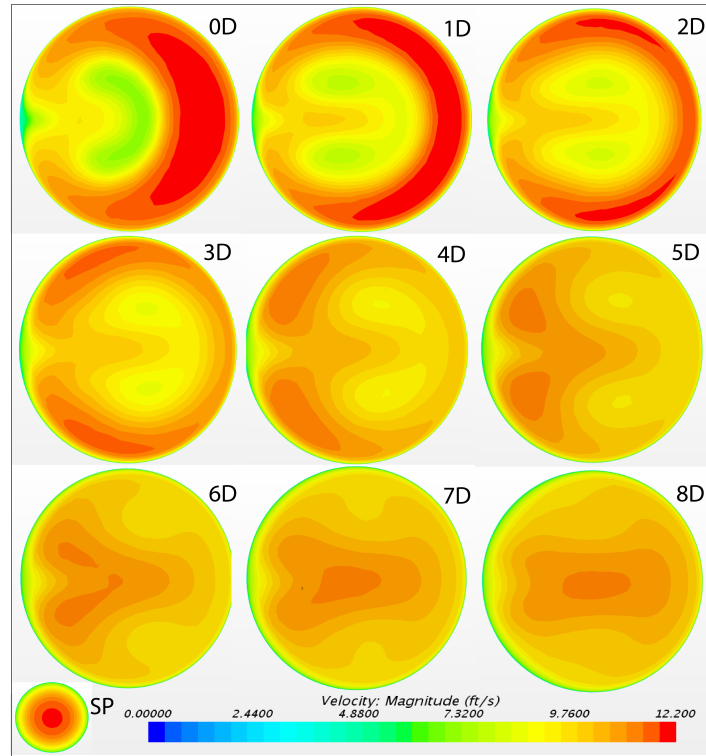
Figure 4.12: Velocity Profile of 10 ft/s Contours Downstream of 90-degree Elbow

The results of the gate valve simulation are shown in Figure 4.13.
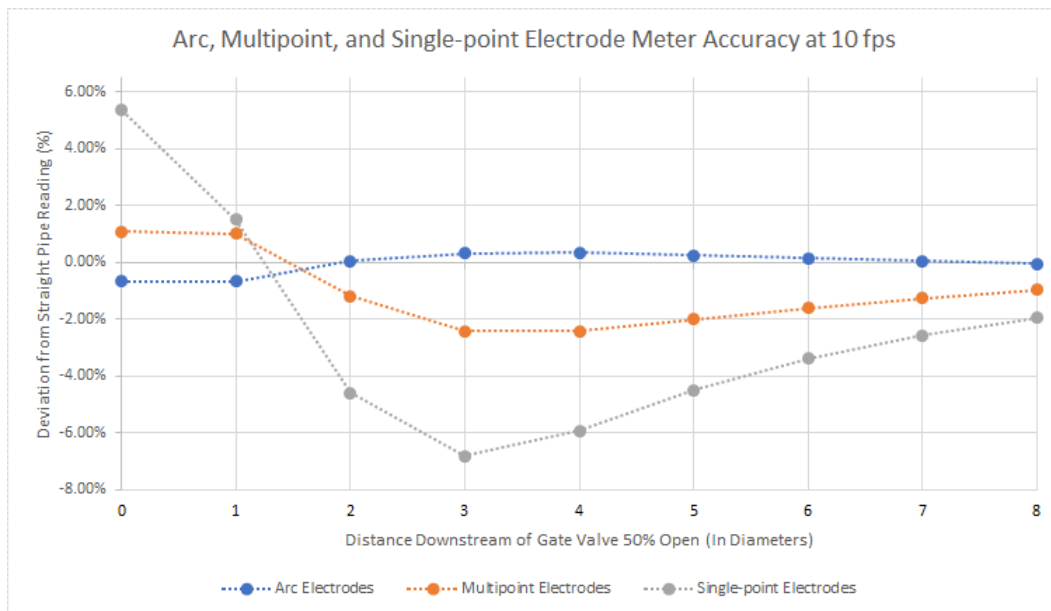
Figure 4.13: Accuracy comparison for arc, multipoint, and single-point electrode configurations downstream of gate valve 50% open at a mean pipe velocity of 10 ft/s

The velocity profile contours for the gate valve (50% open) simulation at each of the diameters shown on the plot in Figure 4.13 corresponding to a mean pipeline velocity of 10 ft/s are shown in Figure 4.14 along with the straight pipe contour, labeled SP, representing the fully developed flow profile.
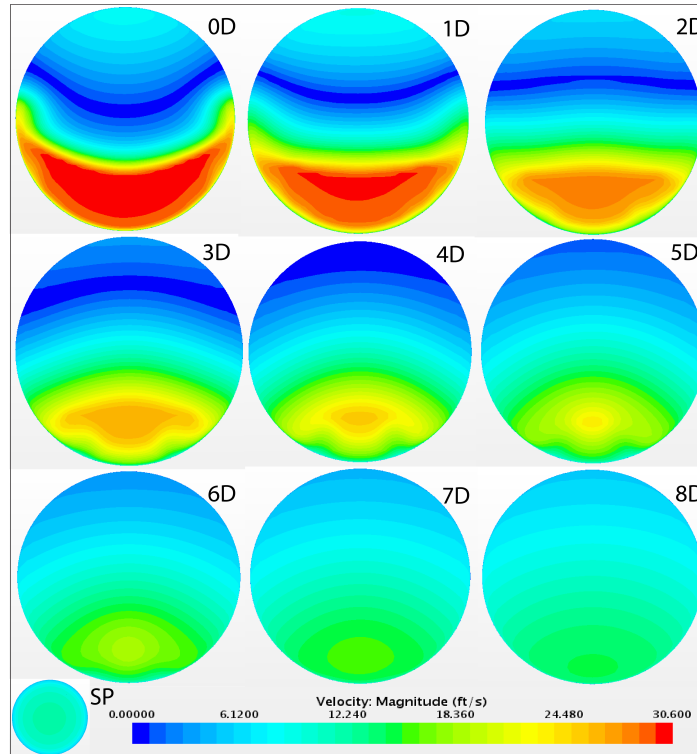
Figure 4.14: Velocity Profile of 10 ft/s Contours Downstream of Gate Valve 50% Open

4.6   Conclusions and Limitations

The authors conclude that the superior performance of the arc electrode magnetic flowmeter immediately downstream (0D) of a 90-degree elbow and a gate valve 50% open is remarkable. Although this research was conducted numerically without laboratory data, it does indicate that the optimized arc electrode magnetic flowmeter is superior to the optimized multipoint and single-point magnetic flowmeters as demonstrated in Figures 4.10, 4.11, and 4.13. It also warrants further exploration of the optimized arc electrode flowmeter in a laboratory setting to determine the effect of necessary components that were beyond

the scope of this paper (e.g., a real non-uniform magnetic field and potential electrode fouling). It is not possible to definitively state that the arc electrode flowmeter will always be "x" times better than the multipoint or single-point electrode because the accuracy of the meter is dependent upon the specific and distinct nature of the distorted velocity profile caused by the installation condition in question. However, the examples presented in this study support the assertion that the arc electrode flowmeter is superior to the multipoint and single-point electrode flowmeter (assuming the magnetic field used in practice follows industry best practices such as those noted by Frenzel et al. (2011)). This superior performance of the arc electrode flowmeter is because the arc electrodes reduce the dispersion of the weight function so much more than the multipoint and single-point electrode weight functions which is readily apparent from a careful review of weight function values presented in Figures 4.4, 4.7, and 4.8.

Another relevant finding is that the accuracy increase from the single-point electrode to the multipoint electrode flowmeter is significant. The gain of accuracy from the multipoint electrode to the arc electrode flowmeter is less significant. However, the deviation of the multipoint flowmeter is still subject to the same oscillatory behavior of the single-point electrode meter, but the magnitude of the deviation is less. In contrast to the multipoint and single-point flowmeter, the arc electrode flowmeter has a much more predictable performance trend and varies less than 0.20% and 1.05% throughout the 90-degree elbow simulations and the gate valve simulations, respectively. Again, this demonstrates the superior performance of the arc electrode flowmeter. As noted earlier, this is not surprising when comparing the values of the weight functions shown in Figures 4.4, 4.7, and 4.8. The arc electrode flowmeter has the most uniform weight function distribution, which renders it less sensitive to distorted velocity profiles than the other two flowmeters.

Although this study is a numerical study, it reinforces the observations made by Beck et al. (2018) that many times the manufacturer's recommendation of 3-5D downstream of 90-elbows is not sufficient to meet the manufacturer's accuracy claims for the meter. Figures 4.10 and 4.11 indicate that at 3-5D downstream, the deviation of the single-point electrode

flowmeter is still outside $\pm 1\%$. Consequently, with single-point electrode flowmeters comprising the majority of magnetic flowmeters available to users, a laboratory calibration is recommended to ensure the expected performance of the flowmeter in adverse installation conditions like those presented herein.

This research demonstrates that the optimized arc electrode flowmeter produces significant performance improvements as compared to the optimized multipoint and single-point electrode flowmeters in adverse installation conditions and ought to be researched further in laboratory settings.

CHAPTER 5

WEIGHT FUNCTION METHOD VERSUS MAGNETOHYDRODYNAMICS
COUPLED WITH NAVIER-STOKES SOLVER: A COMPARATIVE STUDY

5.1 Abstract

The weight function method (WFM) is compared with the magnetohydrodynamics (MHD) coupled solver approach for single-point and multipoint magnetic flowmeters in distorted flows. A review of the literature appears to indicate that researchers who are interested in magnetic flowmeter accuracy and performance either have been unaware of or not capable of analyzing magnetic flowmeters using the WFM. The study also examines whether any differences are apparent between modeling the single-point electrodes and omitting the electrodes from the model. The results of the study indicate differences less than 0.50% between the WFM and the MHD approach. The results also demonstrate that for single-point flowmeters, modeling the electrodes is not necessary. This research eliminates the barrier of deriving a weight function to model magnetic flowmeters.

5.2 Introduction

As of 2017, magnetic flowmeters had more market share of the drinking water distribution and wastewater collection industry than any other flowmeter and their use continues to expand (FlowResearch 2017). Magnetic flowmeters are a type of volumetric flowmeter and when noting the strengths and characteristics of flow measurement devices, the magnetic flowmeter is markedly unique. The measurement technique itself is based on the coupling of two branches of physics: electromagnetism and fluid mechanics, commonly called magnetohydrodynamics (MHD). MHD is the umbrella under which the interaction of electrically conducting fluids and magnetic fields is studied. In contrast to differential pressure flowmeters, Coriolis meters, and turbine meters, magnetic flowmeters do not cause any system

energy losses and can be very accurate and repeatable when installed and calibrated correctly (Beck et al. 2018). When many water systems rely on pumping, this equates directly to a long-term operational saving in pumping costs. Figure 5.1 presents a typical magnetic flowmeter with two diametrically opposed point electrodes located at the springline of the pipe. The magnetic field B_y is in the negative y direction and flow is in the positive z direction (i.e., out of the page).
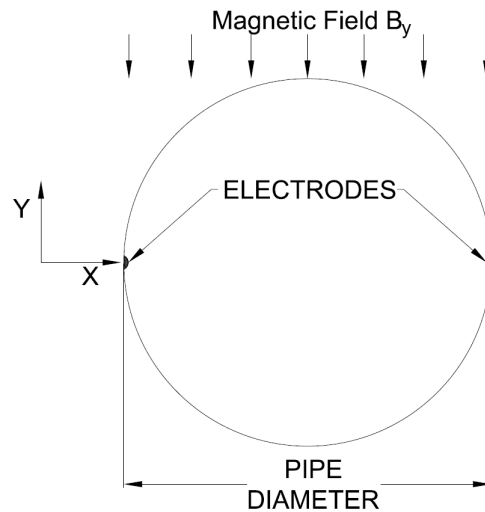
Figure 5.1: Magnetic Flowmeter Schematic

This paper reviews the development of magnetic flowmeter analysis methods and presents the results of a comparative study between the traditional weight function method (WFM) and a coupled MHD solver approach using commercially available software.

5.2.1 The Evolution of Magnetic Flowmeter Analysis Methods

This section describes the evolution of magnetic flowmeter analysis methods and provides the backdrop against which the significance of the present study becomes apparent. The specific articles highlighted in this review do not represent a comprehensive list of all the researchers who have contributed to the field over the years. Rather, the articles discussed herein are intended to highlight studies that show the shift toward a more holistic and cohesive approach to magnetic flowmeter analysis made possible by an aggregated

understanding of previous research and the advancement of computational software.

As the following paragraphs illustrate, researchers were often limited by the available tools and had to make assumptions about the velocity profile, magnetic field, or both when analyzing magnetic flowmeter performance. Furthermore, it is apparent from the literature that other researchers who are very interested in the sensitivity and accuracy of magnetic flowmeters in varied hydraulic conditions either do not appear to be aware of or are incapable of analyzing magnetic flowmeters performance numerically and thus rely on other correlative methods like those described by Martim et al. (2019) and Beck et al. (2019) as a substitute. In some cases, researchers appear to be as comfortable with the fluid mechanics involved in solving the flow field as they are in understanding the computations required to produce a voltage output for the magnetic flowmeter being modeled. However, this appears to be the exception rather than the norm. Thus, the interest in enabling the many researchers interested in the measurement errors that are produced from common magnetic flowmeter installation conditions.

Even research conducted by some magnetic flowmeter manufacturers like SeaMetrics (Peery 2006) appears to indicate a gap between the way manufacturers develop and test magnetic flowmeters and the present capabilities of software when used correctly to model magnetic flowmeter performance. Thus, from both a design and operational perspective, the present study is of significant interest.

The genesis of magnetic flowmeter analysis can be traced back to Shercliff (1954) who was the first to note the sensitivity of magnetic flowmeter performance to the shape of the velocity profile at the cross section of measurement. To predict the influence that a given velocity profile would have on a single-point electrode magnetic flowmeter, Shercliff (1962) proposed a weight function to compensate for the effect of the velocity profile on the output signal of the flowmeter. The weight function is dependent on the shape of the flowmeter and the geometry of the electrodes. For many years the weight function became the standard method of analysis for determining the performance of magnetic flowmeters.

Building upon the work of Shercliff (1962), Bevir (1969) expanded the weight function

to three dimensions using what he called a weight vector. Around the same time, Smyth (1971) derived weight functions using a similar approach and produced a similar weight function to Shercliff (1962). Using the weight function method, Bevir et al. (1981) presented a method for which the performance of a magnetic flowmeter could be predicted based upon constraints on the velocity profile being "rectilinear and axisymmetric" (i.e., no distortion in the flow). Later, O'Sullivan and Wyatt (1983) presented a method employing the weight function that removed the axisymmetric but not the rectilinear flow restriction.

Luntta and Halttunen (1989) used the computer program PHEONICS to model the flow profile for a distorted flow and, using the weight function, computed the expected error for a magnetic flowmeter. Lim and Chung (1998) modeled the flow field and compared the results of the WFM with a solution to the flowmeter equation using the finite volume method (they do not state whether they wrote the code or used a commercial package). They noted that the results of each method were sensitive to the direction and combination of various grid refinements. Wang et al. (2006) created a 3D model for a magnetic flowmeter and employed a numerical weight function based on the work of Shercliff (1962) including a numerical solution of the flow field. Fu et al. (2010) proposed a method for calibrating magnetic flowmeters by coupling the weight function, magnetic field, and velocity profile data using a finite element solver in MatLab. It appears that Lu et al. (2013) was the first to use commercially available software that employed both the magnetohydrodynamic equations and the Navier-Stokes equations to analyze magnetic flowmeters. They concluded that the MHD coupled solver method agreed well with the weight function method for a laminar and turbulent flow in straight pipe conditions without modeling the actual electrodes and the associated solid-fluid interaction. They also evaluated the effect of the Lorentz force on the magnetic flowmeter output for both a laminar and turbulent flow. They concluded that the effect of the Lorentz force was "negligible" for the fluid modeled which had a low electric conductivity. However, unlike this work, Lu et al. (2013) only compared the WFM and MHD for straight pipe conditions and did not evaluate the capability of the MHD method to model alternative electrode configurations (e.g., multipoint electrodes). There

does not appear to be any literature that compares the WFM with the MHD method for flows downstream of distortions or with alternative electrode configurations (e.g., multipoint electrodes).

5.2.2 Objective and Significance

The purpose of this study is to demonstrate the MHD coupled solver approach and the traditional WFM produce similar results. The significance of this research is that it demonstrates the capabilities of multiphysics solvers when used correctly to model the primary elements of a magnetic flowmeter holistically thereby eliminating the need for the weight function.

5.3 Magnetohydrodynamic (MHD) Fundamentals

This section reviews the fundamental equations of MHD which govern the analysis of magnetic flowmeters. The solution to the governing flowmeter equation by means of the WFM and the MHD coupled solver method, respectively, is addressed. The Reynolds Magnetic Number (Re_{mag}) is introduced in the concluding portion of the section.

The MHD equations describe the interaction between magnetic fields and electrically conducting fluids. Ohm's law for the case when a conducting fluid passes through a magnetic field is given by

$$\mathbf{J} = \sigma(\mathbf{E} + \mathbf{v} \times \mathbf{B}), \tag{5.1}$$

where $\mathbf{J}$ is the current density vector, σ the fluid conductivity, $\mathbf{E}$ is the electric field, $\mathbf{v}$ is the fluid velocity vector, and $\mathbf{B}$ is the magnetic field (Hughes and Young 1966). $\mathbf{E}$ can be substituted with $-\nabla U$, where U is the electric potential and because of conservation of charge the induced electric current within the meter satisfies Equation 5.2

$$\nabla \cdot \mathbf{J} = 0. \tag{5.2}$$

Using the identity that $\nabla \cdot (\nabla U) = \nabla^2 U$ and assuming isotropic conductivity Equation 5.1 can be rearranged as,

$$\nabla^2 U = \nabla \cdot (\mathbf{v} \times \mathbf{B}) \tag{5.3}$$

which is commonly called the flowmeter equation (Shercliff 1962).

At the time of Shercliff, it appears that numerical computational methods were not robust enough to solve the flowmeter equation directly. Consequently, Shercliff proposed the weight function as an alternative method of solution to the flowmeter equation. The process for deriving the weight function as presented by Bevir (1969) is summarized in what follows. Let G be a potential function that satisfies Laplace's equation (Equation 5.4) and has boundary conditions of a positive and negative unit voltage on opposing electrodes as shown in Equation 5.5 (Bevir 1969).

$$\nabla^2 G = 0. \tag{5.4}$$

$$\frac{\partial G}{\partial r}\bigg|_{r=R} = \begin{cases} \text{right electrode} = 1 \\ \text{left electrode} = -1 \\ \text{otherwise} = 0 \end{cases} \tag{5.5}$$

The weight function is obtained by taking the gradient of G perpendicular to the flow direction (z) and the magnetic field (negative y)

$$\nabla G = j_x, \tag{5.6}$$

where j_x represents the values of the weight function at each point in the flowmeter. Using the weight function method, the flowmeter signal is found by solving Equation 5.7

$$\Delta U = \int_\Omega v_z j_x B_y d\Omega, \tag{5.7}$$

where ΔU is the voltage difference between the electrodes, v_z is the velocity profile in the pipe, j_x is the weight function, B_y is the y-component of the magnetic field in the meter, and Ω is the measuring volume or plane for a 3D or 2D analysis, respectively (Bevir 1969).

The solution to Equation 5.7 requires the derivation of the weight function of the flowmeter and a knowledge of the magnetic field and velocity data at each grid of the domain. Thus, it often requires writing one's own post-processing code to solve Equation 5.7, which can be extensive effort beyond that of solving the flow field of interest. Hence, it is desirable to eliminate any unnecessary steps in the process without compromising the fidelity of the magnetic flowmeter analysis.

In contrast to the WFM, many commercial multiphysics solvers have the capability to solve the flowmeter equation directly without the need for the weight function. For example, the commercial software Simcenter STAR CCM+, which is used in this study, solves for the voltage by discretizing an integral form of Equation 5.3 over the entire domain using the finite volume method (SIEMENS 2021). The ability to solve Equation 5.7 directly is a significant advantage when considering the time savings and flexibility of a comprehensive solver.

Another important concept to introduce is the Reynolds Magnetic Number (Re_{mag}) which is a dimensionless number that relates the ratio of the induced and prescribed magnetic flux densities and is defined as,

$$Re_{mag} = \mu_0 \sigma U L \tag{5.8}$$

where μ_0 is the permeability constant, σ is the electric conductivity of the fluid, U is the characteristic flow velocity in the pipe, and L is the diameter of the pipe (SIEMENS 2021). For low Re_{mag} values, the induced magnetic flux densities are negligible. Due to the low electrical conductivity of water, the present study falls in the low Re_{mag} regime.

5.4 Methodology

This section presents the process employed for deriving the weight functions that were used in the analyses, reviews the process of grid generation to determine the uncertainty due to discretization, outlines the project scope, and explains the assumptions and limitations of the study.

5.4.1 Weight Function Derivations

The weight functions for the single-point and multipoint electrodes were produced using the Partial Differential Equation (PDE) Toolbox in MatLab. A potential function G is found using the boundary conditions described in Equation 5.5. The weight function for the flowmeter is obtained by employing Equation 5.6. The weight functions corresponding to the single-point and multipoint (2 diametrically opposed pairs of 3 electrodes with 25-degrees between electrodes) flowmeters are shown in Figures 5.2 and 5.3. Several contour lines are shown in black with white labels indicating the value of the weight function.
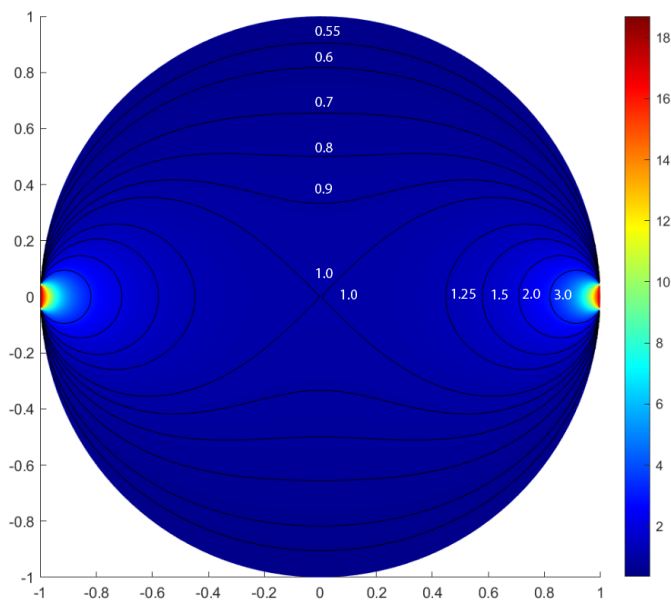
Figure 5.2: Weight Function of Single-point Electrode Flowmeter
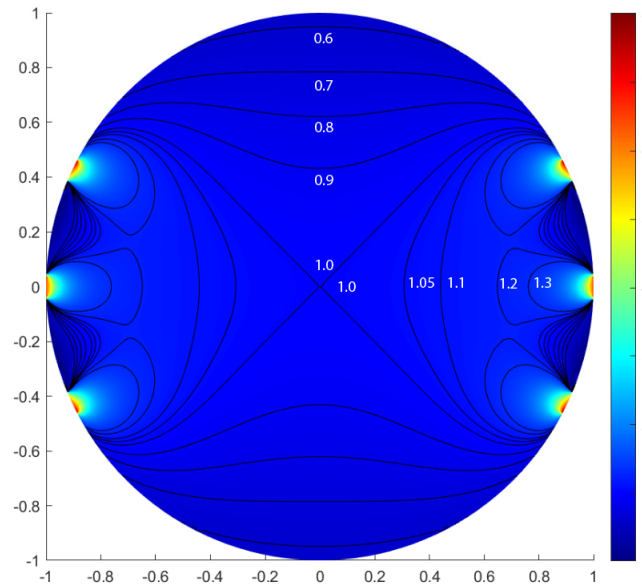
Figure 5.3: Weight Function of Multipoint Electrode Flowmeter

5.4.2 Study Scope

This section describes the simulated geometry, numerical modeling setup, and the type of magnetic flowmeters modeled. A 6-inch 90-degree long radius (1.5D) elbow was used as the flow disturbance for the study (see Figure 5.4). The software used to conduct the numerical modeling was Simcenter STAR CCM+ version 13.06.012. The flow was modeled as a constant density fluid with the Reynolds-averaged Navier-Stokes (RANS) equations, segregated flow solver, $\kappa - \epsilon$ turbulence model, and the two layer all y+ wall treatment. The electromagnetism model, electrodynamic potential model, and one-way coupled MHD solvers were not activated until the flow field reached convergence (i.e., residuals were below 1e-04 or the velocity field was unchanging with iterations). Four flowrates were simulated corresponding to mean pipeline velocities of 2, 6, 10, and 15 feet-per-second (ft/s). Fully developed flow profiles for each flowrate were created by prescribing a periodic boundary condition on a pipe segment and letting the simulation iterate until the velocity profiles were no longer changing as iterations increased. These fully developed profiles were used as the inlet boundary conditions for simulations in straight pipe and the geometry shown in

Figure 5.4. Both single-point and multipoint electrode configurations were modeled in both straight pipe and downstream of the elbow. The straight pipe simulations for each of the four flowrates were used as the reference datum for the corresponding flowrates downstream of the elbow. For the single-point electrode MHD simulations, electrodes were modeled to determine if there were any differences in the voltage output between the electrode reading and the voltage in the fluid cell nearest to the electrode at the pipe wall.
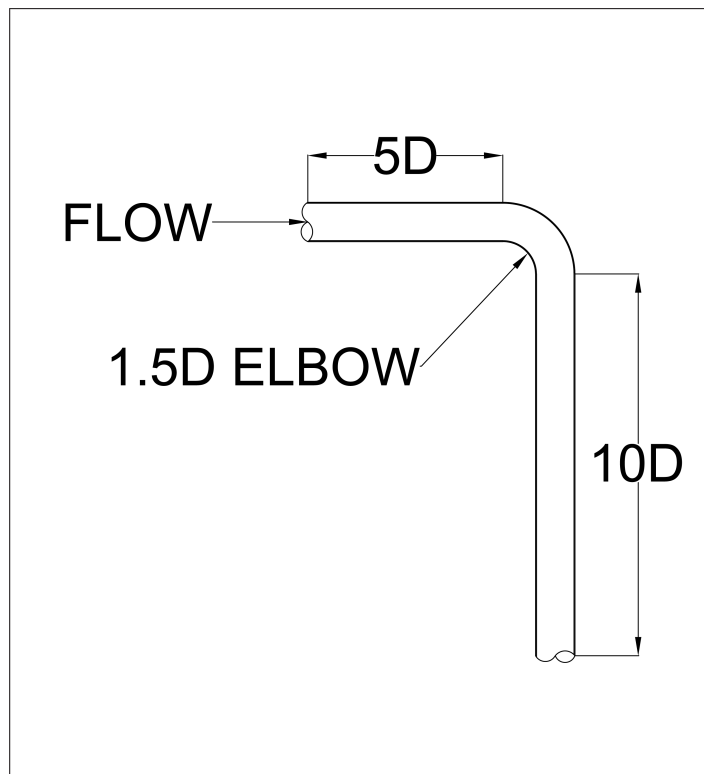
Figure 5.4: Numerical Model Geometry

5.4.3 Grid Generation

The polyhedral mesher and prism layer meshers were used to mesh the fluid domain. In order to produce consistent results, the prism layer thickness was held constant throughout the viscous boundary layer (i.e. prism layer stretching was equal to one) which produced wall y+ values that were in the high y+ range, yet were still in compliance with STAR CCM+'s wall y+ guidelines. Although this mesh may not be the best hydraulic mesh, the

purpose of the study was to test the relative differences between the WFM and the MHD coupled approach.

The process for determining the uncertainties due to the mesh as described by Celik et al. (2008) was followed. The same mesh was used for all simulations; therefore, grid convergence tests were only conducted on the highest and lowest flowrates for both single-point and multipoint simulations. The 15 ft/s single-point and multipoint uncertainty due to the mesh was 0.02% and 0.40%, respectively, while the 2 ft/s single-point and multipoint uncertainties were 0.06% and 0.12%, respectively.

For the single-point and multipoint WFM analysis, the number of cells in the mesh created in the PDE Toolbox in MatLab was more than doubled and the results changed less than 0.01% and 0.06%, respectively.

5.4.4 Assumptions and Intent

By design, it is the intent of the authors to isolate the WFM and the MHD coupled solver method to compare the relative differences between the two methods. Consequently, the exact same velocity profiles at the exact same locations were used as inputs for the WFM results, thereby eliminating any dependence on the velocity profile. Thus, the results are all comparable because they have the same velocity profile and magnetic field data and only the differences in the voltage calculations are apparent. Furthermore, the analysis assumed a uniform magnetic field which is not possible in practice but was used in this study for a comparison of relative differences.

5.5 Results and Practical Applications

The results are presented in terms of deviation from the straight pipe voltage. The deviation was determined by subtracting the straight pipe voltage value from the voltage at the *ith* diameter downstream and dividing by the straight pipe voltage value as shown in Equation 5.9.

$$\%Deviation = \frac{(V_{iD} - V_{straight})}{V_{straight}} \times 100\% \qquad (5.9)$$

It was assumed that the length of a 6-inch flowmeter is 12-inches with the electrodes located at the center of the flowmeter. The 0D location represents the minimum physical distance possible between the electrodes and the elbow, in which the downstream flange of the elbow is bolted to the upstream flange of the flowmeter. The voltage was calculated for each simulation from 0 to 8 diameters downstream of the elbow as shown in Figure 5.4. Figures 5.5-5.8 present the single-point flowmeter data with deviation and distance on the y-axis and x-axis, respectively. For each of these four figures, there are three data sets. The WFM dataset represents the deviation in flowmeter reading calculated by the weight function method as explained in this study. The MHD (no electrode) dataset represents the deviation in flowmeter reading that was determined using the voltage from the grid cell nearest to the electrode. The MHD (electrode) data set represents the deviation in flowmeter reading obtained from numerically modeling the single-point electrodes and the associated solid-fluid interaction.
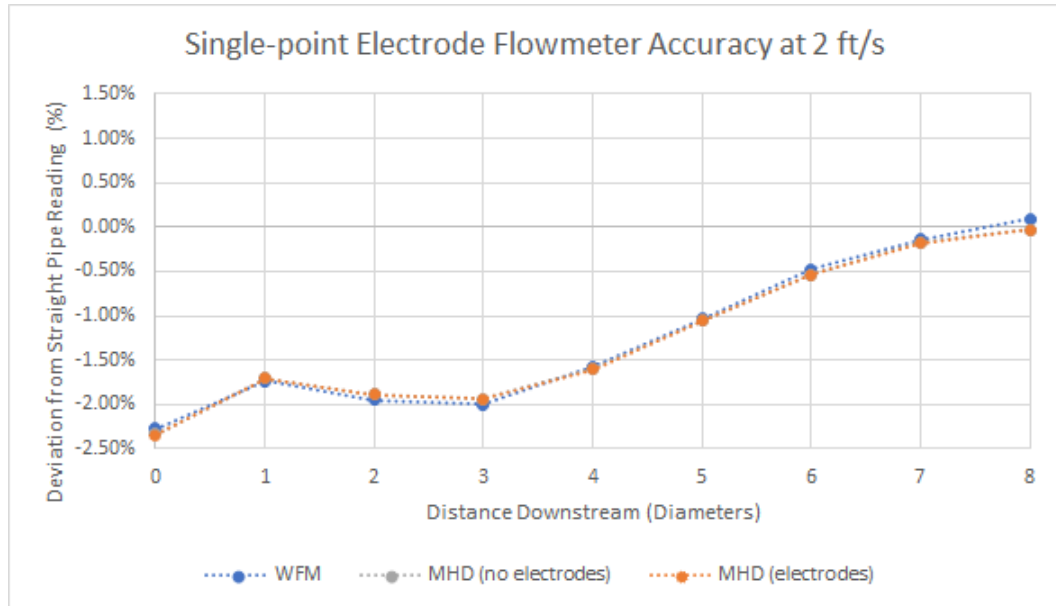
Figure 5.5: WFM vs MHD Single-point Electrode Flowmeter Accuracy Downstream of a Long-Radius Elbow Mean Pipeline Velocity of 2 ft/s
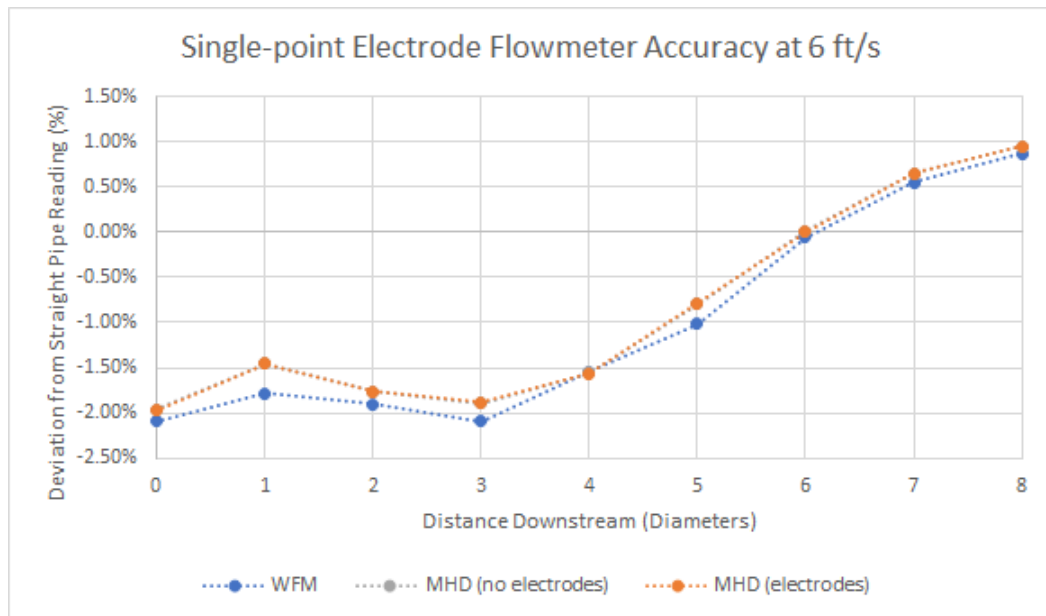
Figure 5.6: WFM vs MHD Single-point Electrode Flowmeter Accuracy Downstream of a Long-Radius Elbow Mean Pipeline Velocity of 6 ft/s
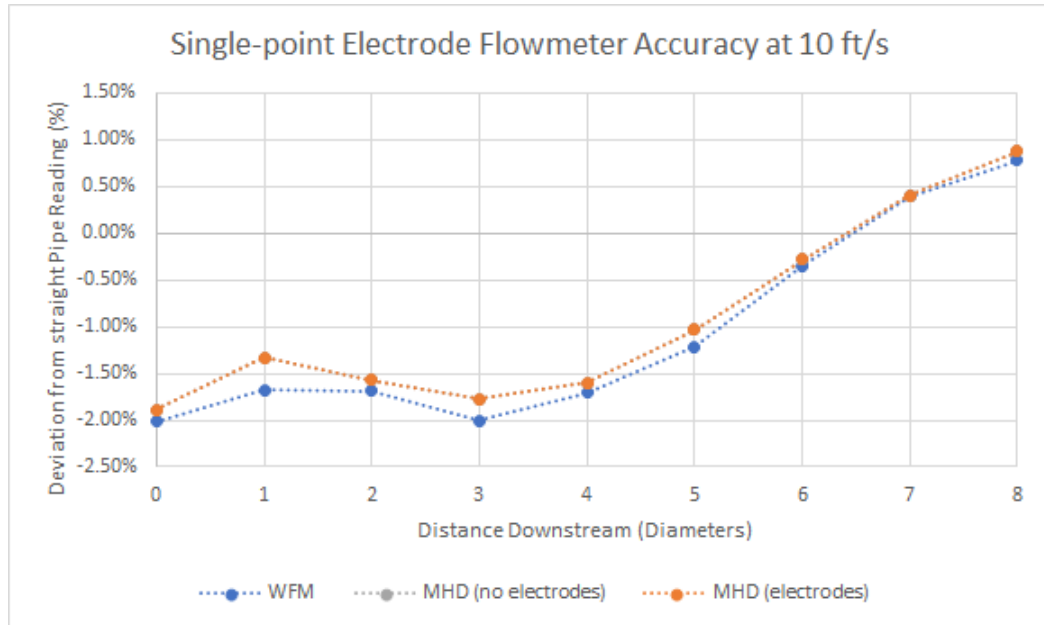
Figure 5.7: WFM vs MHD Single-point Electrode Flowmeter Accuracy Downstream of a Long-Radius Elbow Mean Pipeline Velocity of 10 ft/s
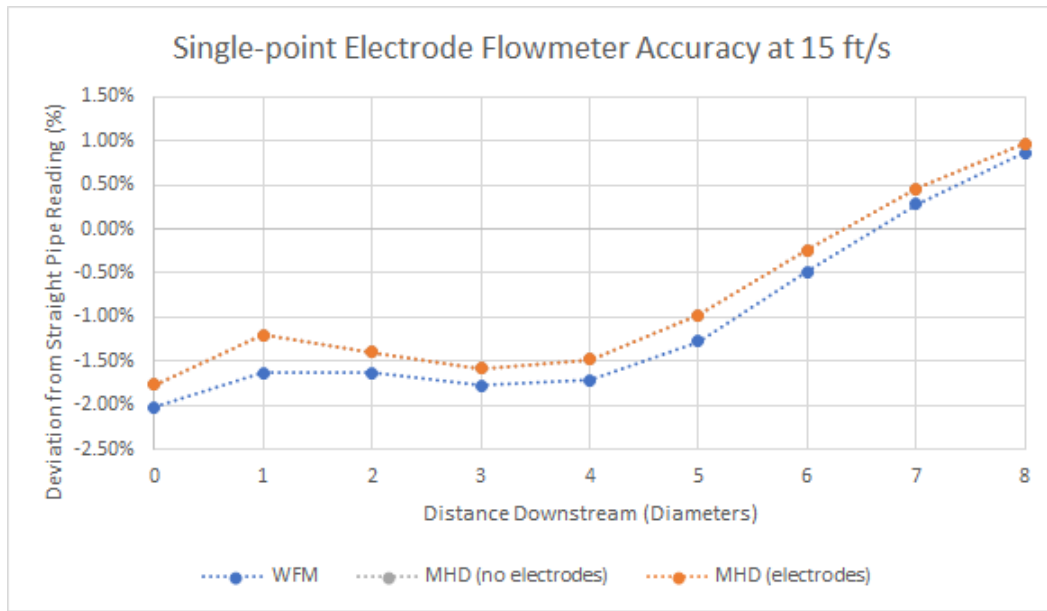
Figure 5.8: WFM vs MHD Single-point Electrode Flowmeter Accuracy Downstream of a Long-Radius Elbow Mean Pipeline Velocity of 15 ft/s

Figures 5.9-5.12 present the multipoint flowmeter data with deviation and distance on the y-axis and x-axis, respectively. For each of these four figures, the two data sets represented are the WFM and the MHD approach which required modeling the multipoint electrode configuration.
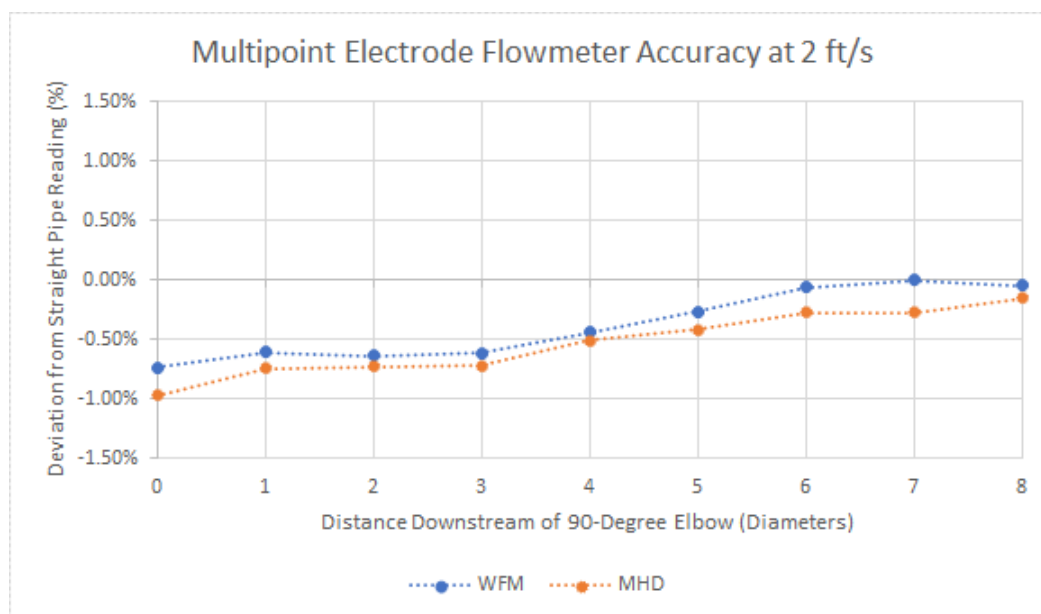
Figure 5.9: WFM vs MHD Single-point Electrode Flowmeter Accuracy Downstream of a Long-Radius Elbow Mean Pipeline Velocity of 2 ft/s
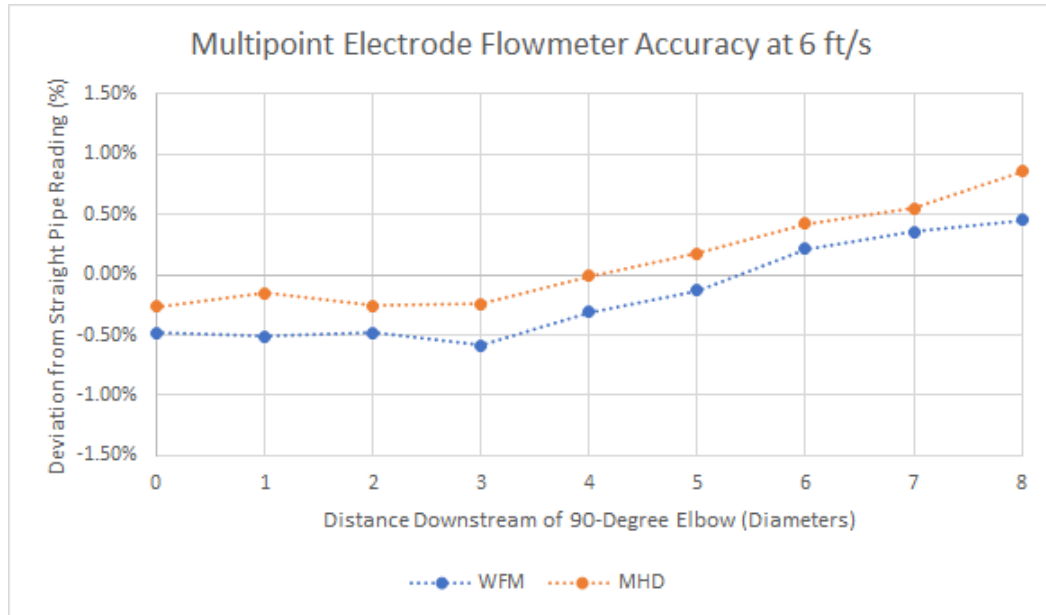
Figure 5.10: WFM vs MHD Single-point Electrode Flowmeter Accuracy Downstream of a Long-Radius Elbow Mean Pipeline Velocity of 6 ft/s
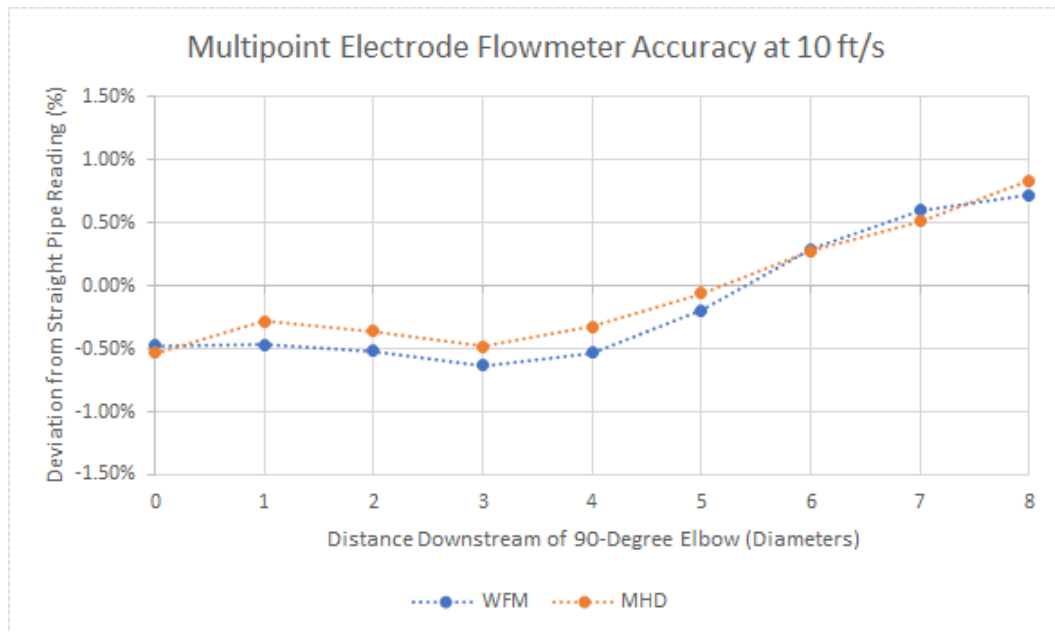
Figure 5.11: WFM vs MHD Single-point Electrode Flowmeter Accuracy Downstream of a Long-Radius Elbow Mean Pipeline Velocity of 10 ft/s
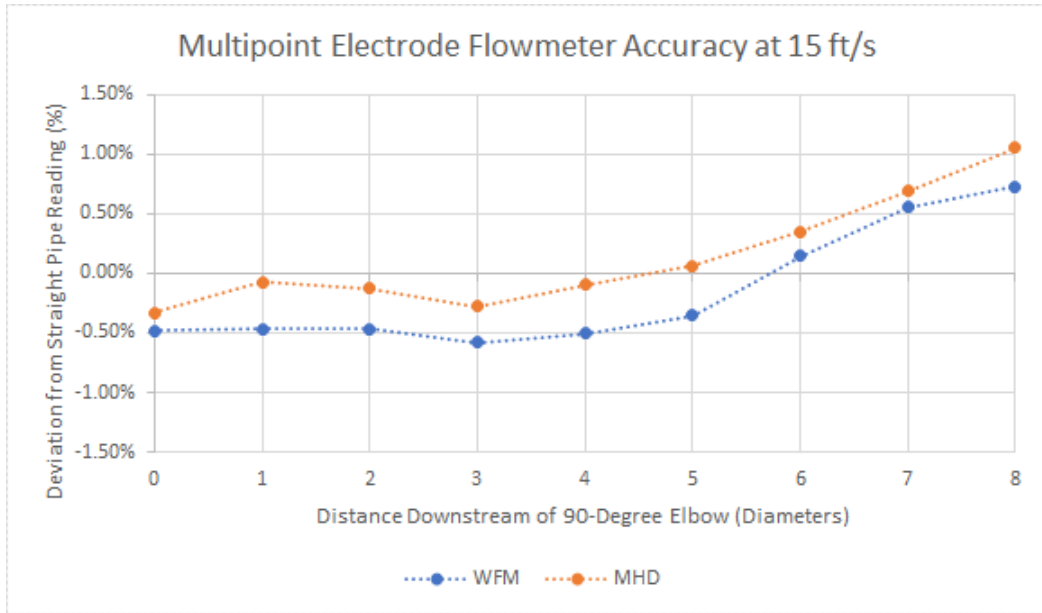
Figure 5.12: WFM vs MHD Single-point Electrode Flowmeter Accuracy Downstream of a Long-Radius Elbow Mean Pipeline Velocity of 15 ft/s

Figure 5.13 presents the data with deviation on the y-axis and flowrate on the x-axis, respectively.
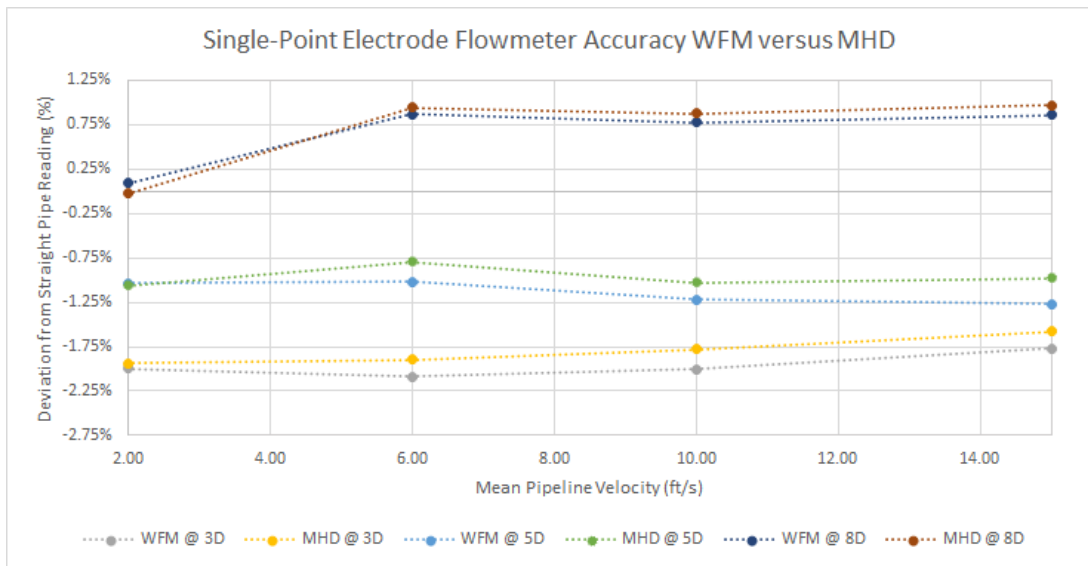
Figure 5.13: WFM vs MHD Single-point Electrode Flowmeter Accuracy at 3D, 5D, and 8D Downstream of a Long-Radius Elbow Mean Pipeline Velocities of 2, 6, 10, and 15 ft/s

Table 5.1 presents the mean, maximum, and minimum deviations between the MHD coupled solver approach and WFM for the single-point and multipoint flowmeter results shown in Figures 5.5-5.12.

Table 5.1: Deviation Between MHD and WFM for the Single-point and Multipoint Flowmeter

Single-point Electrode				
	2 (ft/s)	**6 (ft/s)**	**10 (ft/s)**	**15 (ft/s)**
Mean	0.05%	0.14%	0.14%	0.24%
Max	0.12%	0.33%	0.35%	0.43%
Min	0.02%	0.02%	0.02%	0.10%
Multipoint Electrode				
	2 (ft/s)	**6 (ft/s)**	**10 (ft/s)**	**15 (ft/s)**
Mean	0.15%	0.28%	0.12%	0.30%
Max	0.27%	0.40%	0.20%	0.42%
Min	0.07%	0.19%	0.01%	0.13%

The maximum variation between the MHD (no electrode) and MHD (electrode) results shown in Figures 5.5-5.8 is 0.01%. This indicates that the voltage reading extracted from the modeled electrodes and the voltage in the fluid cell nearest to the electrode provides essentially the same answer, thus indicating no benefit to modeling single-point electrodes. The largest deviation in the single-point electrode data set between the WFM and the MHD approach is 0.43%.

The deviations shown in Figures 5.9-5.12 vary more than the single-point electrode data set from diameter to diameter for both the MHD and WFM. The largest deviation between the WFM and the MHD approach is 0.42% for the multipoint electrode data sets. Figure 5.13 demonstrates that there is very little change in deviation at the same location downstream of the elbow for increasing flowrates which matches what is often seen

in laboratory settings.

5.6   Conclusions and Considerations

The authors conclude that the WFM and the MHD coupled solver approach appear to agree well with each other. The study demonstrates the validity of the MHD coupled solver approach to reproduce similar results as the WFM downstream of disturbances and for alternative electrode configurations like the multipoint flowmeter modeled herein. This is significant as allows researchers who are interested in magnetic flowmeter performance to analyze magnetic flowmeters without deriving the weight function on their own. For some researchers, this will simplify the analysis process and add greater flexibility.

Another noteworthy conclusion of the study is that when evaluating single-point electrode flowmeters using the MHD coupled approach, one does not even need to take the time to model the actual electrodes and set up the solid fluid interaction as the data shows essentially the same results when using the voltage from the cell nearest the electrode on the pipe wall. As most magnetic flowmeters in use today are single-point electrodes this is a significant time savings from a numerical modeling perspective.

It would be an erroneous use of this data to assume that any magnetic flowmeter will respond in accordance with the data presented in this study. Magnetic flowmeters have a distinct separation between the primary and secondary metering elements. The primary elements consist of the electrodes and the magnetic field. The secondary elements include proprietary things such as the sampling rate and algorithm, signal amplification and post-processing of the signal etc. This numerical study is analogous to measuring only the raw voltage of a magnetic flowmeter and therefore does not account for the other parameters mentioned above. Furthermore, no laboratory data was taken to validate the absolute values of the deviations shown in the data as the intent of the study was focused only on the relative differences between the two methods. Thus, it appears that physical laboratory magnetic flowmeter calibrations are required to determine the exact response of a magnetic flowmeter to adverse installation conditions.

This research demonstrates that using coupled MHD and Navier-Stokes equations available in a commercial solver for magnetic flowmeter analysis offers greater flexibility, eliminates post-processing computations to provide the flowmeter signal, and provides a cohesive and holistic analysis. This research eliminates what appears to have been a significant barrier to other researchers interested in magnetic flowmeter analysis by demonstrating an alternative method that produces similar results as the WFM for magnetic flowmeter analysis.

CHAPTER 6

THE EFFECT OF HIGHER FIDELITY FLOW FIELD MODELS ON MAGNETIC
FLOWMETER ANALYSIS

6.1 Abstract

The current research is unclear regarding the sensitivity of the output of a magnetic flowmeter analysis to the fidelity of the simulated flow field. This study evaluates the effects of higher fidelity models on magnetic flowmeter analysis. An eddy viscosity model, second-moment closure model, and a Large-Eddy simulation were compared to laboratory velocity profile data 0.67D downstream of a 1.58D elbow at a Reynolds number of 34,000. The Large-Eddy simulation results matched the laboratory velocity profile data best. The authors conclude that the fidelity of the flow field model does cause differences in the analysis of the flowmeter voltage output.

6.2 Introduction

Accurate flow measurement continues to be a critical component in many sectors of the economy. However, the forces that have driven innovations and improvements to flow measurement devices vary from sector to sector. For example, custody transfer standards drove much of the research surrounding orifice plates and their use as flow measurement devices for the oil and gas industry (Beck et al. 2019). In contrast, water scarcity continues to be the driving force behind improving flow measurement in the drinking water and wastewater sectors. AWWA has stated, "No tool available to water [managers] has played a greater part in the conservation of water than the water meter" (AWWA 2002). According to The World Market for Magnetic Flowmeters, magnetic flowmeters have more market share of the drinking water distribution and wastewater collection industry than any other flowmeter and their use continues to increase (FlowResearch 2017). Magnetic flowmeters

employ electromagnetic induction to correlate the voltage output of the flowmeter with the volumetric flowrate. Generally, these flowmeters do not cause any system energy losses and can be very accurate when calibrated and installed properly (Beck et al. 2018). A typical magnetic flowmeter has two diametrically opposed point electrodes located at the springline of the pipe with the magnetic field B_y in the negative y direction and flow is in the positive z direction (i.e., out of the page) as shown in Figure 6.1.
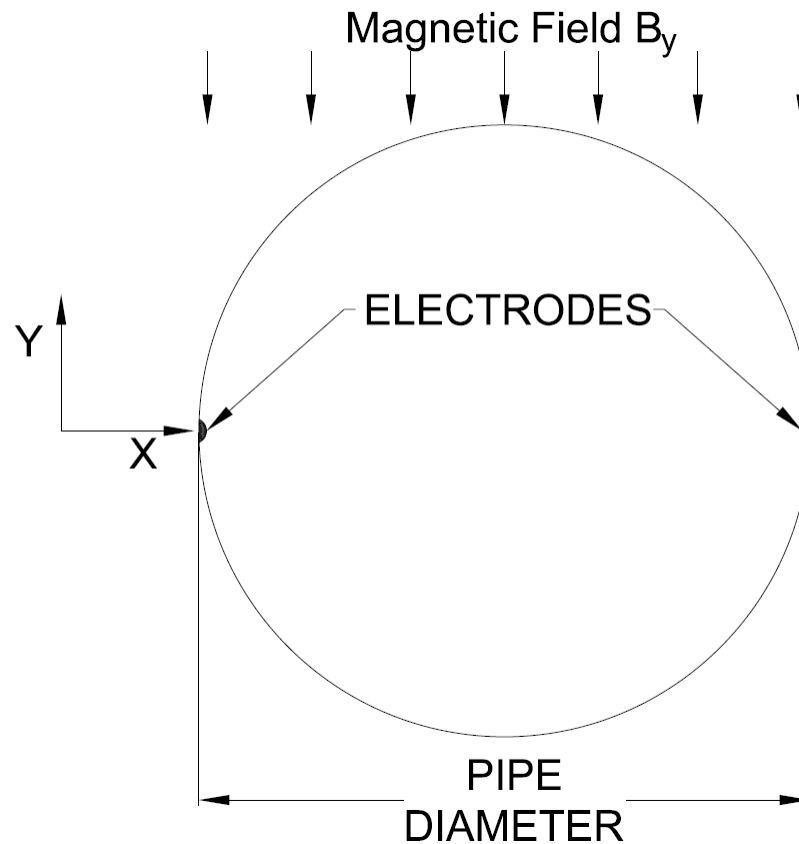
Figure 6.1: Magnetic Flowmeter Schematic

Magnetic flowmeters are often installed in conditions where there is little to no straight pipe upstream of the flowmeter. Fittings such as tees, valves, and elbows etc. distort the flow profile at the cross section of measurement. Without long lengths of straight pipe to produce an axisymmetric flow profile, the magnetic flowmeter accuracy is susceptible to these distortions as Shercliff (1954) noted. Shercliff (1962) introduced the weight function

as a means of predicting the effect of the velocity profile at each point in the flowmeter and its contribution to the voltage output. Using the weight function as the primary method of magnetic flowmeter analysis, many researchers have explored ways to improve the performance of magnetic flowmeters. These methods can be broadly grouped into four categories: changing the electrode geometry to improve the weight function, optimizing the magnetic field, improving the flow profile by using a device like a flow conditioner, and improving the secondary elements such as signal amplification and post processing. Consequently, a large majority of the magnetic flowmeter analysis research has been focused on aspects of the meter itself (e.g., electrodes and magnetic field) and not on the flow field. Thus, very few researchers have even included the flow field in their research.

A limited number of studies have incorporated an evaluation of the flow field to varying degrees of complexity. At the most basic level, some researchers like Al-Khazraji (1979) and Bevir (1969) employed velocity log laws for straight pipe turbulent flow in their analyses. Luntta and Halttunen (1989) employed the numerical code Phoenics to analyze a magnetic flowmeter in a distorted flow condition. Later, Lim and Chung (1999) evaluated the flowmeter signal with laminar flow because "the numerical solution of [turbulent flows] depends strongly on the model adopted, [and] it is almost impossible to distinguish the true installation effects from erroneous results due to the inadequate turbulence model." In a study conducted by Fu et al. (2010), the velocity profile was modeled in an attempt to validate an approach to dry calibrating magnetic flowmeters. However, the authors do not state how they solved the flow field other than stating they solved the Navier-Stokes equations, and they acknowledge that the uncertainty of the flow field is a significant factor in fluid mechanics and higher fidelity models. Furthermore, all of the testing was conducted using a reference flowmeter. The upstream piping of reference flowmeters could introduce additional errors if they not calibrated properly and thus leave some questions as to the absolute errors associated with Fu et al.'s work. Later, Cao et al. (2014) optimized the magnetic field to reduce the effect of a distorted velocity profile on the flowmeter output using the commercial CFD solver FLUENT. Cao et al. (2014) did not state which turbu-

lence model was employed for the numerical modeling as it appears the focus was on the relative difference of between the unoptimized and optimized magnetic fields. In a similar way, Beck et al. (2021) also included the flow field using the Reynolds-average Navier-Stokes (RANS) equations with the κ-ϵ turbulence model as they were only evaluating the relative differences. In another magnetic flowmeter analysis study Lu et al. (2013) used the κ-ϵ turbulence model in COMSOL to model the flow field in straight pipe conditions. Simão et al. (2018) used the κ-ϵ turbulence model and COMSOL as well and acknowledged the tradeoff between higher fidelity models and the associated computation cost increases accompanying those models. Other researchers have long explored the deficiencies of RANS models compared to higher fidelity models in distorted flow conditions like those downstream of an elbow. In a study conducted by Kumar et al. (2014), the recovery of flow downstream of a 90-degree elbow was evaluated using Simcenter STAR CCM+ and the flow field was solved using a large-eddy simulation (LES), Reynolds Stress Model (RSM), κ-ϵ, and what appears to be a variation of the κ-Ω model called the Shear Stress Transport (SST). They conducted the simulations at a Reynolds number of 20,000 and compared to particle image velocimetry (PIV) data obtained by Kalpakli and Örlü (2013) at a Reynolds number of 20,000. They noted that the SST model matched the laboratory data the worst. They also noted that the κ-ϵ predicts slower decay of disturbances. In a review of turbulent flow in curved pipes, Vester et al. (2016) noted that RANS models struggle to predict the flow accurately due to "the anisotropic nature of turbulence [and] the secondary motion imposed by the curvature." However, it is unclear how much this apparent limitation of RANS models influences the flowmeter output.

6.2.1 Objective and Significance

In contrast to the research mentioned above, the objective of this research is to explore and evaluate the effect of higher fidelity computational fluid dynamic (CFD) turbulent models on the output signal of a magnetic flowmeter in a distorted turbulent flow downstream of a 90-degree elbow. As far as the authors are aware, there is no existing research evaluating the voltage output of a magnetic flowmeter using a large-eddy simulation (LES).

6.3   Methodology

This section describes the computational methodology employed for the numerical study. An overview of computational fluid dynamics is provided and the way various solvers approach resolving the flow field is reviewed. The discretization process is also discussed, and the study scope is presented.

6.3.1   Modeling Turbulent Flows

CFD employs numerical methods to solve the Navier-Stokes equations which describe the flow of fluid. For laminar flows, analytical solutions exist. However, for turbulent flows, analytical treatment becomes impossible. Modeling flow fields has a tradeoff between the cost to run the model and the associated accuracy of the model. For example, the most basic methods for modeling turbulent flows are called one-equation or eddy viscosity models. These include the K-Omega and K-Epsilon models and have the least computational demand, thus are employed widely in industry. Another group of models are called second moment closure models. These include the Reynolds stress model which solves for the generation of turbulent kinetic energy in the flow field by solving the symmetric Reynolds stress tensor. These models are generally viewed as a higher fidelity model as the generation of turbulence is physically based. However, the Reynolds Stress Model solves for the six additional unknowns of the Symmetric Reynolds stress tensor and is thus more computationally expensive than the one-equation models mentioned above (There are many sources available explaining the strengths and weaknesses of various turbulence models. As an example, the reader is referred to Launder et al. (2002) Chapters 1 and 2 for more information regarding eddy viscosity and second moment closure models). For large-eddy simulations, STAR CCM+ solves the Navier-Stokes using a spatial filtering process and account for the unsteady nature inherent in turbulent flows (SIEMENS 2021). In contrast to LES, the eddy viscosity models and the second moment closure models are solved using the Reynolds-averaged Navier-Stokes equations because they do not account for the unsteady nature of turbulent flows and are only an attempt to capture the mean flow field statistics. According to El Khoury et al. (2013), Reynolds numbers in the range of 34,000 are considered mod-

erately high Reynolds numbers for LES modeling due to the constraints imposed by the length scales of the turbulent flows and the Courant-Friedrichs-Lewy stability condition on the time-step (Deville et al. 2002).

6.3.2   Study Scope

The simulations completed as part of the study scope are summarized in Table 6.1. Four flowrates corresponding to mean pipeline velocities with units of feet-per-second (ft/s) are listed in the far-left column. The remaining columns indicate the turbulence models employed to solve the flow field, the radius of curvature of the 90-degree elbow (1.58D or 1.5D), and the distance downstream of the elbow for which numerical data was extracted.

Table 6.1: Test Matrix Summary

Test Matrix Summary					
	LES	**RSM**	**K-Epsilon**	**90-Degree Elbow**	**Distance Downstream of Elbow**
0.645 (ft/s)	x	x	x	1.58D	10D
2 (ft/s)	NA	x	x	1.5D	40D
6 (ft/s)	NA	x	x	1.5D	40D
10 (ft/s)	NA	**x**	**x**	1.5D	40D

Particle Image Velocimetry (PIV) Laboratory data from Kalpakli and Örlü (2013) of the velocity profile at a Reynolds number of 34,000 downstream of a 90-degree 1.58D radius elbow was used to validate the LES model for this research. Consequently, for all the Re = 34,000 (mean pipeline velocity was = 0.645 ft/s), a 6-inch 1.58D 90-degree with 10 diameters of straight pipe downstream of the elbow was used in the model simulation in order to match the geometry of the elbow used by Kalpakli and Örlü (Figure 6.2).
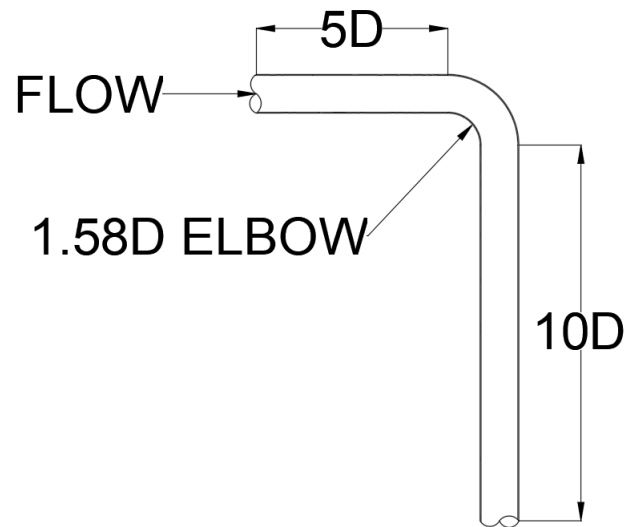
Figure 6.2: Mean Pipeline Velocity of 0.645 ft/s Numerical Model Geometry

However, for all other simulations the standard 6-inch 1.5D 90-degree elbow was used with 41 diameters of straight pipe downstream of the elbow (Figure 6.3). Only κ-ϵ and Reynolds Stress Model simulations were completed at these three higher flowrates due to computational cost.
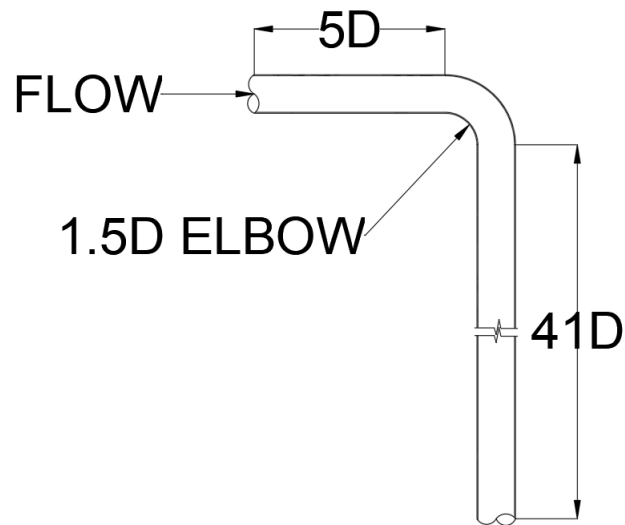
Figure 6.3: RANS Numerical Model Geometry

Each test downstream of the elbow used a straight pipe condition as a baseline voltage for calculating the meter accuracy deviation. The deviation was determined by subtracting the straight pipe voltage value from the voltage at the ith diameter downstream and dividing by the straight pipe voltage value as shown in Equation 6.1

$$\% Deviation = \frac{(V_{iD} - V_{straight})}{V_{straight}} \times 100\%.$$

(6.1)

It was assumed that the length of a 6-inch flowmeter is 12-inches with the electrodes located at the center of the flowmeter. The 0D location represents the minimum physical distance possible between the electrodes and the elbow, in which the downstream flange of the elbow is bolted to the upstream flange of the flowmeter. The -0.33D location represents the location where the laboratory data was taken and used as a validation of the LES model. The voltage was calculated for each simulation at varying diameters downstream of the elbow as shown in Figures 6.2 and 6.3.

A uniform magnetic field was assumed for the analysis, which is not practical to achieve in practice but was used in this study to evaluate relative differences. The electromagnetism, electrodynamics, and one-way coupled MHD packages were employed in Simcenter STAR CCM+ to solve for the flowmeter signal. A RANS solution using κ-ϵ turbulence model was solved on the same mesh and same geometry. Once the residuals of this solution were no longer changing with time, the synthetic eddy method was used to initiate the LES model. For the LES model, monitors were created to monitor the the voltage and the velocity profiles over time. This data was then exported, and a time average was taken and used to compare to the RANS solution.

6.3.3 Grid Generation

The uncertainty of the numerical model due to the discretization was determined using the process described by Celik et al. (2008). For the 2 ft/s κ-ϵ and RSM the uncertainty due to discretization was less than 0.01%. For the 10 ft/s κ-ϵ and RSM the uncertainty due to discretization was less than 0.01% and 0.46%, respectively.

The grid size for the LES model was selected following the criteria described in the Simcenter STAR CCM+ User Guide that the cell base size should be less than the Taylor Micro Scale but greater than the Kolmogorov Length Scale. Furthermore, the Courant-Friedrichs-Lewy (CFL) number was kept ≤ 0.3 for the simulations. A cell base size of 0.08 inches with a polyhedral and prism layer mesh and a time step of 0.002 s was used with a second order solver in STAR CCM+. Ultimately, the LES model was validated using laboratory data obtained at the same Reynolds number as the LES model. The κ-ϵ realizable 2-layer model and RSM 2-layer simulations for the same Reynolds number used the same base size and polyhedral and prism layer mesh as the LES model with wall y+ values at approximately equal to 1. A preliminary model was run using the κ-Ω model and performed poorly, thus it was excluded from other testing. This poor performance of the κ-Ω model appears to agree with what Kumar et al. (2014) found.

6.3.4 Assumptions and Intent

Although the Reynolds number of 34,000 is considered moderately high for LES runs, at the pipe size in this study it equates to a velocity of 0.645 ft/s. This velocity is nearly always avoided in the design of pipelines for economic reasons. Consequently, most magnetic flowmeter manufacturer's accuracy claims do not begin until after 1 ft/s. However, the intent of the study was to highlight the difference in general trends between the RANS modeling and the LES model. Thus, the intent of this study is to determine the effect of the method of the flow field solution on the magnetic flowmeter signal. Furthermore, the flowmeter signal is in microvolts and often is very difficult to capture at such low flow rates as magnetic flowmeter manufacturers are not designing meters for this condition.

6.4 Results and Practical Applications

Figure 6.4 presents the dimensionless laboratory data obtained by Kalpakli and Örlü (2013) at a Reynolds number of 34,000, along with the LES, RSM, and $\kappa - \epsilon$ data produced in the present study at the same Reynolds number. The velocity profiles depicted are in plane with the elbow. As can be seen from Figure 6.4, the LES data agrees better with

the laboratory data than the $\kappa - \epsilon$ and RSM data do. Orlu and Kalpaki do not state the uncertainty associated with the laboratory data they obtained using particle image velocimetry. Thus, it is unclear how much confidence can be placed in the absolute values of the laboratory data. Nevertheless, for the purposes of this study it is emphasized that the LES data matches the laboratory data better than the RSM or $\kappa - \epsilon$ data.
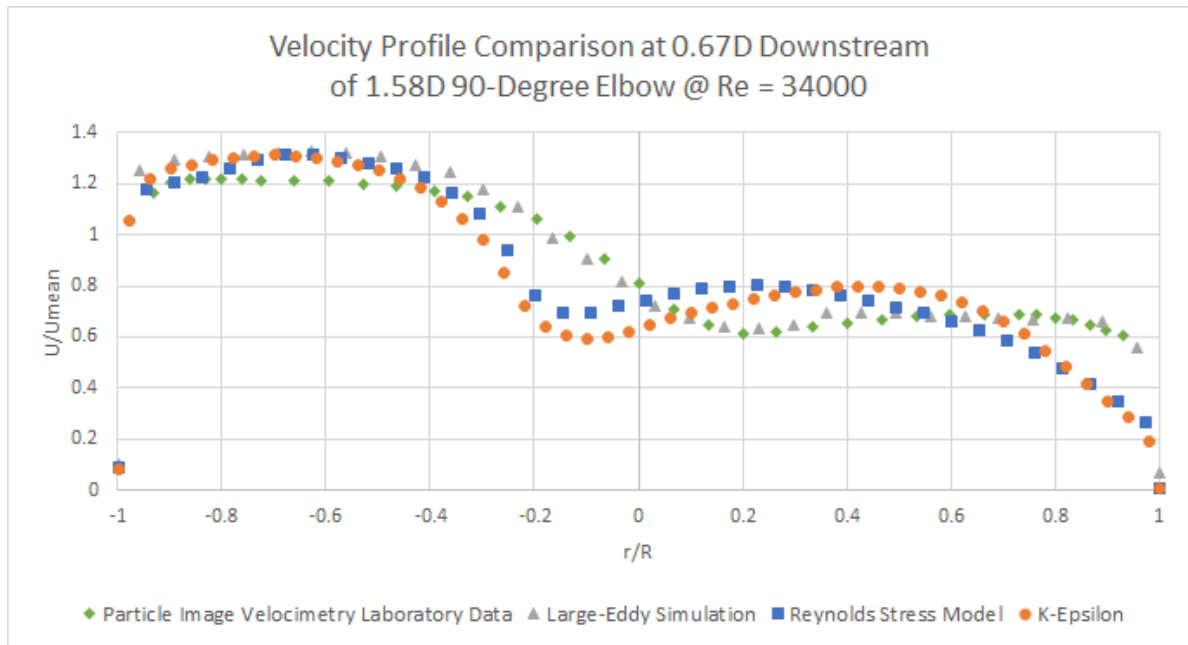
Figure 6.4: Velocity Profile Comparison at 0.67D Downstream of 1.58D 90-Degree Elbow

Figures 6.5 and 6.6 present the velocity profile data in plane with the elbow and out of plane with the elbow, respectively, at different diameters downstream of the elbow. The -0.33D is the exact same location as the 0.67D downstream of the elbow but is stated this way to account for the actual length that a magnetic flowmeter spool has. For the remainder of the paper, this location will be referred to as -0.33D because it represents an impractical condition of a magnetic flowmeter installation.
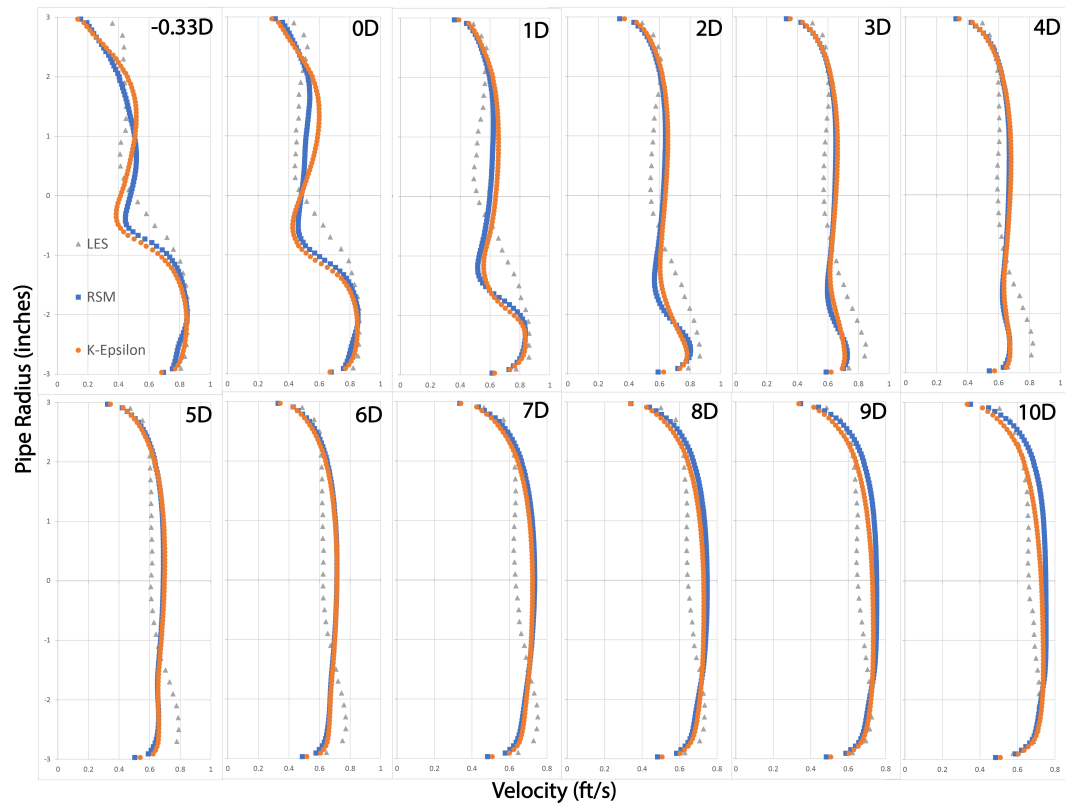
Figure 6.5: Velocity Profiles
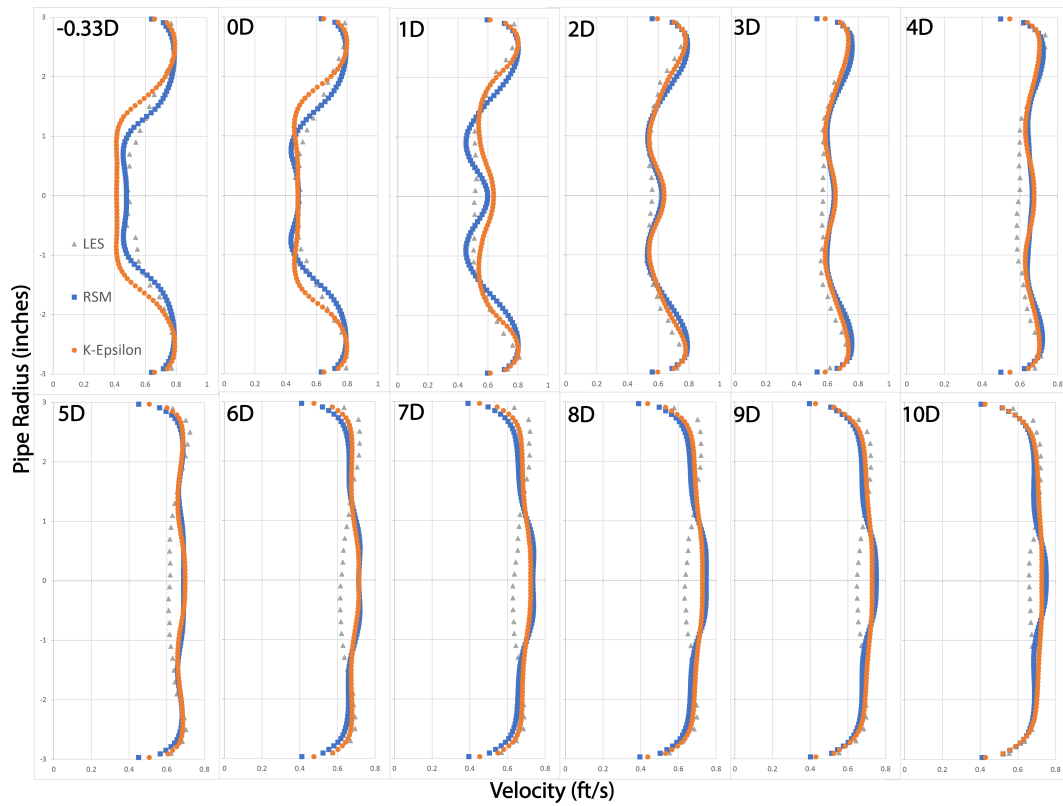
Figure 6.6: Vertical Velocity Profiles

Figure 6.7 presents the flowmeter accuracy for each of the three models in terms of deviation from straight pipe accuracy on the y-axis and distance downstream on the x-axis. From 1D to 10D for the LES data, the mean deviation is -0.75% with a maximum of -0.50% and a minimum of -0.96%. The other two models have a much larger swing in deviation.
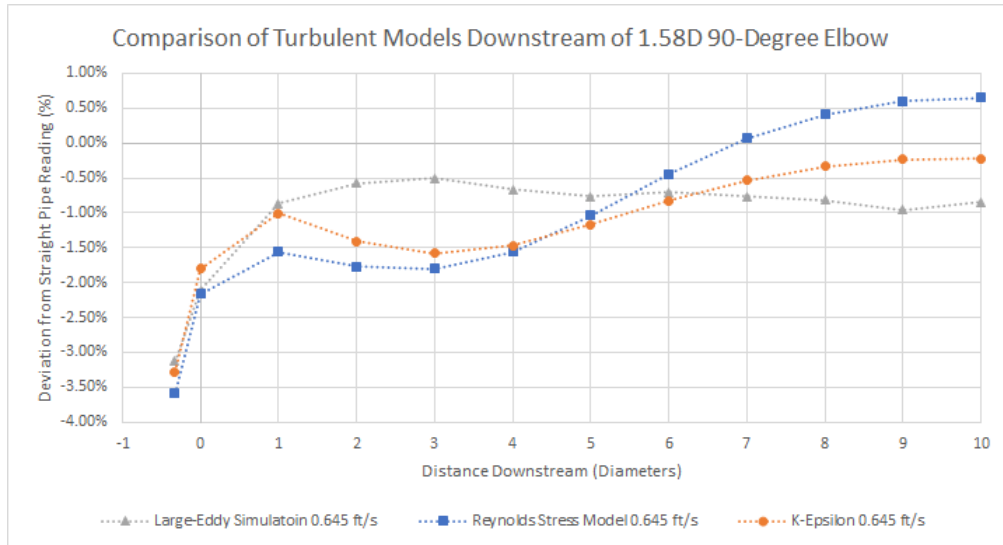
Figure 6.7: Flowmeter Accuracy for LES, K-Epsilon, and Reynolds Stress Simulations at Reynolds Number of 34,000 Downstream of 1.58D 90-Degree Elbow

Figures 6.8-6.10 present the results of the 10, 6, and 2 ft/s mean pipeline velocity simulations from 0D to 40D downstream of a 1.5D 90-degree elbow.
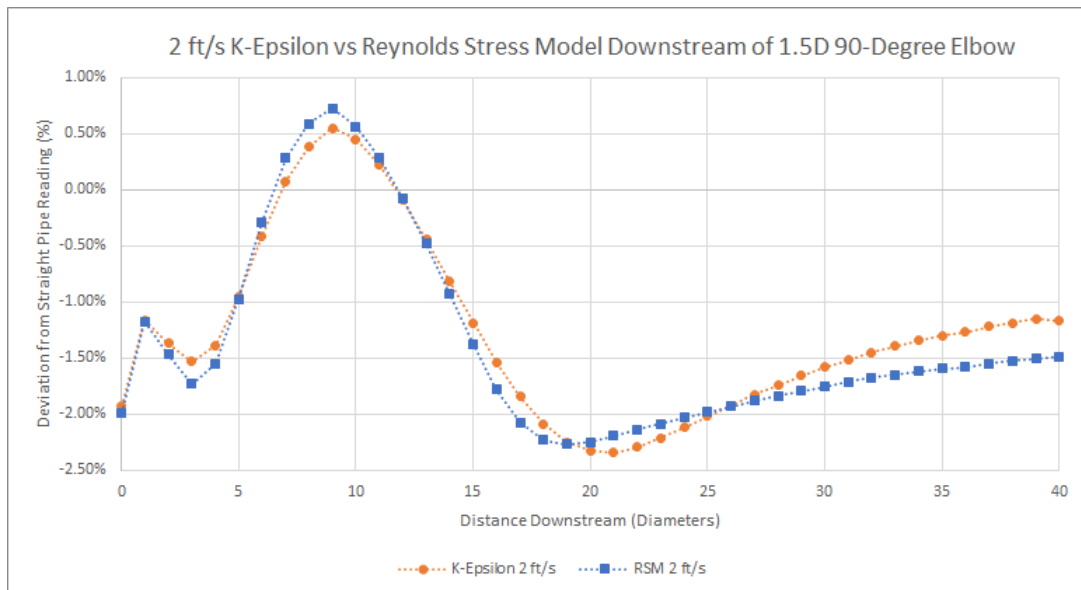
Figure 6.8: Flowmeter Accuracy for K-Epsilon and Reynolds Stress Model for a Mean Pipeline Velocity of 2 ft/s
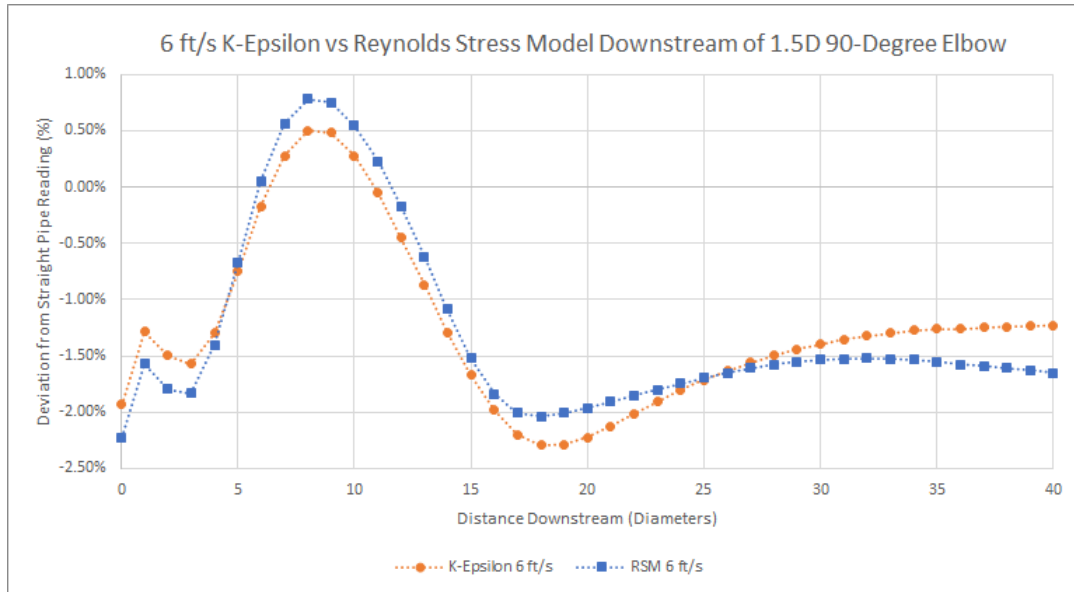
Figure 6.9: Flowmeter Accuracy for K-Epsilon and Reynolds Stress Model for a Mean Pipeline Velocity of 6 ft/s
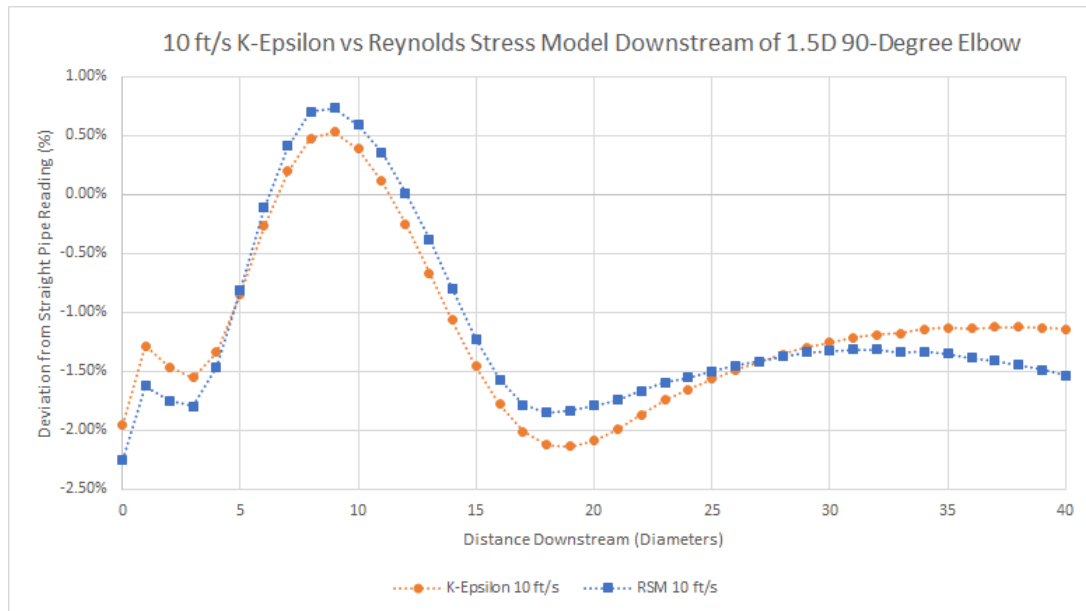
Figure 6.10: Flowmeter Accuracy for K-Epsilon and Reynolds Stress Model for a Mean Pipeline Velocity of 10 ft/s

Figures 6.11 and 6.12 present the flowmeter accuracy for the mean pipeline velocities of 10, 6, and 2 ft/s using the $\kappa - \epsilon$ and RSM models, respectively.
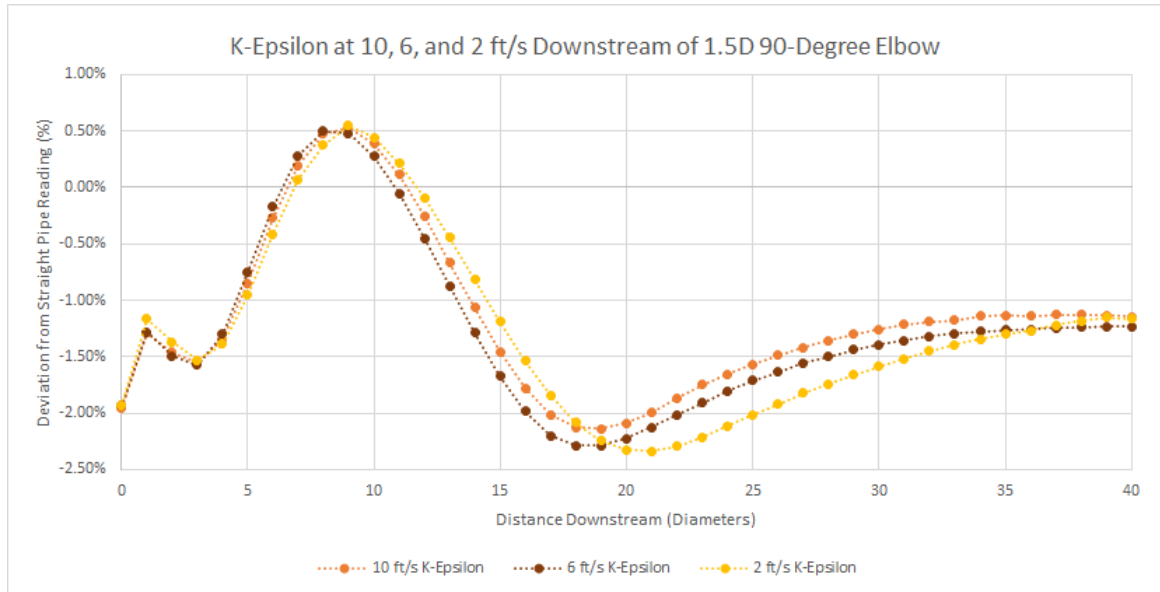
Figure 6.11: Flowmeter Accuracy for Mean Pipeline Velocities of 10, 6, and 2 ft/s using K-Epsilon
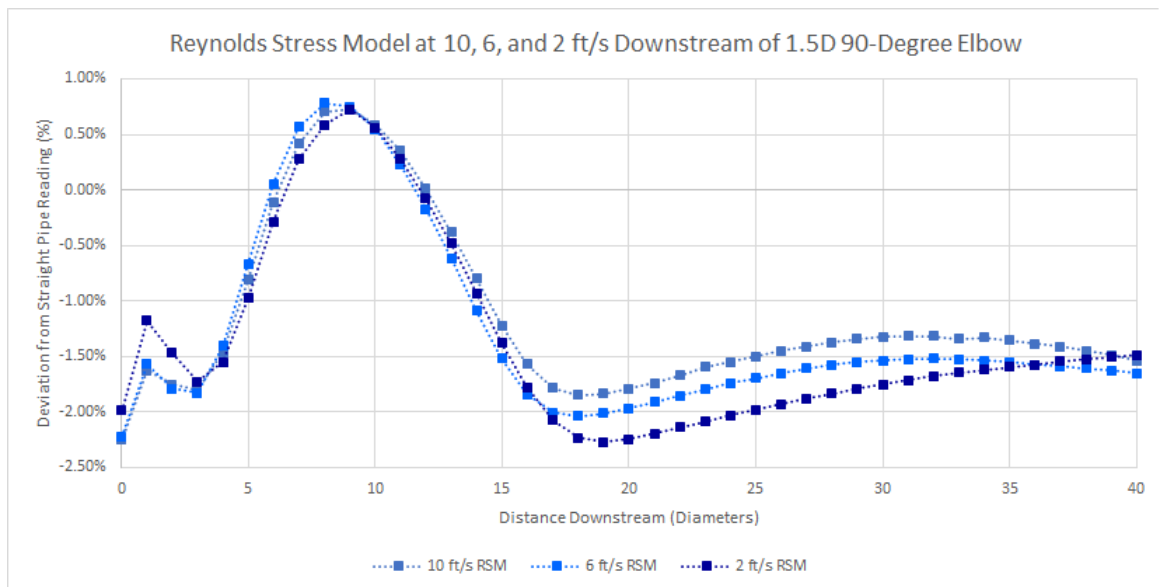
Figure 6.12: Flowmeter Accuracy for Mean Pipeline Velocities of 10, 6, and 2 ft/s using Reynolds Stress Model

Although there are differences in the magnitudes of the deviation from straight pipe accuracy between the κ ϵ data and the RSM data, the exhibit a similar behavior as the flow recovers downstream of the elbow. Using the κ-ϵ solver at a mean velocity of 2 ft/s, a simulation was conducted to evaluate the effect of pipe roughness on recovery of the flow. The pipe roughness height (e) was equal to 0.01 in which is representative of a cast iron pipe. The results were compared to the hydraulically smooth simulation at the same conditions and the difference in flowmeter signal was less than 0.03%.

6.5   Conclusions and Considerations

The authors conclude that the fidelity of the flow field model ought to be considered when attempting to analyze magnetic flowmeter performance in adverse installation conditions. Although there is not laboratory data to validate the LES model at other distances downstream, the results presented in Figure 6.7, appear to support the findings of Röhrig et al. (2015) that RANS models which underpredict the turbulence result in a poor recovery of the flow downstream of the disturbance. Increased levels of turbulence indicate a greater diffusion of momentum and thus dissipate the effect of a flow disturbance and return to axisymmetric flow more quickly than lower levels of turbulence would.

The data presented in Figures 6.8-6.12 does not support what some of the authors experiences have been calibrating magnetic flowmeters over many years. It would appear that magnetic flowmeter analysis is limited by the ability of the flow field model to accurately predict the recovery of the fully developed profile. As a laboratory that calibrates magnetic flowmeters often, this assertion compares well with several of the authors experiences as the deviations as shown in Figures 6.8-6.12 at those pipeline velocities beyond 15-20 diameters of an elbow has not occurred, thus indicating that at some point between the elbow and farther downstream the RANS and LES models differ significantly in the capturing the recovery of the velocity profile for a 90-degree elbow. Furthermore, this research appears to suggest that any claims of dry calibrating a magnetic flowmeter in any practical condition of interest (i.e., where the flow is distorted and a dry calibration may be especially useful) that uses a RANS model without validating and comparing that model to laboratory data

would be unlikely.

It would also appear that although RANS models can provide insight and understanding in many flow conditions, their inability to accurately capture the turbulent mixing is a severe limitation when it comes to magnetic flowmeter analysis. However, at the present time, it does not appear feasible to carry out LES simulations at higher Reynolds number for which magnetic flowmeters are often installed.

CHAPTER 7

SUMMARY AND CONCLUSIONS

This chapter summarizes the research completed and highlights the contributions of that research to the field of magnetic flowmeter analysis. Improving the understanding of the most common and widely used flowmeters in the water industry directly affects water conservation. The accomplishment of the objectives of this study provides additional information to assist magnetic flowmeter designers and users improve flowmeter performance. Each of the chapters is summarized below.

7.1 Chapter 1

In the first chapter, the relationship of the magnetic flowmeter to water conservation was delineated. The magnetic flowmeter and its benefits were also briefly introduced along with an overview of the dissertation.

7.2 Chapter 2

In the second chapter, the history and development of the magnetic flowmeter as a measuring device was presented. Following a presentation of magnetic flowmeter analysis methods, three gaps in the literature were clearly identified. The breadth of magnetic flowmeter research was also briefly presented to provide a backdrop against which the present study can be better appreciated. The chapter concluded with the three research objectives corresponding to the three gaps in the literature. The objectives were: optimizing arc and multipoint electrode flowmeters and an evaluation of their performance compared to single-point flowmeters in distorted flows; an assessment and comparison of the MHD and WFM methods in distorted flows with various electrode configurations; and determining the effect of higher fidelity flow field models on magnetic flowmeter analysis.

7.3   Chapter 3

The third chapter reviewed the fundamental physics of electromagnetism and MHD. The methodology used to analyze magnetic flowmeters was reviewed and CFD was introduced and briefly described.

7.4   Chapter 4

The fourth chapter presented the first standalone original research paper. The first objective was to optimize the arc electrode and multi-point (six-electrode) flowmeter using the weight function coefficient of variation as the basis for optimization. This was completed using MatLab's PDE Solver Toolbox. The arc electrode flowmeter was considered optimized at an angle of 130 degrees and the multipoint electrode flowmeter was considered optimized with an equidistant spacing of 25 degrees between the three electrodes on either side of the meter. These optimized meters were then tested against a traditional single-point electrode flowmeter downstream of a 90-degree elbow and a 50% open gate valve. The arc electrode flowmeter showed much less sensitivity to the distorted profiles than either the multi-point or the singlepoint electrode flowmeter. It appears that more accurate electrode configurations exist than are presently commercially available. Thus, this study appears to warrant further testing and research in a laboratory to explore the optimized multi-point and arc electrode flowmeters. The author recognizes that corrosion of the arc electrodes is a valid concern but asserts there may be conditions where corrosion would not present an issue, thus providing a highly robust meter to velocity profile distortions. This significance of this research is that with a more accurate flowmeter under adverse flow conditions, water conservation could be improved.

7.5   Chapter 5

In the fifth chapter the second objective of the study, which was to determine whether a commercially available software could solve the flowmeter equation in distorted flow conditions in good agreement with the traditional WFM, was explored. This was completed using MatLab's PDE Toolbox to compute the weight function for the optimized multi-point

electrode and singlepoint electrode flowmeter and compare the results with a numerically modelled single-point and multipoint flowmeter using STAR CCM+. It was observed that the maximum deviation between the two methods was less than 0.5% for both the single-point and multipoint analyses. The significance of this research is to enable other researchers interested in magnetic flowmeter performance and analysis the tools to do so without requiring them to understand the significant effort required to derive a weight function by hand and write their own post processing code.

7.6   Chapter 6

The sixth chapter addressed the third objective, which was to determine whether or not magnetic flowmeter analyses are sensitive to the fidelity of the flow field model. Nearly all of the magnetic flowmeter research has been conducted to improve the physical components of the flowmeter itself. Thus, the fidelity of the flow field model and its effect on the output of the flowmeter appear to be uncertain. This research compared three numerical models at a Reynolds number of 34,000 to laboratory velocity profile data 0.67D downstream of a 1.58D 90-degree elbow. The results indicate at that location there was a difference in voltage output of 0.8%. However, farther downstream, where laboratory data was not available, the voltage output differs more substantially in magnitude and trend from the lower fidelity models. This appears to confirm what other researchers have found, that RANS models significantly underpredict the levels of turbulence and thus recover poorly to a fully developed profile. The LES model data indicates the fidelity of the flow field, the Reynolds number, and the distance from the disturbance are all key components and need to be carefully monitored when conducting magnetic flowmeter analyses. The significance of this research was to demonstrate that the fidelity of the flow field does influence to output signal of a magnetic flowmeter downstream of a 90-degree elbow.

7.7   Further Research

This section briefly presents a few possible areas of focus to extend the current research. Laboratory testing could be conducted for arc electrode flowmeters to validate the numerical

accuracy gains as shown in Chapter 4. Laboratory testing could also be completed to collect velocity profile data at varying diameters downstream of a 90-degree elbow to be compared with the LES data produced in Chapter 6.

REFERENCES

Al-Khazraji, Y. (1979). "Electromagnetic flowmeters with large electrodes." *Ph.D Thesis, Imperial College London.*

AWWA (2002). "Cold-water meters—displacement type, bronze main case." *AWWA Standard.*

Beck, K. J., Barfuss, S. L., and Johnson, M. C. (2019). "Assessing the effects of local turbulence and velocity profiles on electromagnetic flowmeter accuracy." *AWWA Water Science*, 1(5), e1156.

Beck, K. J., Barfuss, S. L., Moon, T. K., and Sharp, Z. B. (2021). "The superior accuracy of the arc electrode magnetic flowmeter: A numerical study." *AWWA Water Science*, 3(2), e1220.

Beck, K. J., Weller, R. P., Barfuss, S. L., and Johnson, M. C. (2018). "The effects of a short-radius elbow on electromagnetic flowmeter accuracy." *Journal-American Water Works Association*, 110(7), E12–E17.

Bevir, M. (1969). "Induced voltage electromagnetic flowmeter." *Ph. D Thesis, University of Warwick.*

Bevir, M., O'sullivan, V., and Wyatt, D. (1981). "Computation of electromagnetic flowmeter characteristics from magnetic field data." *Journal of Physics D: Applied Physics*, 14(3), 373.

Cao, Z., Song, W., Peng, Z., and Xu, L. (2014). "Coil shape optimization of the electromagnetic flowmeter for different flow profiles." *Flow measurement and Instrumentation*, 40, 256–262.

Celik, I. B., Ghia, U., Roache, P. J., and Freitas, C. J. (2008). "Procedure for estimation and reporting of uncertainty due to discretization in cfd applications." *Journal of fluids Engineering-Transactions of the ASME*, 130(7).

Cha, J.-E., Ahn, Y.-C., and Kim, M.-H. (2002). "Flow measurement with an electromagnetic flowmeter in two-phase bubbly and slug flow regimes." *Flow measurement and instrumentation*, 12(5-6), 329–339.

Davidović, D., Aničin, B., and Babović, V. (1991). "An electrostatic interpretation of the weighted flow theorem of electromagnetic flowmeters." *Archiv für Elektrotechnik*, 74(4), 267–273.

Deville, M. O., Fischer, P. F., and Mund, E. H. (2002). *High-Order Methods for Incompressible Fluid Flow*. Cambridge Monographs on Applied and Computational Mathematics. Cambridge University Press.

El Khoury, G. K., Schlatter, P., Noorani, A., Fischer, P. F., Brethouwer, G., and Johansson, A. V. (2013). "Direct numerical simulation of turbulent pipe flow at moderately high reynolds numbers." *Flow, turbulence and combustion*, 91(3), 475–495.

Engl, W. (1970). "Der induktive durchflußmesser mit inhomogenem magnetfeld." *Archiv für Elektrotechnik*, 53(6), 344–359.

FlowResearch (2017). "The world market for electromagnetic flowmeters 5th edition." *Flow Research*.

Frenzel, F., Grothey, H., Habersetzer, C., Hiatt, M., Hogrefe, W., Kirchner, M., Lütkepohl, G., Marchewka, W., Mecke, U., Ohm, M., et al. (2011). "Industrial flow measurement basics and practice." *ABB automation products Gmbh*, 290.

Fu, X., Hu, L., Lee, K., Zou, J., Ruan, X., and Yang, H. (2010). "Dry calibration of electromagnetic flowmeters based on numerical models combining multiple physical phenomena (multiphysics)." *Journal of Applied Physics*, 108(8), 083908.

Ge, L., Chen, J., Tian, G., Zeng, W., Huang, Q., and Hu, Z. (2020). "Study on a new electromagnetic flow measurement technology based on differential correlation detection." *Sensors*, 20(9).

Horner, B. (1998). "A novel profile-insensitive multi-electrode induction flowmeter suitable for industrial use." *Measurement*, 24(3), 131–137.

Horner, B. and Mesch, F. (1995). "An induction flowmeter insensitive to asymmetric flow profiles." *Process Tomography 1995, 6–8 April 1995, Bergen, Norway*, 321–330.

Horner, B., Mesch, F., and Trächtler, A. (1996). "A multi-sensor induction flowmeter reducing errors due to non-axisymmetric flow profiles." *Measurement Science and Technology*, 7(3), 354.

Hughes, W. F. and Young, F. J. (1966). "The electromagnetodynamics of fluids." *The electromagnetodynamics of fluids*.

Ismael, M. A., Laftah, R. M., and Falih, M. N. (2017). "Measurement of liquid level in partially-filled pipes using a noise of electromagnetic flowmeter." *Al-Qadisiyah Journal for Engineering Sciences*, 10(4), 550–564.

Kalpakli, A. and Örlü, R. (2013). "Turbulent pipe flow downstream a 90 pipe bend with and without superimposed swirl." *International Journal of Heat and Fluid Flow*, 41, 103–111.

Katutis, R. and Virbalis, J. A. (2007). "Development of battery–driven electromagnetic flow converter." *Electronics and Electrical Engineering*, 4, 79–82.

Kong, L.-f., Du, S., and Li, Y. (2015). "Simulation research on weight function of multi-electrode electromagnetic flowmeter." *Acta Metrologica Sinica*, 36(1), 58–62.

Kumar, V., Kissling, B., Papathanasiou, P., and Aydin, F. (2014). "Large-eddy simulation of typical industrial bends." *STAR Global Conference*.

Launder, B., Sandham, N., and for Mathematical Sciences, I. N. I. (2002). *Closure Strategies for Turbulent and Transitional Flows*. Online access with purchase: Cambridge Books Online. Cambridge University Press, <https://books.google.com/books?id=1xaln_9vJMC>.

Li, Y., Yang, Y., Ma, S., Li, L., Wang, Y., Liu, X., and Xie, R. (2019). "Theoretical model construction and structure optimization of electromagnetic flow transducer based on neural network." *Journal of Intelligent & Fuzzy Systems*, 37(3), 3489–3498.

Lim, K. W. and Chung, M. K. (1998). "Relative errors in evaluating the electromagnetic flowmeter signal using the weight function method and the finite volume method." *Flow Measurement and Instrumentation*, 9(4), 229–235.

Lim, K. W. and Chung, M. K. (1999). "Numerical investigation on the installation effects of electromagnetic flowmeter downstream of a 90 elbow–laminar flow case." *Flow Measurement and Instrumentation*, 10(3), 167–174.

Lim, S. (2008). "The improvement of meter performance em sensing flowmeters using software modelling." Ph.D. thesis, Cranfield University, Bedford, United Kingdom, <https://dspace.lib.cranfield.ac.uk/handle/1826/3751>.

Liu, T. and Zhang, G. (2014). "Magnetic circuit design for electromagnetic flow transducer with locally shrunk measurement pipe." *2014 International Conference on Future Computer and Communication Engineering (ICFCCE 2014)*, Atlantis Press, 11–14.

Lu, B., Xu, L., and Zhang, X. (2013). "Three-dimensional mhd simulations of the electromagnetic flowmeter for laminar and turbulent flows." *Flow Measurement and Instrumentation*, 33, 239–243.

Lucas, G. and Leeungculsatien, T. (2010). "A new method of measuring velocity profiles using a multielectrode electromagnetic flow meter." *6th World Congress on Industrial Process Tomography*, 1016–1025, <http://eprints.hud.ac.uk/id/eprint/9091/> (September).

Luntta, E. and Halttunen, J. (1989). "The effect of velocity profile on electromagnetic flow measurement." *Sensors and Actuators*, 16(4), 335–344.

Martim, A. L. S. S., Dalfré Filho, J. G., De Lucca, Y. d. F. L., and Genovez, A. I. B. (2019). "Electromagnetic flowmeter evaluation in real facilities: Velocity profiles and error analysis." *Flow Measurement and Instrumentation*, 66, 44–49.

Michalski, A., Starzynski, J., and Wincenciak, S. (2001). "Electromagnetic flowmeters for open channels - two-dimensional approach to design procedures." *IEEE Sensors Journal*, 1(1), 52–61.

O'Sullivan, V. and Wyatt, D. (1983). "Computation of electromagnetic flowmeter characteristics from magnetic field data. iii. rectilinear weight functions." *Journal of Physics D: Applied Physics*, 16(8), 1461.

Peery, J. T. (2006). "How much straight pipe is enough?." *Process Instrumentation*, <https://www.piprocessinstrumentation.com/home/article/15551180/how-much-straight-pipe-is-enough> (Mar. 17, 2021).

Powers, D. L. (2014). *Boundary value problems*. Elsevier.

Renzetti, S. and Dupont, D. P. (2016). *Water policy and governance in Canada*, Vol. 17. Springer.

Röhrig, R., Jakirlić, S., and Tropea, C. (2015). "Comparative computational study of turbulent flow in a 90 pipe elbow." *International Journal of Heat and Fluid Flow*, 55, 120–131.

Shercliff, J. (1954). "Relation between the velocity profile and the sensitivity of electromagnetic flowmeters." *Journal of Applied Physics*, 25(6), 817–818.

Shercliff, J. A. (1962). *The theory of electromagnetic flow-measurement.* CUP Archive.

Shi, Y., Wang, M., Shen, M., and Wang, H. (2015). "Optimization of an electromagnetic flowmeter for dual-parameter measurement of vertical air-water flows." *Journal of Mechanical Science and Technology*, 29(7), 2889–2895.

SIEMENS (2021). *Simcenter STAR CCM+ Theory Guide.* SIEMENS, Munich, Germany.

Simão, M., Besharat, M., Carravetta, A., and Ramos, H. M. (2018). "Flow velocity distribution towards flowmeter accuracy: Cfd, udv, and field tests." *Water*, 10(12), 1807.

Smyth, C. (1971). "Derivation of weight functions for the circular and rectangular channel magnetic flowmeters, by means of green's theorem and conformal mapping." *Journal of Physics E: Scientific Instruments*, 4(1), 29.

Vester, A., Örlü, R., and Alfredsson, P. H. (2016). "Turbulent flows in curved pipes: recent advances in experiments and simulations." *Applied Mechanics Reviews*, 68(5).

Wang, J., Gong, C., Tian, G., and Lucas, G. (2006). "Numerical simulation modelling for velocity measurement of electromagnetic flow meter." *Journal of Physics: Conference Series*, Vol. 48, IOP Publishing, 007.

Wang, J., Tian, G., and Lucas, G. (2007). "Relationship between velocity profile and distribution of induced potential for an electromagnetic flow meter." *Flow Measurement and Instrumentation*, 18(2), 99–105.

Watral, Z., Jakubowski, J., and Michalski, A. (2015). "Electromagnetic flow meters for open channels: Current state and development prospects." *Flow measurement and Instrumentation*, 42, 16–25.

Xu, L., Han, J., and Wang, Y. (2005). "Design of electrode array of inductance flowmeter." *IEEE Sensors Journal*, 5(5), 929–933.

Yin, S. and Li, B. (2013). "A new approach for solving weight functions of electromagnetic flowmeters using resistive network modeling." *Journal of Applied Mathematics*, 2013.

APPENDICES

APPENDIX A

MatLab Code

A.1   Code to Derive Single-point Electrode Weight Function Using PDE Toolbox

%PDE Nonconstant Boundary Conditions Solver with unique shapes

R1=↙
[2,144,1,0.999048221581858,0.996194698091746,0.991444861373810,0.984807753012208,0.976296 ↙
007119933,0.965925826289068,0.953716950748227,0.939692620785908,0.923879532511287,0.90630 ↙
7787036650,0.887010833178222,0.866025403784439,0.843391445812886,0.819152044288992,0.7933 ↙
53340291235,0.766044443118978,0.737277336810124,0.707106781186548,0.675590207615660,0.642 ↙
787609686539,0.608761429008721,0.573576436351046,0.537299608346824,0.500000000000000,0.46 ↙
1748613235034,0.422618261740699,0.382683432365090,0.342020143325669,0.300705799504273,0.2 ↙
58819045102521,0.216439613938103,0.173648177666930,0.130526192220052,0.0871557427476581,0 ↙
.0436193873653360,6.12323399573677e-17,-0.0436193873653359,-0.0871557427476580, ↙
-0.130526192220051,-0.173648177666930,-0.216439613938103,-0.258819045102521, ↙
-0.300705799504273,-0.342020143325669,-0.382683432365090,-0.422618261740699, ↙
-0.461748613235034,-0.500000000000000,-0.537299608346824,-0.573576436351046, ↙
-0.608761429008721,-0.642787609686539,-0.675590207615660,-0.707106781186548, ↙
-0.737277336810124,-0.766044443118978,-0.793353340291235,-0.819152044288992, ↙
-0.843391445812886,-0.866025403784439,-0.887010833178222,-0.906307787036650, ↙
-0.923879532511287,-0.939692620785908,-0.953716950748227,-0.965925826289068, ↙
-0.976296007119933,-0.984807753012208,-0.991444861373810,-0.996194698091746, ↙
-0.999048221581858,-1,-0.999048221581858,-0.996194698091746,-0.991444861373811, ↙
-0.984807753012208,-0.976296007119933,-0.965925826289068,-0.953716950748227, ↙
-0.939692620785908,-0.923879532511287,-0.906307787036650,-0.887010833178222, ↙
-0.866025403784439,-0.843391445812886,-0.819152044288992,-0.793353340291235, ↙
-0.766044443118978,-0.737277336810124,-0.707106781186548,-0.675590207615660, ↙
-0.642787609686540,-0.608761429008721,-0.573576436351046,-0.537299608346824, ↙
-0.500000000000000,-0.461748613235034,-0.422618261740700,-0.382683432365090, ↙
-0.342020143325669,-0.300705799504273,-0.258819045102521,-0.216439613938104, ↙
-0.173648177666930,-0.130526192220052,-0.0871557427476583,-0.0436193873653361, ↙
-1.83697019872103e- ↙
16,0.0436193873653358,0.0871557427476579,0.130526192220051,0.173648177666930,0.2164396139 ↙
38102,0.258819045102520,0.300705799504273,0.342020143325669,0.382683432365090,0.422618261 ↙
740699,0.461748613235033,0.499999999999999,0.537299608346824,0.573576436351046,0.60876142 ↙
9008721,0.642787609686539,0.675590207615660,0.707106781186547,0.737277336810124,0.7660444 ↙
43118978,0.793353340291235,0.819152044288992,0.843391445812886,0.866025403784439,0.887010 ↙
833178221,0.906307787036650,0.923879532511287,0.939692620785908,0.953716950748227,0.96592 ↙
5826289068,0.976296007119933,0.984807753012208,0.991444861373810,0.996194698091746,0.9990 ↙
48221581858,0,0.0436193873653360,0.0871557427476582,0.130526192220052,0.173648177666930,0 ↙
.216439613938103,0.258819045102521,0.300705799504273,0.342020143325669,0.382683432365090, ↙
0.422618261740699,0.461748613235034,0.500000000000000,0.537299608346824,0.573576436351046 ↙
,0.608761429008721,0.642787609686539,0.675590207615660,0.707106781186548,0.73727733681012 ↙
4,0.766044443118978,0.793353340291235,0.819152044288992,0.843391445812886,0.8660254037844 ↙
39,0.887010833178222,0.906307787036650,0.923879532511287,0.939692620785908,0.953716950748 ↙
227,0.965925826289068,0.976296007119933,0.984807753012208,0.991444861373810,0.99619469809 ↙
1746,0.999048221581858,1,0.999048221581858,0.996194698091746,0.991444861373811,0.98480775 ↙
3012208,0.976296007119934,0.965925826289068,0.953716950748227,0.939692620785908,0.9238795 ↙
32511287,0.906307787036650,0.887010833178222,0.866025403784439,0.843391445812886,0.819152 ↙
044288992,0.793353340291235,0.766044443118978,0.737277336810124,0.707106781186548,0.67559 ↙
0207615660,0.642787609686540,0.608761429008721,0.573576436351046,0.537299608346824,0.5000 ↙
00000000000,0.461748613235034,0.422618261740700,0.382683432365090,0.342020143325669,0.300 ↙
705799504273,0.258819045102521,0.216439613938103,0.173648177666930,0.130526192220052,0.08 ↙
71557427476582,0.0436193873653361,1.22464679914735e-16,-0.0436193873653358, ↙
-0.0871557427476579,-0.130526192220051,-0.173648177666930,-0.216439613938103, ↙
-0.258819045102520,-0.300705799504273,-0.342020143325669,-0.382683432365090, ↙
-0.422618261740699,-0.461748613235034,-0.500000000000000,-0.537299608346824, ↙
-0.573576436351046,-0.608761429008720,-0.642787609686539,-0.675590207615660, ↙
-0.707106781186548,-0.737277336810124,-0.766044443118978,-0.793353340291235, ↙

```
-0.819152044288992,-0.843391445812886,-0.866025403784439,-0.887010833178222,↵
-0.906307787036650,-0.923879532511287,-0.939692620785908,-0.953716950748227,↵
-0.965925826289068,-0.976296007119933,-0.984807753012208,-0.991444861373810,↵
-0.996194698091746,-0.999048221581858,-1,-0.999048221581858,-0.996194698091746,↵
-0.991444861373811,-0.984807753012208,-0.976296007119934,-0.965925826289068,↵
-0.953716950748227,-0.939692620785908,-0.923879532511287,-0.906307787036650,↵
-0.887010833178222,-0.866025403784439,-0.843391445812886,-0.819152044288992,↵
-0.793353340291235,-0.766044443118978,-0.737277336810124,-0.707106781186548,↵
-0.675590207615661,-0.642787609686540,-0.608761429008721,-0.573576436351047,↵
-0.537299608346823,-0.500000000000000,-0.461748613235034,-0.422618261740700,↵
-0.382683432365090,-0.342020143325669,-0.300705799504273,-0.258819045102521,↵
-0.216439613938103,-0.173648177666930,-0.130526192220053,-0.0871557427476583,↵
-0.0436193873653362]';
R2=[2,720,-0.00436332312997498,-0.0130896371059753,-0.0218149542554314,↵
-0.0305386101116610,-0.0392599403344955,-0.0479782807608725,-0.0566929674554144,↵
-0.0654033367609885,-0.0741087253492489,-0.0828084702711504,-0.0915019090074347,↵
-0.100188379519084,-0.108867220297738,-0.117537770416070,-0.126199369578118,↵
-0.134851358169572,-0.143493077308004,-0.152123868893043,-0.160743075656494,↵
-0.169350041212391,-0.177944110106985,-0.186524627868655,-0.195090941057754,↵
-0.203642397316366,-0.212178345417989,-0.220698135317126,-0.229201118198791,↵
-0.237686646527917,-0.246154074098670,-0.254602756083655,-0.263032049083029,↵
-0.271441311173496,-0.279829901957189,-0.288197182610443,-0.296542515932440,↵
-0.304865266393738,-0.313164800184666,-0.321440485263594,-0.329691691405061,↵
-0.337917790247774,-0.346118155342458,-0.354292162199562,-0.362439188336816,↵
-0.370558613326638,-0.378649818843379,-0.386712188710413,-0.394745108947060,↵
-0.402747967815342,-0.410720155866573,-0.418661065987767,-0.426570093447874,↵
-0.434446635943832,-0.442290093646434,-0.450099869246009,-0.457875367997909,↵
-0.465615997767798,-0.473321169076753,-0.480990295146144,-0.488622791942331,↵
-0.496218078221131,-0.503775575572088,-0.511294708462519,-0.518774904281343,↵
-0.526215593382686,-0.533616209129268,-0.540976187935545,-0.548294969310635,↵
-0.555571995901003,-0.562806713532899,-0.569998571254564,-0.577147021378189,↵
-0.584251519521620,-0.591311524649818,-0.598326499116059,-0.605295908702876,↵
-0.612219222662748,-0.619095913758510,-0.625925458303513,-0.632707336201496,↵
-0.639441030986202,-0.646126029860702,-0.652761823736449,-0.659347907272048,↵
-0.665883778911740,-0.672368940923594,-0.678802899437414,-0.685185164482349,↵
-0.691515250024207,-0.697792674002466,-0.704016958366984,-0.710187629114411,↵
-0.716304216324278,-0.722366254194787,-0.728373281078284,-0.734324839516416,↵
-0.740220476274964,-0.746059742378363,-0.751842193143893,-0.757567388215540,↵
-0.763234891597532,-0.768844271687545,-0.774395101309568,-0.779886957746433,↵
-0.785319422772011,-0.790692082683057,-0.796004528330718,-0.801256355151689,↵
-0.806447163199026,-0.811576557172598,-0.816644146449195,-0.821649545112273,↵
-0.826592371981345,-0.831472250641009,-0.836288809469610,-0.841041681667547,↵
-0.845730505285199,-0.850354923250496,-0.854914583396103,-0.859409138486249,↵
-0.863838246243161,-0.868201569373136,-0.872498775592224,-0.876729537651535,↵
-0.880893533362157,-0.884990445619695,-0.889019962428420,-0.892981776925025,↵
-0.896875587401997,-0.900701097330594,-0.904458015383423,-0.908146055456629,↵
-0.911764936691682,-0.915314383496764,-0.918794125567759,-0.922203897908836,↵
-0.925543440852630,-0.928812500080015,-0.932010826639476,-0.935138176966061,↵
-0.938194312899936,-0.941179001704516,-0.944092016084195,-0.946933134201647,↵
-0.949702139694729,-0.952398821692952,-0.955022974833542,-0.957574399277075,↵
-0.960052900722704,-0.962458290422947,-0.964790385198066,-0.967049007450013,↵
-0.969233985175961,-0.971345151981396,-0.973382347092792,-0.975345415369854,↵
-0.977234207317332,-0.979048579096406,-0.980788392535642,-0.982453515141510,↵
-0.984043820108476,-0.985559186328660,-0.986999498401058,-0.988364646640328,↵
-0.989654527085148,-0.990869041506127,-0.992008097413289,-0.993071608063119,↵
-0.994059492465161,-0.994971675388194,-0.995808087365956,-0.996568664702438,↵
```

-0.997253349476731,-0.997862089547437,-0.998394838556645,-0.998851555933453,
-0.999232206897066,-0.999536762459439,-0.999765199427487,-0.999917500404850,
-0.999993653793219,-0.999993653793219,-0.999917500404850,-0.999765199427487,
-0.999536762459439,-0.999232206897066,-0.998851555933453,-0.998394838556645,
-0.997862089547437,-0.997253349476731,-0.996568664702438,-0.995808087365956,
-0.994971675388194,-0.994059492465161,-0.993071608063119,-0.992008097413289,
-0.990869041506127,-0.989654527085148,-0.988364646640328,-0.986999498401058,
-0.985559186328660,-0.984043820108476,-0.982453515141510,-0.980788392535642,
-0.979048579096406,-0.977234207317332,-0.975345415369854,-0.973382347092792,
-0.971345151981396,-0.969233985175961,-0.967049007450013,-0.964790385198066,
-0.962458290422947,-0.960052900722704,-0.957574399277075,-0.955022974833542,
-0.952398821692952,-0.949702139694729,-0.946933134201647,-0.944092016084195,
-0.941179001704516,-0.938194312899936,-0.935138176966061,-0.932010826639476,
-0.928812500080015,-0.925543440852630,-0.922203897908836,-0.918794125567759,
-0.915314383496764,-0.911764936691682,-0.908146055456629,-0.904458015383423,
-0.900701097330594,-0.896875587401997,-0.892981776925025,-0.889019962428420,
-0.884990445619695,-0.880893533362157,-0.876729537651535,-0.872498775592224,
-0.868201569373136,-0.863838246243161,-0.859409138486249,-0.854914583396103,
-0.850354923250496,-0.845730505285199,-0.841041681667547,-0.836288809469610,
-0.831472250641009,-0.826592371981345,-0.821649545112273,-0.816644146449195,
-0.811576557172598,-0.806447163199026,-0.801256355151689,-0.796004528330718,
-0.790692082683057,-0.785319422772011,-0.779886957746433,-0.774395101309568,
-0.768844271687545,-0.763234891597532,-0.757567388215540,-0.751842193143893,
-0.746059742378363,-0.740220476274964,-0.734324839516416,-0.728373281078284,
-0.722366254194787,-0.716304216324278,-0.710187629114411,-0.704016958366984,
-0.697792674002466,-0.691515250024207,-0.685185164482349,-0.678802899437414,
-0.672368940923594,-0.665883778911740,-0.659347907272048,-0.652761823736449,
-0.646126029860702,-0.639441030986202,-0.632707336201496,-0.625925458303513,
-0.619095913758510,-0.612219222662748,-0.605295908702876,-0.598326499116059,
-0.591311524649818,-0.584251519521620,-0.577147021378189,-0.569998571254564,
-0.562806713532899,-0.555571995901003,-0.548294969310635,-0.540976187935545,
-0.533616209129268,-0.526215593382686,-0.518774904281343,-0.511294708462519,
-0.503775575572088,-0.496218078221131,-0.488622791942331,-0.480990295146144,
-0.473321169076753,-0.465615997767798,-0.457875367997909,-0.450099869246009,
-0.442290093646434,-0.434446635943832,-0.426570093447874,-0.418661065987767,
-0.410720155866573,-0.402747967815342,-0.394745108947060,-0.386712188710413,
-0.378649818843379,-0.370558613326638,-0.362439188336816,-0.354292162199562,
-0.346118155342458,-0.337917790247774,-0.329691691405061,-0.321440485263594,
-0.313164800184666,-0.304865266393738,-0.296542515932440,-0.288197182610443,
-0.279829901957189,-0.271441311173496,-0.263032049083029,-0.254602756083655,
-0.246154074098670,-0.237686646527917,-0.229201118198791,-0.220698135317126,
-0.212178345417989,-0.203642397316366,-0.195090941057754,-0.186524627868655,
-0.177944110106985,-0.169350041212391,-0.160743075656494,-0.152123868893043,
-0.143493077308004,-0.134851358169572,-0.126199369578118,-0.117537770416070,
-0.108867220297738,-0.100188379519084,-0.0915019090074347,-0.0828084702711504,
-0.0741087253492489,-0.0654033367609885,-0.0566929674554144,-0.0479782807608725,
-0.0392599403344955,-0.0305386101116610,-0.0218149542554314,-0.0130896371059753,
-0.00436332312997498,0.00436332312997498,0.0130896371059753,0.0218149542554314,0.03053861
01116610,0.0392599403344955,0.0479782807608725,0.0566929674554144,0.0654033367609885,0.07
41087253492489,0.0828084702711504,0.0915019090074347,0.100188379519084,0.108867220297738,
0.117537770416070,0.126199369578118,0.134851358169572,0.143493077308004,0.152123868893043
,0.160743075656494,0.169350041212391,0.177944110106985,0.186524627868655,0.19509094105775
4,0.203642397316366,0.212178345417989,0.220698135317126,0.229201118198791,0.2376866465279
17,0.246154074098670,0.254602756083655,0.263032049083029,0.271441311173496,0.279829901957
189,0.288197182610443,0.296542515932440,0.304865266393738,0.313164800184666,0.32144048526
3594,0.329691691405061,0.337917790247774,0.346118155342458,0.354292162199562,0.3624391883

36816,0.370558613326638,0.378649818843379,0.386712188710413,0.394745108947060,0.402747967
815342,0.410720155866573,0.418661065987767,0.426570093447874,0.434446635943832,0.44229009
3646434,0.450099869246009,0.457875367997909,0.465615997767798,0.473321169076753,0.4809902
95146144,0.488622791942331,0.496218078221131,0.503775575572088,0.511294708462519,0.518774
904281343,0.526215593382686,0.533616209129268,0.540976187935545,0.548294969310635,0.55557
1995901003,0.562806713532899,0.569998571254564,0.577147021378189,0.584251519521620,0.5913
11524649818,0.598326499116059,0.605295908702876,0.612219222662748,0.619095913758510,0.625
925458303513,0.632707336201496,0.639441030986202,0.646126029860702,0.652761823736449,0.65
9347907272048,0.665883778911740,0.672368940923594,0.678802899437414,0.685185164482349,0.6
91515250024207,0.697792674002466,0.704016958366984,0.710187629114411,0.716304216324278,0.
722366254194787,0.728373281078284,0.734324839516416,0.740220476274964,0.746059742378363,0
.751842193143893,0.757567388215540,0.763234891597532,0.768844271687545,0.774395101309568,
0.779886957746433,0.785319422772011,0.790692082683057,0.796004528330718,0.801256355151689
,0.806447163199026,0.811576557172598,0.816644146449195,0.821649545112273,0.82659237198134
5,0.831472250641009,0.836288809469610,0.841041681667547,0.845730505285199,0.8503549232504
96,0.854914583396103,0.859409138486249,0.863838246243161,0.868201569373136,0.872498775592
224,0.876729537651535,0.880893533362157,0.884990445619695,0.889019962428420,0.89298177692
5025,0.896875587401997,0.900701097330594,0.904458015383423,0.908146055456629,0.9117649366
91682,0.915314383496764,0.918794125567759,0.922203897908836,0.925543440852630,0.928812500
080015,0.932010826639476,0.935138176966061,0.938194312899936,0.941179001704516,0.94409201
6084195,0.946933134201647,0.949702139694729,0.952398821692952,0.955022974833542,0.9575743
99277075,0.960052900722704,0.962458290422947,0.964790385198066,0.967049007450013,0.969233
985175961,0.971345151981396,0.973382347092792,0.975345415369854,0.977234207317332,0.97904
8579096406,0.980788392535642,0.982453515141510,0.984043820108476,0.985559186328660,0.9869
99498401058,0.988364646640328,0.989654527085148,0.990869041506127,0.992008097413289,0.993
071608063119,0.994059492465161,0.994971675388194,0.995808087365956,0.996568664702438,0.99
7253349476731,0.997862089547437,0.998394838556645,0.998851555933453,0.999232206897066,0.9
99536762459439,0.999765199427487,0.999917500404850,0.999993653793219,0.999993653793219,0.
999917500404850,0.999765199427487,0.999536762459439,0.999232206897066,0.998851555933453,0
.998394838556645,0.997862089547437,0.997253349476731,0.996568664702438,0.995808087365956,
0.994971675388194,0.994059492465161,0.993071608063119,0.992008097413289,0.990869041506127
,0.989654527085148,0.988364646640328,0.986999498401058,0.985559186328660,0.98404382010847
6,0.982453515141510,0.980788392535642,0.979048579096406,0.977234207317332,0.9753454153698
54,0.973382347092792,0.971345151981396,0.969233985175961,0.967049007450013,0.964790385198
066,0.962458290422947,0.960052900722704,0.957574399277075,0.955022974833542,0.95239882169
2952,0.949702139694729,0.946933134201647,0.944092016084195,0.941179001704516,0.9381943128
99936,0.935138176966061,0.932010826639476,0.928812500080015,0.925543440852630,0.922203897
908836,0.918794125567759,0.915314383496764,0.911764936691682,0.908146055456629,0.90445801
5383423,0.900701097330594,0.896875587401997,0.892981776925025,0.889019962428420,0.8849904
45619695,0.880893533362157,0.876729537651535,0.872498775592224,0.868201569373136,0.863838
246243161,0.859409138486249,0.854914583396103,0.850354923250496,0.845730505285199,0.84104
1681667547,0.836288809469610,0.831472250641009,0.826592371981345,0.821649545112273,0.8166
44146449195,0.811576557172598,0.806447163199026,0.801256355151689,0.796004528330718,0.790
692082683057,0.785319422772011,0.779886957746433,0.774395101309568,0.768844271687545,0.76
3234891597532,0.757567388215540,0.751842193143893,0.746059742378363,0.740220476274964,0.7
34324839516416,0.728373281078284,0.722366254194787,0.716304216324278,0.710187629114411,0.
704016958366984,0.697792674002466,0.691515250024207,0.685185164482349,0.678802899437414,0
.672368940923594,0.665883778911740,0.659347907272048,0.652761823736449,0.646126029860702,
0.639441030986202,0.632707336201496,0.625925458303513,0.619095913758510,0.612219222662748
,0.605295908702876,0.598326499116059,0.591311524649818,0.584251519521620,0.57714702137818
9,0.569998571254564,0.562806713532899,0.555571995901003,0.548294969310635,0.5409761879355
45,0.533616209129268,0.526215593382686,0.518774904281343,0.511294708462519,0.503775575572
088,0.496218078221131,0.488622791942331,0.480990295146144,0.473321169076753,0.46561599776
7798,0.457875367997909,0.450099869246009,0.442290093646434,0.434446635943832,0.4265700934
47874,0.418661065987767,0.410720155866573,0.402747967815342,0.394745108947060,0.386712188
710413,0.378649818843379,0.370558613326638,0.362439188336816,0.354292162199562,0.34611815

5342458,0.337917790247774,0.329691691405061,0.321440485263594,0.313164800184666,0.3048652 ↵
66393738,0.296542515932440,0.288197182610443,0.279829901957189,0.271441311173496,0.263032 ↵
049083029,0.254602756083655,0.246154074098670,0.237686646527917,0.229201118198791,0.22069 ↵
8135317126,0.212178345417989,0.203642397316366,0.195090941057754,0.186524627868655,0.1779 ↵
44110106985,0.169350041212391,0.160743075656494,0.152123868893043,0.143493077308004,0.134 ↵
851358169572,0.126199369578118,0.117537770416070,0.108867220297738,0.100188379519084,0.09 ↵
15019090074347,0.0828084702711504,0.0741087253492489,0.0654033367609885,0.056692967455414 ↵
4,0.0479782807608725,0.0392599403344955,0.0305386101116610,0.0218149542554314,0.013089637 ↵
1059753,0.00436332312997498,-0.999993653793219,-0.999917500404850,-0.999765199427487, ↵
-0.999536762459439,-0.999232206897066,-0.998851555933453,-0.998394838556645, ↵
-0.997862089547437,-0.997253349476731,-0.996568664702438,-0.995808087365956, ↵
-0.994971675388194,-0.994059492465161,-0.993071608063119,-0.992008097413289, ↵
-0.990869041506127,-0.989654527085148,-0.988364646640328,-0.986999498401058, ↵
-0.985559186328660,-0.984043820108476,-0.982453515141510,-0.980788392535642, ↵
-0.979048579096406,-0.977234207317332,-0.975345415369854,-0.973382347092792, ↵
-0.971345151981396,-0.969233985175961,-0.967049007450013,-0.964790385198066, ↵
-0.962458290422947,-0.960052900722704,-0.957574399277075,-0.955022974833542, ↵
-0.952398821692952,-0.949702139694729,-0.946933134201647,-0.944092016084195, ↵
-0.941179001704516,-0.938194312899936,-0.935138176946061,-0.932010826639476, ↵
-0.928812500080015,-0.925543440852630,-0.922203897908836,-0.918794125567759, ↵
-0.915314383496764,-0.911764936691682,-0.908146055456629,-0.904458015383423, ↵
-0.900701097330594,-0.896875587401997,-0.892981776925025,-0.889019962428420, ↵
-0.884990445619695,-0.880893533362157,-0.876729537651535,-0.872498775592224, ↵
-0.868201569373136,-0.863838246243161,-0.859409138486249,-0.854914583396103, ↵
-0.850354923250496,-0.845730505285199,-0.841041681667547,-0.836288809469610, ↵
-0.831472250641009,-0.826592371981345,-0.821649545112273,-0.816644146449195, ↵
-0.811576557172598,-0.806447163199026,-0.801256355151689,-0.796004528330718, ↵
-0.790692082683057,-0.785319422772011,-0.779886957746433,-0.774395101309568, ↵
-0.768844271687545,-0.763234891597532,-0.757567388215540,-0.751842193143893, ↵
-0.746059742378363,-0.740220476274964,-0.734324839516416,-0.728373281078284, ↵
-0.722366254194787,-0.716304216324278,-0.710187629114411,-0.704016958366984, ↵
-0.697792674002466,-0.691515250024207,-0.685185164482349,-0.678802899437414, ↵
-0.672368940923594,-0.665883778911740,-0.659347907272048,-0.652761823736449, ↵
-0.646126029860702,-0.639441030986202,-0.632707336201496,-0.625925458303513, ↵
-0.619095913758510,-0.612219222662748,-0.605295908702876,-0.598326499116059, ↵
-0.591311524649818,-0.584251519521620,-0.577147021378189,-0.569998571254564, ↵
-0.562806713532899,-0.555571995901003,-0.548294969310635,-0.540976187935545, ↵
-0.533616209129268,-0.526215593382686,-0.518774904281343,-0.511294708462519, ↵
-0.503775575572088,-0.496218078221131,-0.488622791942331,-0.480990295146144, ↵
-0.473321169076753,-0.465615997767798,-0.457875367997909,-0.450099869246009, ↵
-0.442290093646434,-0.434446635943832,-0.426570093447874,-0.418661065987767, ↵
-0.410720155866573,-0.402747967815342,-0.394745108947060,-0.386712188710413, ↵
-0.378649818843379,-0.370558613326638,-0.362439188336816,-0.354292162199562, ↵
-0.346118155342458,-0.337917790247774,-0.329691691405061,-0.321440485263594, ↵
-0.313164800184666,-0.304865266393738,-0.296542515932440,-0.288197182610443, ↵
-0.279829901957189,-0.271441311173496,-0.263032049083029,-0.254602756083655, ↵
-0.246154074098670,-0.237686646527917,-0.229201118198791,-0.220698135317126, ↵
-0.212178345417989,-0.203642397316366,-0.195090941057754,-0.186524627868655, ↵
-0.177944110106985,-0.169350041212391,-0.160743075656494,-0.152123868893043, ↵
-0.143493077308004,-0.134851358169572,-0.126199369578118,-0.117537770416070, ↵
-0.108867220297738,-0.100188379519084,-0.0915019090074347,-0.0828084702711504, ↵
-0.0741087253492489,-0.0654033367609885,-0.0566929674554144,-0.0479782807608725, ↵
-0.0392599403344955,-0.0305386101116610,-0.0218149542554314,-0.0130896371059753, ↵
-0.00436332312997498,0.00436332312997498,0.0130896371059753,0.0218149542554314,0.03053861 ↵
01116610,0.0392599403344955,0.0479782807608725,0.0566929674554144,0.0654033367609885,0.07 ↵
41087253492489,0.0828084702711504,0.0915019090074347,0.100188379519084,0.108867220297738, ↵

0.117537770416070,0.126199369578118,0.134851358169572,0.143493077308004,0.152123868893043
,0.160743075656494,0.169350041212391,0.177944110106985,0.186524627868655,0.19509094105775
4,0.203642397316366,0.212178345417989,0.220698135317126,0.229201118198791,0.2376866465279
17,0.246154074098670,0.254602756083655,0.263032049083029,0.271441311173496,0.279829901957
189,0.288197182610443,0.296542515932440,0.304865266393738,0.313164800184666,0.32144048526
3594,0.329691691405061,0.337917790247774,0.346118155342458,0.354292162199562,0.3624391883
36816,0.370558613326638,0.378649818843379,0.386712188710413,0.394745108947060,0.402747967
815342,0.410720155866573,0.418661065987767,0.426570093447874,0.434446635943832,0.44229009
3646434,0.450099869246009,0.457875367997909,0.465615997767798,0.473321169076753,0.4809902
95146144,0.488622791942331,0.496218078221131,0.503775575572088,0.511294708462519,0.518774
904281343,0.526215593382686,0.533616209129268,0.540976187935545,0.548294969310635,0.55557
1995901003,0.562806713532899,0.569998571254564,0.577147021378189,0.584251519521620,0.5913
11524649818,0.598326499116059,0.605295908702876,0.612219222662748,0.619095913758510,0.625
925458303513,0.632707336201496,0.639441030986202,0.646126029860702,0.652761823736449,0.65
9347907272048,0.665883778911740,0.672368940923594,0.678802899437414,0.685185164482349,0.6
91515250024207,0.697792674002466,0.704016958366984,0.710187629114411,0.716304216324278,0.
722366254194787,0.728373281078284,0.734324839516416,0.740220476274964,0.746059742378363,0
.751842193143893,0.757567388215540,0.763234891597532,0.768844271687545,0.774395101309568,
0.779886957746433,0.785319422772011,0.790692082683057,0.796004528330718,0.801256355151689
,0.806447163199026,0.811576557172598,0.816644146449195,0.821649545112273,0.82659237198134
5,0.831472250641009,0.836288809469610,0.841041681667547,0.845730505285199,0.8503549232504
96,0.854914583396103,0.859409138486249,0.863838246243161,0.868201569373136,0.872498775592
224,0.876729537651535,0.880893533362157,0.884990445619695,0.889019962428420,0.89298177692
5025,0.896875587401997,0.900701097330594,0.904458015383423,0.908146055456629,0.9117649366
91682,0.915314383496764,0.918794125567759,0.922203897908836,0.925543440852630,0.928812500
080015,0.932010826639476,0.935138176966061,0.938194312899936,0.941179001704516,0.94409201
6084195,0.946933134201647,0.949702139694729,0.952398821692952,0.955022974833542,0.9575743
99277075,0.960052900722704,0.962458290422947,0.964790385198066,0.967049007450013,0.969233
985175961,0.971345151981396,0.973382347092792,0.975345415369854,0.977234207317332,0.97904
8579096406,0.980788392535642,0.982453515141510,0.984043820108476,0.985559186328660,0.9869
99498401058,0.988364646640328,0.989654527085148,0.990869041506127,0.992008097413289,0.993
071608063119,0.994059492465161,0.994971675388194,0.995808087365956,0.996568664702438,0.99
7253349476731,0.997862089547437,0.998394838556645,0.998851555933453,0.999232206897066,0.9
99536762459439,0.999765199427487,0.999917500404850,0.999993653793219,0.999993653793219,0.
999917500404850,0.999765199427487,0.999536762459439,0.999232206897066,0.998851555933453,0
.998394838556645,0.997862089547437,0.997253349476731,0.996568664702438,0.995808087365956,
0.994971675388194,0.994059492465161,0.993071608063119,0.992008097413289,0.990869041506127
,0.989654527085148,0.988364646640328,0.986999498401058,0.985559186328660,0.98404382010847
6,0.982453515141510,0.980788392535642,0.979048579096406,0.977234207317332,0.9753454153698
54,0.973382347092792,0.971345151981396,0.969233985175961,0.967049007450013,0.964790385198
066,0.962458290422947,0.960052900722704,0.957574399277075,0.955022974833542,0.95239882169
2952,0.949702139694729,0.946933134201647,0.944092016084195,0.941179001704516,0.9381943128
99936,0.935138176966061,0.932010826639476,0.928812500080015,0.925543440852630,0.922203897
908836,0.918794125567759,0.915314383496764,0.911764936691682,0.908146055456629,0.90445801
5383423,0.900701097330594,0.896875587401997,0.892981776925025,0.889019962428420,0.8849904
45619695,0.880893533362157,0.876729537651535,0.872498775592224,0.868201569373136,0.863838
246243161,0.859409138486249,0.854914583396103,0.850354923250496,0.845730505285199,0.84104
1681667547,0.836288809469610,0.831472250641009,0.826592371981345,0.821649545112273,0.8166
44146449195,0.811576557172598,0.806447163199026,0.801256355151689,0.796004528330718,0.790
692082683057,0.785319422772011,0.779886957746433,0.774395101309568,0.768844271687545,0.76
3234891597532,0.757567388215540,0.751842193143893,0.746059742378363,0.740220476274964,0.7
34324839516416,0.728373281078284,0.722366254194787,0.716304216324278,0.710187629114411,0.
704016958366984,0.697792674002466,0.691515250024207,0.685185164482349,0.678802899437414,0
.672368940923594,0.665883778911740,0.659347907272048,0.652761823736449,0.646126029860702,
0.639441030986202,0.632707336201496,0.625925458303513,0.619095913758510,0.612219222662748
,0.605295908702876,0.598326499116059,0.591311524649818,0.584251519521620,0.57714702137818

9,0.569998571254564,0.562806713532899,0.555571995901003,0.548294969310635,0.5409761879355 ↙
45,0.533616209129268,0.526215593382686,0.518774904281343,0.511294708462519,0.503775575572 ↙
088,0.496218078221131,0.488622791942331,0.480990295146144,0.473321169076753,0.46561599776 ↙
7798,0.457875367997909,0.450099869246009,0.442290093646434,0.434446635943832,0.4265700934 ↙
47874,0.418661065987767,0.410720155866573,0.402747967815342,0.394745108947060,0.386712188 ↙
710413,0.378649818843379,0.370558613326638,0.362439188336816,0.354292162199562,0.34611815 ↙
5342458,0.337917790247774,0.329691691405061,0.321440485263594,0.313164800184666,0.3048652 ↙
66393738,0.296542515932440,0.288197182610443,0.279829901957189,0.271441311173496,0.263032 ↙
049083029,0.254602756083655,0.246154074098670,0.237686646527917,0.229201118198791,0.22069 ↙
8135317126,0.212178345417989,0.203642397316366,0.195090941057754,0.186524627868655,0.1779 ↙
44110106985,0.169350041212391,0.160743075656494,0.152123868893043,0.143493077308004,0.134 ↙
851358169572,0.126199369578118,0.117537770416070,0.108867220297738,0.100188379519084,0.09 ↙
15019090074347,0.0828084702711504,0.0741087253492489,0.0654033367609885,0.056692967455414 ↙
4,0.0479782807608725,0.0392599403344955,0.0305386101116610,0.0218149542554314,0.013089637 ↙
1059753,0.00436332312997498,-0.00436332312997498,-0.0130896371059753,-0.0218149542554314, ↙
-0.0305386101116610,-0.0392599403344955,-0.0479782807608725,-0.0566929674554144, ↙
-0.0654033367609885,-0.0741087253492489,-0.0828084702711504,-0.0915019090074347, ↙
-0.100188379519084,-0.108867220297738,-0.117537770416070,-0.126199369578118, ↙
-0.134851358169572,-0.143493077308004,-0.152123868893043,-0.160743075656494, ↙
-0.169350041212391,-0.177944110106985,-0.186524627868655,-0.195090941057754, ↙
-0.203642397316366,-0.212178345417989,-0.220698135317126,-0.229201118198791, ↙
-0.237686646527917,-0.246154074098670,-0.254602756083655,-0.263032049083029, ↙
-0.271441311173496,-0.279829901957189,-0.288197182610443,-0.296542515932440, ↙
-0.304865266393738,-0.313164800184666,-0.321440485263594,-0.329691691405061, ↙
-0.337917790247774,-0.346118155342458,-0.354292162199562,-0.362439188336816, ↙
-0.370558613326638,-0.378649818843379,-0.386712188710413,-0.394745108947060, ↙
-0.402747967815342,-0.410720155866573,-0.418661065987767,-0.426570093447874, ↙
-0.434446635943832,-0.442290093646434,-0.450099869246009,-0.457875367997909, ↙
-0.465615997767798,-0.473321169076753,-0.480990295146144,-0.488622791942331, ↙
-0.496218078221131,-0.503775575572088,-0.511294708462519,-0.518774904281343, ↙
-0.526215593382686,-0.533616209129268,-0.540976187935545,-0.548294969310635, ↙
-0.555571995901003,-0.562806713532899,-0.569998571254564,-0.577147021378189, ↙
-0.584251519521620,-0.591311524649818,-0.598326499116059,-0.605295908702876, ↙
-0.612219222662748,-0.619095913758510,-0.625925458303513,-0.632707336201496, ↙
-0.639441030986202,-0.646126029860702,-0.652761823736449,-0.659347907272048, ↙
-0.665883778911740,-0.672368940923594,-0.678802899437414,-0.685185164482349, ↙
-0.691515250024207,-0.697792674002466,-0.704016958366984,-0.710187629114411, ↙
-0.716304216324278,-0.722366254194787,-0.728373281078284,-0.734324839516416, ↙
-0.740220476274964,-0.746059742378363,-0.751842193143893,-0.757567388215540, ↙
-0.763234891597532,-0.768844271687545,-0.774395101309568,-0.779886957746433, ↙
-0.785319422772011,-0.790692082683057,-0.796004528330718,-0.801256355151689, ↙
-0.806447163199026,-0.811576557172598,-0.816644146449195,-0.821649545112273, ↙
-0.826592371981345,-0.831472250641009,-0.836288809469610,-0.841041681667547, ↙
-0.845730505285199,-0.850354923250496,-0.854914583396103,-0.859409138486249, ↙
-0.863838246243161,-0.868201569373136,-0.872498775592224,-0.876729537651535, ↙
-0.880893533362157,-0.884990445619695,-0.889019962428420,-0.892981776925025, ↙
-0.896875587401997,-0.900701097330594,-0.904458015383423,-0.908146055456629, ↙
-0.911764936691682,-0.915314383496764,-0.918794125567759,-0.922203897908836, ↙
-0.925543440852630,-0.928812500080015,-0.932010826639476,-0.935138176966061, ↙
-0.938194312899936,-0.941179001704516,-0.944092016084195,-0.946933134201647, ↙
-0.949702139694729,-0.952398821692952,-0.955022974833542,-0.957574399277075, ↙
-0.960052900722704,-0.962458290422947,-0.964790385198066,-0.967049007450013, ↙
-0.969233985175961,-0.971345151981396,-0.973382347092792,-0.975345415369854, ↙
-0.977234207317332,-0.979048579096406,-0.980788392535642,-0.982453515141510, ↙
-0.984043820108476,-0.985559186328660,-0.986999498401058,-0.988364646640328, ↙
-0.989654527085148,-0.990869041506127,-0.992008097413289,-0.993071608063119, ↙

```matlab
    -0.994059492465161,-0.994971675388194,-0.995808087365956,-0.996568664702438,↙
    -0.997253349476731,-0.997862089547437,-0.998394838556645,-0.998851555933453,↙
    -0.999232206897066,-0.999536762459439,-0.999765199427487,-0.999917500404850,↙
    -0.999993653793219]';
geom=[R2];

%Names for the geometric objects
ns=(char('R2'))';

%set formula
sf='R2';

%create geometry
g=decsg(geom,sf,ns);

%create geometry model
model = createpde;

%include the geometry in the model and view the geometry
geometryFromEdges(model,g);
pdegplot(model, 'Edgelabels', 'on')



%Defining boundary conditions for the scalar problem
% applyBoundaryCondition(model, 'neumann', 'Edge', 1:13, 'g', 1);
% applyBoundaryCondition(model, 'neumann', 'Edge', 67:70, 'g', 1);
% applyBoundaryCondition(model, 'neumann', 'Edge', 23:49, 'g', -1);% q = 0 by default
% applyBoundaryCondition(model, 'neumann', 'Edge', 14:22, 'g',0);
% applyBoundaryCondition(model, 'neumann', 'Edge', 58:71, 'g', 1);
% applyBoundaryCondition(model, 'neumann', 'Edge', 50:57, 'g',0);
% applyBoundaryCondition(model, 'neumann', 'Edge', 1:10, 'g', 1);
% % applyBoundaryCondition(model, 'neumann', 'Edge', 67:70, 'g', 1);
% applyBoundaryCondition(model, 'neumann', 'Edge', 26:46, 'g', -1);% q = 0 by default
% applyBoundaryCondition(model, 'neumann', 'Edge', 11:25, 'g',0);
% applyBoundaryCondition(model, 'neumann', 'Edge', 61:71, 'g', 1);
% applyBoundaryCondition(model, 'neumann', 'Edge', 47:60, 'g',0);
applyBoundaryCondition(model, 'neumann', 'Edge', 536:544, 'g',1);
applyBoundaryCondition(model, 'neumann', 'Edge', 545:720, 'g',0);
applyBoundaryCondition(model, 'neumann', 'Edge', 176:184, 'g',-1);
applyBoundaryCondition(model, 'neumann', 'Edge', 1:175, 'g',0);
applyBoundaryCondition(model, 'neumann', 'Edge', 185:535, 'g',0);


%Edges 2 and 4 need functions that perform the linear interpolation. Each
%edge can use the same function that returns the value u(x,y)=52+20x
%you can implement this simple interpolation in an anonymous function

% myufunction =@(location, state)52+20*location.x;
% applyBoundaryCondition(model,'dirichlet', 'Edge', [2,4], 'u', myufunction,↙
'Vectorized', 'on');

%Solve an elliptic PDE with these boundary conditions, using the parameters
%c = 1, a = 0, and f=10. Because the shorter rectangular side has length
%0.8, to ensure that the mesh is not too coarse choose a maxmum mesh size
%Hmax = 0.1
```

```matlab
specifyCoefficients(model, 'm', 0, 'd', 0, 'c', 1, 'a', 0, 'f', 0);
generateMesh(model, 'Hmax', 0.006);
results = solvepde(model);
u = results.NodalSolution;
%% Normalize Xgradient data
xgrad=results.XGradients;
x=model.Mesh.Nodes(1,:)';
y=model.Mesh.Nodes(2,:)';
ref=zeros(size(y));
xdiff=abs(x)-abs(ref);%Finds difference between 0 and all x values
ydiff=abs(y)-abs(ref);%Finds difference between 0 and all y values
[center, centeridx]=min(abs(xdiff)+abs(ydiff)); %Finds min of both x, y difference and ↙
names as center
normal=xgrad(centeridx);
xgradn=abs(xgrad./normal);
new=xgradn(centeridx);
pdeplot(model, 'XYData', xgradn,'Contour', 'on' , 'Colormap', 'jet', 'Levels', [.9;0.95;.↙
98;0.99;1.0;1.01;1.05;1.1])

% contour(x,y,xgradn',[.51,.65,.85,1.0,1.2,2.5], 'showtext', 'on')
S=std(xgradn);
M=mean(xgradn);
Cv=S/M;

% [gu] = gradient(un);
% pdeplot(model, 'XYData', gu);

ylim([-1.0 1.0])
xlim([-1.0 1.0])
```

A.2 Code to Derive Optimized Multipoint Electrode Weight Function Using PDE Toolbox

```
%PDE Nonconstant Boundary Conditions Solver with unique shapes

R1=↙
[2,144,1,0.999048221581858,0.996194698091746,0.991444861373810,0.984807753012208,0.976296↙
007119933,0.965925826289068,0.953716950748227,0.939692620785908,0.923879532511287,0.90630↙
7787036650,0.887010833178222,0.866025403784439,0.843391445812886,0.819152044288992,0.7933↙
53340291235,0.766044443118978,0.737277336810124,0.707106781186548,0.675590207615660,0.642↙
787609686539,0.608761429008721,0.573576436351046,0.537299608346824,0.500000000000000,0.46↙
1748613235034,0.422618261740699,0.382683432365090,0.342020143325669,0.300705799504273,0.2↙
58819045102521,0.216439613938103,0.173648177666930,0.130526192220052,0.0871557427476581,0↙
.0436193873653360,6.12323399573677e-17,-0.0436193873653359,-0.0871557427476580,↙
-0.130526192220051,-0.173648177666930,-0.216439613938103,-0.258819045102521,↙
-0.300705799504273,-0.342020143325669,-0.382683432365090,-0.422618261740699,↙
-0.461748613235034,-0.500000000000000,-0.537299608346824,-0.573576436351046,↙
-0.608761429008721,-0.642787609686539,-0.675590207615660,-0.707106781186548,↙
-0.737277336810124,-0.766044443118978,-0.793353340291235,-0.819152044288992,↙
-0.843391445812886,-0.866025403784439,-0.887010833178222,-0.906307787036650,↙
-0.923879532511287,-0.939692620785908,-0.953716950748227,-0.965925826289068,↙
-0.976296007119933,-0.984807753012208,-0.991444861373810,-0.996194698091746,↙
-0.999048221581858,-1,-0.999048221581858,-0.996194698091746,-0.991444861373811,↙
-0.984807753012208,-0.976296007119933,-0.965925826289068,-0.953716950748227,↙
-0.939692620785908,-0.923879532511287,-0.906307787036650,-0.887010833178222,↙
-0.866025403784439,-0.843391445812886,-0.819152044288992,-0.793353340291235,↙
-0.766044443118978,-0.737277336810124,-0.707106781186548,-0.675590207615660,↙
-0.642787609686540,-0.608761429008721,-0.573576436351046,-0.537299608346824,↙
-0.500000000000000,-0.461748613235034,-0.422618261740700,-0.382683432365090,↙
-0.342020143325669,-0.300705799504273,-0.258819045102521,-0.216439613938104,↙
-0.173648177666930,-0.130526192220052,-0.0871557427476583,-0.0436193873653361,↙
-1.83697019872103e-↙
16,0.0436193873653358,0.0871557427476579,0.130526192220051,0.173648177666930,0.2164396139↙
38102,0.258819045102520,0.300705799504273,0.342020143325669,0.382683432365090,0.422618261↙
740699,0.461748613235033,0.499999999999999,0.537299608346824,0.573576436351046,0.60876142↙
9008721,0.642787609686539,0.675590207615660,0.707106781186547,0.737277336810124,0.7660444↙
43118978,0.793353340291235,0.819152044288992,0.843391445812886,0.866025403784439,0.887010↙
833178221,0.906307787036650,0.923879532511287,0.939692620785908,0.953716950748227,0.96592↙
5826289068,0.976296007119933,0.984807753012208,0.991444861373810,0.996194698091746,0.9990↙
48221581858,0,0.0436193873653360,0.0871557427476582,0.130526192220052,0.173648177666930,0↙
.216439613938103,0.258819045102521,0.300705799504273,0.342020143325669,0.382683432365090,↙
0.422618261740699,0.461748613235034,0.500000000000000,0.537299608346824,0.573576436351046↙
,0.608761429008721,0.642787609686539,0.675590207615660,0.707106781186548,0.73727733681012↙
4,0.766044443118978,0.793353340291235,0.819152044288992,0.843391445812886,0.8660254037844↙
39,0.887010833178222,0.906307787036650,0.923879532511287,0.939692620785908,0.953716950748↙
227,0.965925826289068,0.976296007119933,0.984807753012208,0.991444861373810,0.99619469809↙
1746,0.999048221581858,1,0.999048221581858,0.996194698091746,0.991444861373811,0.98480775↙
3012208,0.976296007119934,0.965925826289068,0.953716950748227,0.939692620785908,0.9238795↙
32511287,0.906307787036650,0.887010833178222,0.866025403784439,0.843391445812886,0.819152↙
044288992,0.793353340291235,0.766044443118978,0.737277336810124,0.707106781186548,0.67559↙
0207615660,0.642787609686540,0.608761429008721,0.573576436351046,0.537299608346824,0.5000↙
00000000000,0.461748613235034,0.422618261740700,0.382683432365090,0.342020143325669,0.300↙
705799504273,0.258819045102521,0.216439613938103,0.173648177666930,0.130526192220052,0.08↙
71557427476582,0.0436193873653361,1.22464679914735e-16,-0.0436193873653358,↙
-0.0871557427476579,-0.130526192220051,-0.173648177666930,-0.216439613938103,↙
-0.258819045102520,-0.300705799504273,-0.342020143325669,-0.382683432365090,↙
-0.422618261740699,-0.461748613235034,-0.500000000000000,-0.537299608346824,↙
-0.573576436351046,-0.608761429008720,-0.642787609686539,-0.675590207615660,↙
-0.707106781186548,-0.737277336810124,-0.766044443118978,-0.793353340291235,↙
```

```matlab
-0.819152044288992,-0.843391445812886,-0.866025403784439,-0.887010833178222, ↙
-0.906307787036650,-0.923879532511287,-0.939692620785908,-0.953716950748227, ↙
-0.965925826289068,-0.976296007119933,-0.984807753012208,-0.991444861373810, ↙
-0.996194698091746,-0.999048221581858,-1,-0.999048221581858,-0.996194698091746, ↙
-0.991444861373811,-0.984807753012208,-0.976296007119934,-0.965925826289068, ↙
-0.953716950748227,-0.939692620785908,-0.923879532511287,-0.906307787036650, ↙
-0.887010833178222,-0.866025403784439,-0.843391445812886,-0.819152044288992, ↙
-0.793353340291235,-0.766044443118978,-0.737277336810124,-0.707106781186548, ↙
-0.675590207615661,-0.642787609686540,-0.608761429008721,-0.573576436351047, ↙
-0.537299608346823,-0.500000000000000,-0.461748613235034,-0.422618261740700, ↙
-0.382683432365090,-0.342020143325669,-0.300705799504273,-0.258819045102521, ↙
-0.216439613938103,-0.173648177666930,-0.130526192220053,-0.0871557427476583, ↙
-0.0436193873653362]';

geom=[R1];

%Names for the geometric objects
ns=(char('R1'))';

%set formula
sf='R1';

%create geometry
g=decsg(geom,sf,ns);

%create geometry model
model = createpde;

%include the geometry in the model and view the geometry
geometryFromEdges(model,g);
pdegplot(model, 'Edgelabels', 'on')



%Defining boundary conditions for the scalar problem

applyBoundaryCondition(model, 'neumann', 'Edge', 10:11, 'g',-1);
applyBoundaryCondition(model, 'neumann', 'Edge', 1, 'g',-1);
applyBoundaryCondition(model, 'neumann', 'Edge', 144, 'g',-1);
applyBoundaryCondition(model, 'neumann', 'Edge', 134:135, 'g',-1);
applyBoundaryCondition(model, 'neumann', 'Edge', 62:63, 'g',1);
applyBoundaryCondition(model, 'neumann', 'Edge', 72:73, 'g',1);
applyBoundaryCondition(model, 'neumann', 'Edge', 82:83, 'g',1);
applyBoundaryCondition(model, 'neumann', 'Edge', 2:9, 'g',0);
applyBoundaryCondition(model, 'neumann', 'Edge', 12:61, 'g',0);
applyBoundaryCondition(model, 'neumann', 'Edge', 64:71, 'g',0);
applyBoundaryCondition(model, 'neumann', 'Edge', 74:81, 'g',0);
applyBoundaryCondition(model, 'neumann', 'Edge', 84:133, 'g',0);
applyBoundaryCondition(model, 'neumann', 'Edge', 136:143, 'g',0);


%Edges 2 and 4 need functions that perform the linear interpolation. Each
%edge can use the same function that returns the value u(x,y)=52+20x
%you can implement this simple interpolation in an anonymous function

% myufunction =@(location, state)52+20*location.x;
```

```matlab
% applyBoundaryCondition(model,'dirichlet', 'Edge', [2,4], 'u', myufunction, ↙
'Vectorized', 'on');


%Solve an elliptic PDE with these boundary conditions, using the parameters
%c = 1, a = 0, and f=10. Because the shorter rectangular side has length
%0.8, to ensure that the mesh is not too coarse choose a maxmum mesh size
%Hmax = 0.1
specifyCoefficients(model, 'm', 0, 'd', 0, 'c', 1, 'a', 0, 'f', 0);
generateMesh(model, 'Hmax', 0.01);
results = solvepde(model);
u = results.NodalSolution;
%% Normalize Xgradient data
xgrad=results.XGradients;
x=model.Mesh.Nodes(1,:)';
y=model.Mesh.Nodes(2,:)';
ref=zeros(size(y));
xdiff=abs(x)-abs(ref);%Finds difference between 0 and all x values
ydiff=abs(y)-abs(ref);%Finds difference between 0 and all y values
[center, centeridx]=min(abs(xdiff)+abs(ydiff)); %Finds min of both x, y difference and↙
names as center
normal=xgrad(centeridx);
xgradn=abs(xgrad./normal);
new=xgradn(centeridx);
pdeplot(model, 'XYData', xgradn,'Contour', 'on' , 'Colormap', 'jet', 'Levels', [0.6,0.7,↙
0.8, 0.9, 1.0, 1.05, 1.1, 1.2, 1.3])
% contour(x,y,xgradn',[.51,.65,.85,1.0,1.2,2.5], 'showtext', 'on')
S=std(xgradn);
M=mean(xgradn);
Cv=S/M;
ax.XAxis.FontSize = 15;
ax.YAxis.FontSize = 15;
% [gu] = gradient(un);
% pdeplot(model, 'XYData', gu);

ylim([-1.0 1.0])
xlim([-1.0 1.0])
```

A.3 Code to Derive Optimized Arc Electrode Weight Function Using PDE Toolbox

%PDE Nonconstant Boundary Conditions Solver with unique shapes

R1=↙
[2,144,1,0.999048221581858,0.996194698091746,0.991444861373810,0.984807753012208,0.976296↙
007119933,0.965925826289068,0.953716950748227,0.939692620785908,0.923879532511287,0.90630↙
7787036650,0.887010833178222,0.866025403784439,0.843391445812886,0.819152044288992,0.7933↙
53340291235,0.766044443118978,0.737277336810124,0.707106781186548,0.675590207615660,0.642↙
787609686539,0.608761429008721,0.573576436351046,0.537299608346824,0.500000000000000,0.46↙
1748613235034,0.422618261740699,0.382683432365090,0.342020143325669,0.300705799504273,0.2↙
58819045102521,0.216439613938103,0.173648177666930,0.130526192220052,0.0871557427476581,0↙
.0436193873653360,6.12323399573677e-17,-0.0436193873653359,-0.0871557427476580,↙
-0.130526192220051,-0.173648177666930,-0.216439613938103,-0.258819045102521,↙
-0.300705799504273,-0.342020143325669,-0.382683432365090,-0.422618261740699,↙
-0.461748613235034,-0.500000000000000,-0.537299608346824,-0.573576436351046,↙
-0.608761429008721,-0.642787609686539,-0.675590207615660,-0.707106781186548,↙
-0.737277336810124,-0.766044443118978,-0.793353340291235,-0.819152044288992,↙
-0.843391445812886,-0.866025403784439,-0.887010833178222,-0.906307787036650,↙
-0.923879532511287,-0.939692620785908,-0.953716950748227,-0.965925826289068,↙
-0.976296007119933,-0.984807753012208,-0.991444861373810,-0.996194698091746,↙
-0.999048221581858,-1,-0.999048221581858,-0.996194698091746,-0.991444861373811,↙
-0.984807753012208,-0.976296007119933,-0.965925826289068,-0.953716950748227,↙
-0.939692620785908,-0.923879532511287,-0.906307787036650,-0.887010833178222,↙
-0.866025403784439,-0.843391445812886,-0.819152044288992,-0.793353340291235,↙
-0.766044443118978,-0.737277336810124,-0.707106781186548,-0.675590207615660,↙
-0.642787609686540,-0.608761429008721,-0.573576436351046,-0.537299608346824,↙
-0.500000000000000,-0.461748613235034,-0.422618261740700,-0.382683432365090,↙
-0.342020143325669,-0.300705799504273,-0.258819045102521,-0.216439613938104,↙
-0.173648177666930,-0.130526192220052,-0.0871557427476583,-0.0436193873653361,↙
-1.83697019872103e-↙
16,0.0436193873653358,0.0871557427476579,0.130526192220051,0.173648177666930,0.2164396139↙
38102,0.258819045102520,0.300705799504273,0.342020143325669,0.382683432365090,0.422618261↙
740699,0.461748613235033,0.499999999999999,0.537299608346824,0.573576436351046,0.60876142↙
9008721,0.642787609686539,0.675590207615660,0.707106781186547,0.737277336810124,0.7660444↙
43118978,0.793353340291235,0.819152044288992,0.843391445812886,0.866025403784439,0.887010↙
833178221,0.906307787036650,0.923879532511287,0.939692620785908,0.953716950748227,0.96592↙
5826289068,0.976296007119933,0.984807753012208,0.991444861373810,0.996194698091746,0.9990↙
48221581858,0,0.0436193873653360,0.0871557427476582,0.130526192220052,0.173648177666930,0↙
.216439613938103,0.258819045102521,0.300705799504273,0.342020143325669,0.382683432365090,↙
0.422618261740699,0.461748613235034,0.500000000000000,0.537299608346824,0.573576436351046↙
,0.608761429008721,0.642787609686539,0.675590207615660,0.707106781186548,0.73727733681012↙
4,0.766044443118978,0.793353340291235,0.819152044288992,0.843391445812886,0.8660254037844↙
39,0.887010833178222,0.906307787036650,0.923879532511287,0.939692620785908,0.953716950748↙
227,0.965925826289068,0.976296007119933,0.984807753012208,0.991444861373810,0.99619469809↙
1746,0.999048221581858,1,0.999048221581858,0.996194698091746,0.991444861373811,0.98480775↙
3012208,0.976296007119934,0.965925826289068,0.953716950748227,0.939692620785908,0.9238795↙
32511287,0.906307787036650,0.887010833178222,0.866025403784439,0.843391445812886,0.819152↙
044288992,0.793353340291235,0.766044443118978,0.737277336810124,0.707106781186548,0.67559↙
0207615660,0.642787609686540,0.608761429008721,0.573576436351046,0.537299608346824,0.5000↙
00000000000,0.461748613235034,0.422618261740700,0.382683432365090,0.342020143325669,0.300↙
705799504273,0.258819045102521,0.216439613938103,0.173648177666930,0.130526192220052,0.08↙
71557427476582,0.0436193873653361,1.22464679914735e-16,-0.0436193873653358,↙
-0.0871557427476579,-0.130526192220051,-0.173648177666930,-0.216439613938103,↙
-0.258819045102520,-0.300705799504273,-0.342020143325669,-0.382683432365090,↙
-0.422618261740699,-0.461748613235034,-0.500000000000000,-0.537299608346824,↙
-0.573576436351046,-0.608761429008720,-0.642787609686539,-0.675590207615660,↙
-0.707106781186548,-0.737277336810124,-0.766044443118978,-0.793353340291235,↙

```
  -0.819152044288992,-0.843391445812886,-0.866025403784439,-0.887010833178222, ↙
  -0.906307787036650,-0.923879532511287,-0.939692620785908,-0.953716950748227, ↙
  -0.965925826289068,-0.976296007119933,-0.984807753012208,-0.991444861373810, ↙
  -0.996194698091746,-0.999048221581858,-1,-0.999048221581858,-0.996194698091746, ↙
  -0.991444861373811,-0.984807753012208,-0.976296007119934,-0.965925826289068, ↙
  -0.953716950748227,-0.939692620785908,-0.923879532511287,-0.906307787036650, ↙
  -0.887010833178222,-0.866025403784439,-0.843391445812886,-0.819152044288992, ↙
  -0.793353340291235,-0.766044443118978,-0.737277336810124,-0.707106781186548, ↙
  -0.675590207615661,-0.642787609686540,-0.608761429008721,-0.573576436351047, ↙
  -0.537299608346823,-0.500000000000000,-0.461748613235034,-0.422618261740700, ↙
  -0.382683432365090,-0.342020143325669,-0.300705799504273,-0.258819045102521, ↙
  -0.216439613938103,-0.173648177666930,-0.130526192220053,-0.0871557427476583, ↙
  -0.0436193873653362]';


geom=[R1];

%Names for the geometric objects
ns=(char('R1'))';

%set formula
sf='R1';

%create geometry
g=decsg(geom,sf,ns);

%create geometry model
model = createpde;

%include the geometry in the model and view the geometry
geometryFromEdges(model,g);
pdegplot(model, 'Edgelabels', 'on')




%Defining boundary conditions for the scalar problem
% applyBoundaryCondition(model, 'neumann', 'Edge', 1:13, 'g', 1);
% applyBoundaryCondition(model, 'neumann', 'Edge', 67:70, 'g', 1);
% applyBoundaryCondition(model, 'neumann', 'Edge', 23:49, 'g', -1);% q = 0 by default
% applyBoundaryCondition(model, 'neumann', 'Edge', 14:22, 'g',0);
% applyBoundaryCondition(model, 'neumann', 'Edge', 58:71, 'g', 1);
% applyBoundaryCondition(model, 'neumann', 'Edge', 50:57, 'g',0);
% applyBoundaryCondition(model, 'neumann', 'Edge', 1:10, 'g', 1);
% % applyBoundaryCondition(model, 'neumann', 'Edge', 67:70, 'g', 1);
% applyBoundaryCondition(model, 'neumann', 'Edge', 26:46, 'g', -1);% q = 0 by default
% applyBoundaryCondition(model, 'neumann', 'Edge', 11:25, 'g',0);
% applyBoundaryCondition(model, 'neumann', 'Edge', 61:71, 'g', 1);
% applyBoundaryCondition(model, 'neumann', 'Edge', 47:60, 'g',0);
applyBoundaryCondition(model, 'neumann', 'Edge', 119:144, 'g',1/2.26893);
applyBoundaryCondition(model, 'neumann', 'Edge', 1:26, 'g',1/2.26893);
applyBoundaryCondition(model, 'neumann', 'Edge', 47:98, 'g',-1/2.26893);
applyBoundaryCondition(model, 'neumann', 'Edge', 27:46, 'g',0);
applyBoundaryCondition(model, 'neumann', 'Edge', 99:118, 'g',0);


%Edges 2 and 4 need functions that perform the linear interpolation. Each
%edge can use the same function that returns the value u(x,y)=52+20x
```

```matlab
%you can implement this simple interpolation in an anonymous function

% myufunction =@(location, state)52+20*location.x;
% applyBoundaryCondition(model,'dirichlet', 'Edge', [2,4], 'u', myufunction,↙
'Vectorized', 'on');

%Solve an elliptic PDE with these boundary conditions, using the parameters
%c = 1, a = 0, and f=10. Because the shorter rectangular side has length
%0.8, to ensure that the mesh is not too coarse choose a maxmum mesh size
%Hmax = 0.1
specifyCoefficients(model, 'm', 0, 'd', 0, 'c', 1, 'a', 0, 'f', 0);
generateMesh(model, 'Hmax', 0.01);
results = solvepde(model);
u = results.NodalSolution;
%% Normalize Xgradient data
xgrad=results.XGradients;
x=model.Mesh.Nodes(1,:)';
y=model.Mesh.Nodes(2,:)';
ref=zeros(size(y));
xdiff=abs(x)-abs(ref);%Finds difference between 0 and all x values
ydiff=abs(y)-abs(ref);%Finds difference between 0 and all y values
[center, centeridx]=min(abs(xdiff)+abs(ydiff)); %Finds min of both x, y difference and↙
names as center
normal=xgrad(centeridx);
xgradn=xgrad./normal;
new=xgradn(centeridx);
pdeplot(model, 'XYData', xgradn,'Contour', 'on' , 'Colormap', 'jet','Levels', [.9;0.95;.↙
98;0.99;1.0;1.01;1.05;1.1])
% contour(x,y,xgradn',[.51,.65,.85,1.0,1.2,2.5], 'showtext', 'on')
S=std(xgradn);
M=mean(xgradn);
Cv=S/M;

% [gu] = gradient(un);
% pdeplot(model, 'XYData', gu);


ylim([-1.0 1.0])
xlim([-1.0 1.0])
```

A.4 Code to Sort and Process CFD Data Using Weight Function Method

```matlab
%August 17, 2020
%Kade Beck
%Analytic Weighting of Star Data
%% Read Data from Sources
% Reads output table from Star Data with all parameters of interest
% Reads analytic weight function data

clc; clear; close all;
% WeightFunction_two_D_Shi5; %runs analytic weightfunction file
% WeightFunction_Shercliff;
FEMWFNormalizerMP25;
% Rstar=inputdlg('What is the Radius used in the Star CCM+ model?')how can
% I get this to prompt them to put in the radius they used in the model?
SData=readtable('1D MP 15.csv');
% Rstar=inputdlg('What is the Radius used in the Star CCM+ model?')
Rstar=3.0325;
%% Convert Data from Table to Double
SData=table2array(SData);
%% Sort Data to Quandrants to ensure proper matching of Weight Function Values
C1=(SData(:, 7)); %xcoordinates
C2=(SData(:, 8)); %y coordinates
L1=C1 >0; %x coordinates greater than zero test
L2=C2 >0; % y coordinates greater than zero test
Q1= find (L1 ==1 & L2 ==1);  %Extracting the index where true for Q1
Q2= find (L1 ==0 & L2 ==1);  %Extracting the index where true for Q2
Q3= find (L1 ==0 & L2 ==0);  %Extracting the index where true for Q3
Q4= find (L1 ==1 & L2 ==0);  %Extracting the index where true for Q4
SQ1=SData(Q1,:); %Extracting all Star Data for Quandrant 1
SQ2=SData(Q2,:); %Extracting all Star Data for Quandrant 2
SQ3=SData(Q3,:); %Extracting all Star Data for Quandrant 3
SQ4=SData(Q4,:); %Extracting all Star Data for Quandrant 4
SX1=SQ1(:,7)/Rstar;
SY1=SQ1(:,8)/Rstar;
SX2=SQ2(:,7)/Rstar;
SY2=SQ2(:,8)/Rstar;
SX3=SQ3(:,7)/Rstar;
SY3=SQ3(:,8)/Rstar;
SX4=SQ4(:,7)/Rstar;
SY4=SQ4(:,8)/Rstar;
% Xs=table2array(SData(:, [7]))/Rstar;%this normalizes data to match analytic coordinate ↙
output
% Ys=table2array(SData(:, [8]))/Rstar;%this normalizes data to match analytic coordinate ↙
output
% V=table2array(SData(:, [4]));
%Convert matrices to vectors
x=x(:);
y=y(:);
W=xgradn(:);
%Logical operation and index on Weight Function Data
WFL1=x>0;
WFL2=y>0;
WFQ1= find(WFL1 == 1 & WFL2 == 1);
WFQ2= find(WFL1 == 0 & WFL2 == 1);
WFQ3= find(WFL1 == 0 & WFL2 == 0);
WFQ4= find(WFL1 == 1 & WFL2 == 0);
WFX1=x(WFQ1);
```

```matlab
WFY1=y(WFQ1);
WFX2=x(WFQ2);
WFY2=y(WFQ2);
WFX3=x(WFQ3);
WFY3=y(WFQ3);
WFX4=x(WFQ4);
WFY4=y(WFQ4);
WQ1=W(WFQ1);
WQ2=W(WFQ2);
WQ3=W(WFQ3);
WQ4=W(WFQ4);


%% Set Index for Star Data
n1=length(SX1); %create iteration vectors
W1=zeros(size(SX1)); %creates blank vector used to store matching WF values that will be ↙
exported to Excel for processing
%% For Loop to Find Closest Matching Value of Weight Function
for i=1:n1
    Xdiff1=abs(SX1(i))-abs(WFX1); %Finds difference between Xsi and all X values
    Ydiff1=abs(SY1(i))-abs(WFY1); %Finds difference between Ysi and all Y values
    Total=abs(Xdiff1)+abs(Ydiff1);
    [match1, matchIdx1]=min(Total); %Finds min of both X, Y difference and names as match
    W1(i)=WQ1(matchIdx1);
end
%% Set length for Q2
n2=length(SX2); %create iteration vectors
W2=zeros(size(SX2)); %creates blank vector used to store matching WF values that will be ↙
exported to Excel for processing
%% For Loop to Find Closest Matching Value of Weight Function
for i=1:n2
    Xdiff2=abs(SX2(i))-abs(WFX2); %Finds difference between Xsi and all X values
    Ydiff2=abs(SY2(i))-abs(WFY2); %Finds difference between Ysi and all Y values
    Total=abs(Xdiff2)+abs(Ydiff2);
    [match2, matchIdx2]=min(Total); %Finds min of both X, Y difference and names as match
    W2(i)=WQ2(matchIdx2);
end
%% Set length for Q3
n3=length(SX3); %create iteration vectors
W3=zeros(size(SX3)); %creates blank vector used to store matching WF values that will be ↙
exported to Excel for processing
%% For Loop to Find Closest Matching Value of Weight Function
for i=1:n3
    Xdiff3=abs(SX3(i))-abs(WFX3); %Finds difference between Xsi and all X values
    Ydiff3=abs(SY3(i))-abs(WFY3); %Finds difference between Ysi and all Y values
    Total=abs(Xdiff3)+abs(Ydiff3);
    [match3, matchIdx3]=min(Total); %Finds min of both X, Y difference and names as match
    W3(i)=WQ3(matchIdx3);
end
%% Set length for Q4
n4=length(SX4); %create iteration vectors
W4=zeros(size(SX4)); %creates blank vector used to store matching WF values that will be ↙
exported to Excel for processing
%% For Loop to Find Closest Matching Value of Weight Function
for i=1:n4
    Xdiff4=abs(SX4(i))-abs(WFX4); %Finds difference between Xsi and all X values
```

```matlab
    Ydiff4=abs(SY4(i))-abs(WFY4); %Finds difference between Ysi and all Y values
    Total=abs(Xdiff4)+abs(Ydiff4);
    [match4, matchIdx4]=min(Total); %Finds min of both X, Y difference and names as match
    W4(i)=WQ4(matchIdx4);
end

%% Combine Data to tables and one final table to export
StarQ1= [SQ1 W1];
StarQ2= [SQ2 W2];
StarQ3= [SQ3 W3];
StarQ4= [SQ4 W4];

WFinal= [W1; W2; W3; W4];

SFinal=array2table([StarQ1; StarQ2; StarQ3; StarQ4]);
```

APPENDIX B

Discussion Regarding the Analytical Derivation of the Weight Function and Hand
Solution to Coefficients

B.1   Background

The weight function is commonly derived using the Method of Separation of Variables
and finding the coefficients of the Fourier series. This appendix provides the resources the
author used and some excerpts of the author's work for his own derivation. The author's
desire was to understand the entire process and analytical foundation, thus it is included in
this appendix for the careful student who may be interested.

B.2   Derivation

An example of the same math used to derive the weight function is based on solving the
potential on a unit disk using separation of variables (see Powers (2014) page 188). Powers
(2014) provides a thorough guide of that process. However, this only provides the general
form of the equation. In order to compute the weight function for any combination and type
of electrode, the specific boundary conditions must be applied and then the coefficients must
be solved for using those boundary conditions. The following pages include the authors own
solution to the coefficients using the boundary conditions shown.

7/8/2020

NOW WE BEGIN TO UNDERSTAND HOW TO FIND THE COEFFICIENTS.

$$G(r, \theta) = \tfrac{1}{2}c_0 + \sum_{n=1}^{\infty} (c_n \cos n\theta + d_n \sin n\theta) r^n$$

NOW WE TAKE THE PARTIAL OF G w.r.t. r

$$\partial G / \partial r = 0 + \sum_{n=1}^{\infty} n r^{n-1} (c_n \cos n\theta + d_n \sin n\theta)$$

NOW WE USE OUR BOUNDARY CONDITIONS

TO SOLVE THE EQUATION FOR OUR

COEFFICIENTS.

$$\partial G / \partial r |_{r=R} = \begin{cases} \frac{1}{R\theta_0} & (\alpha\theta < \tfrac{1}{2}\theta_0, \ 2\pi - \tfrac{1}{2}\theta_0 < \theta < 2\pi \\ 0 & (\tfrac{1}{2}\theta_0 < \theta < \pi - \tfrac{1}{2}\theta_0 \\ & (\pi + \tfrac{1}{2}\theta_0 < \theta < 2\pi - \tfrac{1}{2}\theta_0 \\ -\tfrac{1}{R\theta_0} & (\pi - \tfrac{1}{2}\theta_0 < \theta < \pi + \tfrac{1}{2}\theta_0 \end{cases}$$

Pg 190 EQ (11) SPECIFIES HOW TO CHOOSING COEFFICIENTS FOR THIS FOURIER SERIES PROBLEM.

$$\frac{\partial G}{\partial r} = 0 + \sum_{n=1}^{\infty} n R^{n-1} (c_n \cos n\theta + d_n \sin n\theta)$$

$$C_n = \frac{1}{\pi R^n} \int_{2\pi - \tfrac{1}{2}\theta_0}^{\tfrac{1}{2}\theta_0} \frac{1}{R\theta_0} \cos n\theta \, d\theta$$

$$C_n = \frac{1}{\pi R^n} \cdot \frac{1}{R\theta_0} \left[\frac{1}{n} \sin n\theta \right]_{-\tfrac{1}{2}\theta_0}^{\tfrac{1}{2}\theta_0}$$

$$C_n = \frac{1}{\pi R^n R\theta_0} \cdot \left[\frac{1}{n} \sin n(+\tfrac{1}{2}\theta_0) + \frac{1}{n} \sin n(+\tfrac{1}{2}\theta_0) \right]$$

$$C_n = \frac{2 \sin n\theta_{1/2}}{\pi R^n R\theta_0 \, n} \quad ?$$

I HAVE IDENTIFIED MY ERROR. I WAS TRYING TO USE THE NORMAL-STANDARD FORM OF THE FOURIER SERIES COEFFICIENTS. HOWEVER, I CANNOT DO THIS BECAUSE MY BOUNDARY CONDITION IS A NUEMANN BOUNDARY CONDITION, NOT A DIRICHLET. THUS I HAVE THE DERIVATIVE OF G W.r.t R NOT G ITSELF.

SO

$$\frac{\partial G}{\partial r}\bigg|_{r=R} = \sum_{n=1}^{\infty} nR^{n-1}(C_n \cos n\theta + d_n \sin n\theta) \qquad \text{✳}$$

NOW WE KNOW WHAT FORM THE COEFFICIENTS SHOULD TAKE

$$C_n = \frac{1}{\pi n R^{n-1}} \int_{2\pi - \frac{1}{2}\theta_0}^{\frac{1}{2}\theta_0} \overbrace{\left(\frac{1}{R\theta_0}\right)}^{f(\theta)} \cos n\theta \, d\theta$$

WE CAN PULL OUT $f(\theta)$ BECAUSE IT IS CONSTANT HERE

$$C_n = \frac{1}{\pi n R^{n-1} R \theta_0} \int_{2\pi - \frac{1}{2}\theta_0}^{\frac{1}{2}\theta_0} \cos n\theta \, d\theta$$

WE KNOW THAT $A^p \cdot A^k = A^{p+k}$ $\therefore$ $R^1 \cdot R^{n-1} = R^n$

$$C_n = \frac{1}{n\pi R^n \theta_0} \int_{-\frac{1}{2}\theta_0}^{\frac{1}{2}\theta_0} \cos n\theta \, d\theta$$
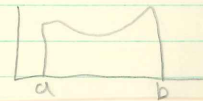
$$C_n = \frac{1}{nR^n \pi \theta_0} \left[\frac{1}{n} \sin n\theta \right]_{-\frac{1}{2}\theta_0}^{\frac{1}{2}\theta_0}$$

$$C_n = \frac{1}{nR^n \pi \theta_0} \left[\left(\frac{1}{n} \sin\left(n \frac{\theta_0}{2}\right) \right) - \left(\frac{1}{n} \sin\left(n \cdot \left(-\frac{1}{2}\theta_0\right)\right) \right) \right]$$

$$C_n = \frac{1}{nR^n \pi \theta_0} \left[\left(\frac{1}{n} \sin\left(n \frac{\theta_0}{2}\right) \right) + \left(\frac{1}{n} \sin\left(n \frac{\theta_0}{2}\right) \right) \right]$$

$$C_n = \frac{2 \sin \frac{n\theta_0}{2}}{n^2 R^n \pi \theta_0} \qquad \text{FOR BOUNDARY (1)}$$

$$C_n = \frac{-1}{nR^{n-1}\pi\theta_0 R} \int_{\pi - \frac{1}{2}\theta_0}^{\pi + \frac{1}{2}\theta_0} \cos n\theta \, d\theta \qquad \text{FOR} \quad \frac{-1}{R\theta_0}$$

$$C_n = \frac{-1}{nR^n \pi \theta_0} \cdot \left[\frac{1}{n} \sin n\theta_0 \right]_{\pi - \frac{1}{2}\theta_0}^{\pi + \frac{1}{2}\theta_0}$$

$$C_n = \frac{-1}{nR^n \pi \theta_0} \left[\left(\frac{1}{n} \sin n(\pi + \frac{1}{2}\theta_0) \right) - \left(\frac{1}{n} \sin n(\pi - \frac{1}{2}\theta_0) \right) \right]$$

NOW USING THE DIFFERENCE FORMULA AND SUM FORMULAS

$$C_n = \frac{-1}{nR^n \pi \theta_0} \left[\frac{1}{n} \left[\sin n\pi \overset{0}{\cos\left(\frac{n}{2}\theta_0\right)} + \left(\cos n\pi \sin \frac{n}{2}\theta_0 \right) \right] \right.$$

$$\left. - \left[\frac{1}{n} \left(\overset{0}{\sin n\pi \cos\left(\frac{n}{2}\theta_0\right)} \right) - \left(\cos n\pi \left(\sin \frac{-n}{2}\theta_0 \right) \right) \right] \right]$$

$$C_n = \frac{-1}{nR^n \pi \theta_0} \left[\frac{1}{n} \left(\cos n\pi \sin \frac{n}{2}\theta_0 \right) \right] + \left[\frac{1}{n} \cos n\pi \sin \frac{n}{2}\theta_0 \right]$$

$$C_n = \frac{-1}{nR^n \pi \theta_0} \left[\frac{2}{n} \left(\cos n\pi \sin \frac{n\theta_0}{2} \right) \right]$$

$$C_n = \frac{-2 (-1)^n \sin \frac{n\theta_0}{2}}{n^2 R^n \pi \theta_0}$$

WHEN n IS EVEN $(C_{n_1} + 2) = C_{n_1} + C_{n_2} = \dfrac{2 \sin \frac{n\theta_0}{2}}{n^2 R^n \pi \theta_0} + \dfrac{-2(-1)^0 \sin \frac{n\theta_0}{2}}{n^2 R^n \pi \theta_0}$

WHEN n IS ODD $(C_n + 2) = C_{n_1} + C_{n_2} = \dfrac{2 \sin \frac{n\theta_0}{2}}{n^2 R^n \pi \theta_0} + \dfrac{+2(-1) \sin \frac{n\theta_0}{2}}{n^2 R^n \pi \theta_0}$

$$\therefore \boxed{C_n = \frac{4 \sin \frac{n\theta_0}{2}}{n^2 R^n \pi \theta_0}}$$

NOW FOR THE OTHER BOUNDARIES FOR C_n

C_0 IS 0 BECAUSE WE DIFFERENTIATED AND IT DOES NOT APPEAR IN OUR NEUMANN BOUNDARY CONDITION.

AS FOR C_n, $f(\theta) = 0$ WHEN $\frac{1}{2}\theta_0 < \theta < \pi - \frac{1}{2}\theta_0$

$$C_n = \frac{1}{\pi n R^{n-1}} \int_{\frac{1}{2}\theta_0}^{\pi - \frac{1}{2}\theta_0} \overbrace{f(\theta)}^{0 \text{ FOR THESE CONDITIONS}} \cos n(\theta) \, d\theta$$

$$d_{n_1} = \frac{1}{\pi n R^{n-1}} \int_{-\frac{1}{2}\theta_0}^{\frac{1}{2}\theta_0} \frac{1}{R\theta_0} \sin n\theta \, d\theta$$

$$d_{n_1} = \frac{1}{\pi n R^n \theta_0} \left[\frac{-1}{n} \cos n\theta \right]_{-\frac{1}{2}\theta_0}^{\frac{1}{2}\theta_0}$$

WE KNOW $\cos(-x) = \cos(x)$

$$d_{n_1} = \frac{1}{\pi n R^n \theta_0} \cdot \left[\frac{-1}{n} \cos n\frac{\theta_0}{2} \right] - \left[\frac{-1}{n} \cos\left(n - \frac{1}{2}\theta_0\right) \right]$$

$$d_{n_1} = \frac{1}{\pi n R^n \theta_0} \cdot \left(\left[\frac{-1}{n} \cos n\frac{\theta_0}{2} \right] + \left[\frac{1}{n} \cos\left(n\frac{1}{2}\theta_0\right) \right] \right) \quad 0$$

$\therefore d_{n_1} = 0$

$$d_{n_2} = \frac{-1}{\pi n R^n \theta_0} \int_{\pi + \frac{1}{2}\theta_0}^{2\pi - \frac{1}{2}\theta_0} \sin n\theta \, d\theta$$

$$d_{n_2} = \frac{-1}{\pi n R^n \theta_0} \left[\frac{-1}{n} \cos n\theta \right]_{\pi + \frac{1}{2}\theta_0}^{2\pi - \frac{1}{2}\theta_0} = \frac{-1}{\pi n R^n \theta_0} \left[\frac{-1}{n} \cos\left(2\pi - \frac{1}{2}\theta_0\right) \right] - \left[\frac{1}{n} \cos n\left(\pi + \frac{1}{2}\theta_0\right) \right]$$

USING SUM AND DIFFERENCE FORMULAS

$$d_{n_2} = \frac{-1}{\pi n R^n \theta_0} \left[\frac{-1}{n} \left(\cos n 2\pi \cos \frac{-n}{2}\theta_0 \right) + \overbrace{\sin n2\pi \sin \frac{-n}{2}\theta_0}^{0} \right] - \left[\frac{1}{n} \left(\cos n2\pi \cos \frac{1}{2}\theta_0 \right) - \overbrace{\sin n\pi \sin \frac{n}{2}\theta_0}^{0} \right]$$

$$d_{n_2} = \frac{-1}{\pi n R^n \theta_0} \left[\frac{-1}{n} \left(\left(\cos n2\pi \cos \frac{n}{2}\theta_0 \right) - \left(\cos n2\pi \cos \frac{n}{2}\theta_0 \right) \right) \right]$$

$$d_{n_2} = 0$$

CURRICULUM VITAE

KADE J. BECK
kadejbeck@gmail.com
(614) 300-6467

education

2019-2021	**UTAH STATE UNIVERSITY**	**LOGAN, UT**

Doctor of Philosophy in Civil Engineering (Fluid Mechanics & Hydraulics
- *Dissertation:* An Analysis of Electromagnetic Flowmeters: A Numerical Study

LOGAN, UT

2017-2018   **Master of Science in Civil Engineering (Fluid Mechanics & Hydraulics**
- *Thesis*: Assessing the Effects of Local Turbulence and Velocity Profiles on Electromagnetic Flowmeter Accuracy.

LOGAN, UT

2013-2017   **Bachelor of Science in Civil Engineering**
- *Thesis:* Design of Logan City's Stormwater Conveyance system.

experience

2018-2020   **FRANSON CIVIL ENGINEERS**   **LOGAN, UT**
Engineer I
Began as entry level engineer and gained technical and project management competency. Began managing project and client relationships directly. Outstanding organizational ability, recognized for strategic thinking of projects to leverage resources, and excellent oral and written communication skills.

2015-2021   **UTAH WATER RESEARCH LABORATORY**   **LOGAN, UT**
Research Assistant
Conducted tests calibrating the accuracy of residential, industrial, and agricultural water metering devices.
- Created proposal and secured $4,500 to conduct personal research under supervision of Professor Barfuss.
- Assisted testing several physical model studies and analyzing and synthesizing data for client recommendations.

May-Sept 2017 **JACOBS (CH2M)**   **TAYLORSVILLE, UT**
Water Engineering Intern
Conducted hydraulic analyses and business development initiatives.
- Reviewed and created hydraulic models of existing pipe networks for rehabilitation.
- Compiled regional database to streamline proposal writing process while only using 60% of budget.

2015-2017   **UTAH STATE UNIVERSITY**   **LOGAN, UT**
AWWA Founding Member and Chapter President
Chartered Utah's first AWWA Student Chapter; organized and directed student chapter involving 20 members.
- Secured funding from Intermountain Section AWWA and Civil Engineering Department for chapter operations.
- Planned and executed 5 tours of water infrastructure and treatment facilities to connect students with industry.

May-Oct 2015 **U. S. BRIDGE**   **NEW ALBANY, OH**
Civil Engineering Intern
Reviewed engineering drawings and performed standard design calculations.
- Analyzed data to build pricing tool to improve time required to produce proposals for customers from several hours to a few seconds. Created over 210 CAD drawings to accompany the proposal price with a schematic of the desired bridge improving overall customer experience.
- Created design aides to reduce computation time for project engineers reducing costs and increasing efficiency.
- As the first engineering intern in company history, developed standard communication and reporting protocol for future interns.

2014-2015   **UTAH STATE UNIVERSITY**   **LOGAN, UT**
College of Engineering Senator
Directed a team of 30 students in identifying, planning, and executing solutions for the College of Engineering.
- Met with all club leadership of the college to identify missing elements of the educational experience. Presented to the Industrial Advisory Board a plan to initiate a college sponsored career exploration program. Built relationships with businesses and college, provided local interns, and increased retention for college.
- Conducted primary research and presented to the Dean's Office and all department heads an execution strategy to incorporate an official interdisciplinary capstone project. Negotiated satisfying credit requirements between departments. Upon approval, the interdisciplinary capstone option was launched in fall 2015.
- Presented to eight other student officers the needs of upgraded teaching technology for USU College of Engineering and secured $7,000.
- Created six new officer positions for the leadership council to improve training and continuity of council.

publications	**Beck, Kade** & Barfuss, Steven & Sharp, Zachary & Johnson, Michael & Dutta, Som & Moon, Todd. (2021). The effect of higher fidelity flow field models on electromagnetic flowmeter analysis. AWWA Water Science. *(Soon to be Submitted)*
	Beck, Kade & Barfuss, Steven & Sharp, Zachary & Moon, Todd. (2021). Weight function method versus magnetohydrodynamics coupled with Navier-Stokes solver: A comparative study. AWWA Water Science *(Submitted)*
	Beck, Kade & Barfuss, Steven & Moon, Todd & Sharp, Zachary. (2021). The superior accuracy of the arc electrode flowmeter: A numerical study. AWWA Water Science. 10.1002/aws2.1220
	Beck, Kade & Barfuss, Steven & Johnson, Michael. (2019). Assessing the effects of local turbulence and velocity profiles on electromagnetic flowmeter accuracy. AWWA Water Science. 1. 10.1002/aws2.1156.
	Beck, Kade & Weller, Ryan & Barfuss, Steven & Johnson, Michael. (2018). The Effects of a Short-Radius Elbow on Electromagnetic Flowmeter Accuracy. Journal - American Water Works Association. 110. 10.1002/awwa.1055.

presentations	**Crockett Pressurized Irrigation System,** Northern Utah Water Conference, April 2019.
	How Close is Close Enough? Utah Water Users Workshop, March 2019.
	The Effects of a Short Radius Elbow on Electromagnetic Flowmeter Accuracy, AWWA Annual Conference and Exposition, June 2018.
	The Effects of a Short Radius Elbow on Electromagnetic Flowmeter Accuracy, AWWA Intermountain Section (1st Place Student Poster Competition) October 2017.
	Field Calibration of Irrigation Flow Measuring Devices, Utah Water Users Workshop, March 2017.

professional associations	American Water Works Association – Member
	American Society of Civil Engineers – Student Member (served as Young Member Forum Chair for Northern Utah Branch from 08/2018-05/2019. Served as Vice President of USU Student Chapter from 01/2014-05/2014).

awards	**Outstanding Master's Student Researcher –** *USU College of Engineering*	04/2018
	Outstanding Master's Student Researcher – *USU Civil and Environmental Engineering Department*	02/2018
	Life Saving Award – *Jacobs Engineering*	07/2017
	Outstanding Senior Achievement Award – *USU College of Engineering*	02/2017
	Outstanding Senior – *USU Civil and Environmental Engineering Department*	01/2017
	A-Pin Recipient – *USU College of Engineering*	10/2016
	Outstanding Emerging Student Leader – *USU Student Involvement and Leadership Center*	05/2015
	Outstanding Student College of Engineering, Utah State University– *Logan Kiwanis Club*	04/2015
	Outstanding Service Award – *USU College of Engineering*	04/2015
	Utah State University President's Award - *USU Student Involvement and Leadership Center*	04/2015

scholarships	**American Society of Civil Engineers J. Waldo Smith Hydraulic Fellowship**	05/2017
	Lawrence O. Canon Scholar	05/2017
	International American Association of Cost Engineering Scholarship	05/2017
	NSF S-STEM Scholarship	05/2017
	Seely Hinckley Scholar	05/2017
	American Water Works Association Honorary Scholar	01/2017
	Lillywhite Presidential Scholar	05/2016
	NSF S-STEM Scholarship	05/2016
	Lyman Willardson Engineering Scholarship	04/2016
	Douglas D. Alder Scholar	04/2016
	American Water Works Association National Neptune Technology Scholarship	03/2016
	American Water Works Association Intermountain Section Engineering Scholarship	01/2016
	Claude J Burtenshaw Scholarship	05/2015
	James and Theresa Moore Scholarship	05/2015
	Arsham Amirikian Engineering Scholarship	05/2015
	Utah State University Student Involvement and Leadership Scholarship	05/2014

community	Volunteer literacy tutor for students with learning disabilities (January-April 2016).
	Lead and directed 250 missionary volunteers for 6 months. Missionary for The Church of Jesus Christ of Latter-day Saints in Ohio (2011-2013).
	Eagle Scout (November 2006).

interests	Enjoy being with wife and four children, mountain biking, playing basketball, reading and board games.